# CAFEE

*Center for Alternative Fuels, Engines & Emissions*

*West Virginia University*

**Final Report**

# In-Use Emissions Testing of Light-Duty Diesel Vehicles in the United States

Prepared by:

**Principal Investigator**

**Dr. Gregory J. Thompson (Principal Investigator)**

**Phone: (304) 293-3254**

**Email: gregory.thompson@mail.wvu.edu**

**Co-Principal Investigators**

**Daniel K. Carder, Marc C. Besch, Arvind Thiruvengadam, Hemanth K. Kappanna**

**Center for Alternative Fuels, Engines & Emissions**

**Dept. of Mechanical & Aerospace Engineering**

**West Virginia University**

**Morgantown WV 26506-6106**

Prepared for:

**Francisco Posada, PhD**

**Researcher - Passenger Vehicle Program**

**International Council on Clean Transportation (ICCT)**

**1225 Eye Street, NW, Suite 900**

**Washington, DC 20005**

**Phone: (202) 534-1605**

**Email: francisco@theicct.org**

**May 15, 2014**

## EXECUTIVE SUMMARY

The Center for Alternative Fuels, Engines and Emissions (CAFEE) at West Virginia University (WVU) was contracted by the International Council on Clean Transportation (ICCT) to conduct in-use testing of three light-duty diesel vehicles, using a portable emissions measurement system (PEMS), over a variety of pre-defined test routes exhibiting diverse driving conditions pertinent to major United States population centers located in the state of California. Additionally, one vehicle was operated over an extended distance of nearly 4000km predominantly composed of highway driving conditions between California and Washington State. Also, two out of the three test vehicles were selected for chassis dynamometer testing at California Air Resources Board's (CARB) El Monte, CA vehicle certification test facility; however, a detailed discussion of these results is not part of this report.

The test vehicles were certified to US-EPA Tier2-Bin5 and California LEV-II ULEV emissions limits and were equipped with $NO_x$ after-treatment technologies, including one lean-$NO_x$ trap (LNT) (*Vehicle A*) and two urea-based selective catalytic reduction (SCR) systems (*Vehicles B* and *C*). Furthermore, all three test vehicles were thoroughly checked for possible engine or after-treatment malfunction codes using an ECU scanning tool prior to selecting a vehicle for this on-road measurement campaign, with none of them showing any fault code or other anomalies. The after-treatment system was assumed to be '*de-greened*' as all three vehicles have accumulated more than 3,000 to 4,000 miles, and no reduction in catalytic activity due to aging was expected as the total mileage was relatively low (< 15,000 miles) for all test vehicles. Gaseous emissions of $NO_x$, CO, THC and $CO_2$ were measured using the OBS-2200 PEMS from Horiba Ltd., while particulate number and mass concentrations were inferred from real-time particle charge measurements employing a Pegasor particle sensor, model PPS-M, from Pegasor.

Real-world $NO_x$ emissions were found to exceed the US-EPA Tier2-Bin5 (at full useful life) standard by a factor of 15 to 35 for the LNT-equipped vehicle, by a factor of 5 to 20 for one and at or below the standard for the second urea-SCR fitted vehicle over five pre-defined routes categorized based on their predominant driving conditions, namely, i) highway, ii) urban/suburban, and iii) rural-up/downhill driving. The second urea-SCR equipped vehicle exceeded the standard only during rural-up/downhill operating conditions by a factor of ~10. Most importantly, distance-specific $NO_x$ emissions for the two high-emitting vehicles were below the US-EPA Tier2-Bin5 standard for the weighted average over the FTP-75 certification

cycle during chassis dynamometer testing at CARB's El Monte facility, with 0.022g/km ±0.006g/km (±1σ, 2 repeats) and 0.016g/km ±0.002g/km (±1σ, 3 repeats) for the LNT and urea-SCR equipped vehicles, respectively. It has to be noted that on-road emissions testing was performed with the engine and after-treatment in warmed-up condition (i.e. warm/hot start). Increased $NO_x$ emissions are usually expected for cold-start as seen during the first portion (i.e. '*Bag-1*') of the FTP-75 cycle, however, not for hot, running conditions as exhibited during '*Bag-2 and 3*' of the FTP-75 cycle or on-road operation of the vehicle.

Generally, distance-specific $NO_x$ emissions were observed to be highest for rural-up/downhill and lowest for high-speed highway driving conditions with relatively flat terrain. The LNT after-treatment based vehicle was observed to emit significantly (> 19% to 90%) more $NO_x$ during diesel particulate filter (DPF) regeneration events. This was speculated to be due to an extended duration of lean exhaust conditions and a lack of frequent enrichment of the exhaust gas ($\lambda < 1$) while DPF regeneration was ongoing, leading to an inhibition of necessary LNT regeneration ($D_eNOx$), and thus, causing the $NO_x$ storage catalyst to become saturated with $NO_x$ emissions that ultimately started to break through. *Vehicles B* and *C* were not observed to exhibit such a predominant increase in $NO_x$ emissions during DPF regeneration events and changes in $NO_x$ emissions rates were generally confounded by driver and traffic pattern influences.

Even though exceeding the US-EPA Tier2-Bin5 standard on average by a factor of 6 (i.e. 0.26g/km ±0.21g/km (±1σ)) during extended highway driving between California and Washington State, *Vehicle B*, the urea-SCR equipped vehicle, was found to have $NO_x$ emissions below the regulatory standard for portions of the route characterized by low or negligible changes in altitude (i.e. near zero road grade), and with the vehicle operated in cruise-control mode at highway speeds (i.e. 120km/h).

In general, CO and THC emissions were observed to be well below the regulatory level for all three test vehicles and driving conditions, with exception of two routes for the LNT-equipped vehicle where THC emissions were observed at slightly elevated levels. Interestingly, chassis dynamometer testing of *Vehicles A* and *B* indicated THC emissions to be primarily composed of methane ($CH_4$/THC ratio > 0.95) which is surprising for diesel fueled vehicle and might be attributed to secondary reactions occurring over the surface of the oxidation catalyst or the LNT in case of *Vehicle A*.

As expected, highway driving showed lowest distance-specific $CO_2$, whereas urban/suburban driving conditions lead to highest $CO_2$ emissions factors for all vehicles.

During PEMS testing, average fuel economy for highway driving with *Vehicles A* and *B* was 45.3 mpg ±8.6mpg (±σ1) and 43.7mpg ±5.7mpg (±σ1), respectively, and 27.3 mpg (no repetition) for *Vehicle C* which is ~39% lower compared to *Vehicles A* and *B*. On the other hand, urban/suburban driving results in average fuel economies of 30.0mpg ±2.9mpg (±σ1) and 26.6 mpg ±1.4mpg (±σ1) for *Vehicles A* and *B*, respectively, and 18.5mpg ±4.0mpg (±σ1) for *Vehicle C* which is 35% lower compared to *Vehicles A* and *B*. Overall, urban/suburban driving leads to a 32-39% reduction in fuel economy over highway driving.

Particulate number emissions, inferred from PPS measurements, were observed below the Euro 5b/b+ standard except during vehicle operation exhibiting DPF regeneration events where PN emissions significantly increased by two to three orders of magnitude, thereby exceeding the Euro 5b/b+ standard under all driving conditions for the LNT and first urea-SCR vehicles. It is noted that PN is not regulated in the United States. Also, for the latter vehicle DPF regeneration frequencies were found to be predominantly based on distance traveled, occurring after every 756km ±29km (±1σ), corresponding to ~7.07hours ±0.06hours for highway driving conditions.

It is noted that only three vehicles were tested as part of this measurement campaign with each vehicle being a different after-treatment technology or vehicle manufacturer; conclusions drawn from the data presented herein are confined to these three vehicles. The limited data set does not necessarily permit drawing more generalized conclusions for a specific vehicle category or after-treatment technology.

## TABLE OF CONTENTS

## LIST OF TABLES

## LIST OF FIGURES

## LIST OF ABBREVIATIONS AND UNITS

| | | |
|---|---|---|
| CAFEE | - | Center for Alternative Fuels, Engines and Emissions |
| CARB | - | California Air Resources Board |
| CLD | - | Chemiluminescence Detector |
| CO | - | Carbon Monoxide |
| $CO_2$ | - | Carbon Dioxide |
| CVS | - | Constant Volume Sampler |
| DPF | - | Diesel Particle Filter |
| EERL | - | Engines and Emissions Research Laboratory |
| EFM | - | Exhaust Flow Meter |
| EPA | - | Environmental Protection Agency |
| EU | - | European Union |
| FTP | - | Federal Test Procedure |
| GPS | - | Global Positioning System |
| FID | - | Flame Ionization Detector |
| LNT | - | Lean $NO_x$ Trap |
| MPG | - | Miles per Gallon |
| NDIR | - | Non-Dispersive Infrared Spectrometer |
| NEDC | - | New European Driving Cycle |
| NO | - | Nitrogen Monoxide |
| $NO_x$ | - | Oxides of Nitrogen |
| NTE | - | Not-to-Exceed |
| OC | - | Oxidation Catalyst |
| PEMS | - | Portable Emissions Measurement System |
| PM | - | Particulate Matter |
| PN | - | Particle Number |
| RPA | - | Relative Positive Acceleration |
| SCR | - | Selective Catalytic Reduction |
| THC | - | Total Hydrocarbons |

# 1 INTRODUCTION

Researchers at the Joint Research Centre (JRC) in Europe have identified off-cycle oxides of nitrogen ($NO_x$) emissions from light-duty diesel vehicles (LDV) to substantially exceed the Euro 3-5 emissions standards on average by a factor of 4 to 7 over specific test routes [1]. Hence, the study concluded that the introduction of tighter emissions limits for the purpose of vehicle/engine certification has not necessarily translated into effective on-road $NO_x$ reductions of the same magnitude [1]. Furthermore, work conducted by other researchers has highlighted the thermodynamic conditions of the exhaust gas and after-treatment components to be a primary limiting factor for achieving high $NO_x$ conversion efficiencies using the aqueous-urea based selective catalytic reduction (SCR) system, especially during low-load, low-speed operation such as frequently encountered during urban driving and stop-and-go traffic on congested highways.

Sparked by these findings, the International Council on Clean Transportation (ICCT) contracted West Virginia University (WVU) to perform on-road emissions measurements in order to study off-cycle emissions performance and fuel economy from three diesel light-duty vehicles (LDV's) under typical United States (US) driving conditions using a portable emissions measurement system (PEMS). The PEMS testing aided in comparing the performance of different $NO_x$ control technologies under off-cycle conditions against United States Environmental Protection Agency (US-EPA) Tier2-Bin5 and California Air Resources Board (CARB) LEV-II ULEV emissions standards.

The test plan covered a wide variety of topological, road and ambient conditions as well as traffic densities over three major urban areas along the West coast, namely, San Diego, Los Angeles, and San Francisco (California). Additionally, one vehicle, specifically one equipped with urea-SCR after-treatment technology, was operated over a total distance of ~4000km between Los Angeles, CA and Seattle, WA to investigate emissions reduction characteristics over extended highway driving conditions. Furthermore, two out of the three test vehicles were selected for chassis dynamometer testing over standardized test cycles at CARB's vehicle certification laboratory in El Monte, CA. This also allowed for comparison of the PEMS against laboratory grade instruments to verify measurement accuracy of the on-board system.

## 1.1 Objectives

The primary objective of this study was to gain insight into real-world emissions of $NO_x$ and other regulated gaseous pollutants from diesel LDVs certified to US-EPA Tier2-Bin5 and CARB LEV-II ULEV (CA) standards. Emissions were measured during typical driving conditions pertinent to major US population centers using on-board instrumentation (PEMS). For a subset of vehicles and test routes, particulate matter mass emissions (PM) and particle number (PN) emission concentrations were also measured on-board.

To that aim, the Center for Alternative Fuels, Engines and Emissions (CAFEE) at WVU conducted light-duty PEMS testing on two 2012 model year (MY) and one MY 2013 vehicles equipped with two different $NO_x$ after-treatment technologies, including lean $NO_x$ trap (LNT) and aqueous urea-based selective catalytic reduction (SCR) system. Gaseous exhaust emissions, including $NO_x$, carbon monoxide (CO), carbon dioxide ($CO_2$) and total hydrocarbons (THC) were measured on a continuous basis utilizing a Horiba OBS-2200 portable emissions measurement system, whereas particle number concentrations and particulate mass emissions were inferred from real-time measurements performed using a Pegasor particle sensor, model PPS-M from Pegasor.

Specifically, the data collected during the course of this study allowed for following analysis and comparisons:

i. comparison of off-cycle $NO_x$ emissions against US-EPA Tier 2-Bin 5 and CARB LEV-II ULEV emissions standards;

ii. evaluation of fuel economy in comparison to standardized chassis dynamometer test cycles and EPA evaluated fuel economy ratings as published on window stickers for new cars sold in the United States [2];

iii. calculation of in-use emissions factors based on the '*Averaging Windows Method*' (AWM) [3] using $CO_2$ emissions emitted over a certification cycle as the threshold value to define the averaging window size;

iv. evaluation of $NO_x$ after-treatment conversion efficiencies of two different technologies as a function of driving conditions, traffic density, ambient conditions and exhaust gas thermodynamic properties;

v. quantification of particle number (PN) emissions concentrations with regard to the particle number limits (i.e. $6.0x10^{11}$ #/km) set forth by the European Union (EU) in 2013 with the introduction of Euro 5b/b+ emission standards [4];

vi. evaluation of diesel particulate filter (DPF) filtration efficiency and frequency of regeneration events; and

vii. quantification of maximum route emissions rates and their respective location along the routes.

## 2 BACKGROUND

The background information given hereafter will be limited to a discussion of United States Environmental Protection Agency's (US-EPA) Tier 2 and California Air Resources Board's (CARB) LEV-II emissions regulations that are applicable to the two light-duty vehicles (LDV) and one light-duty truck (LDT) whos on-road emissions have been evaluated as part of this study.

The ongoing effort by EPA and CARB to comply with National Ambient Air Quality Standards (NAAQS), particularly in several non-attainment regions, has led to ever-increasingly stringent regulations on LDVs emissions. These are currently regulated under EPA's Tier 2 and California LEV-II emissions regulations. EPA's vehicle classification is based on gross vehicle weight rating (GVWR) and is shown in Table 2.1. It has to be noted that medium duty passenger vehicles (MDPV) are regulated under light-duty vehicle emissions regulations.

**Table 2.1: Vehicle classification based on gross vehicle weight rating (GVWR) [5]**

<table>
<tr><th colspan="11">Gross Vehicle Weight Rating (GVWR) [lbs]<br>6,000 8,500 10,500 14,000 16,000 19,500 26,000 33,000 60,000</th></tr>
<tr><td rowspan="4">Federal</td><td colspan="2">LDV</td><td colspan="9">MDPV[c)]</td></tr>
<tr><td colspan="2">LDT</td><td colspan="9">HDV / HDE</td></tr>
<tr><td>LLDT</td><td>HLDT</td><td colspan="5">LHDDE</td><td colspan="2">MHDDE</td><td colspan="2">HHDDE / Urban Bus</td></tr>
<tr><td>LDT 1 & 2[a)]</td><td>LDT 3 & 4[b)]</td><td>HDV2b</td><td>HDV3</td><td>HDV4</td><td>HDV5</td><td>HDV6</td><td>HDV7</td><td>HDV8a</td><td>HDV8b</td></tr>
</table>

[a)] *Light-duty truck (LDT) 1 if loaded vehicle weight (LVW) = 3,750; LDT 2 if LVW > 3,750*

[b)] *LDT 3 if adjusted loaded vehicle weight (ALVW) = 5,750; LDT 4 if ALVW > 5,750*

[c)] *MDPV vehicles will generally be grouped with and treated as HLDTs in the Tier 2 program*

The EPA's Tier 2 emission standards that were phased in over a period of four years, beginning in 2004, for LDV/LLDTs, with an extension of two years for HLDTs, were in full effect starting from MY 2009 for all new passenger cars and light-duty trucks, including pickup trucks, vans, minivans and sport-utility vehicles. The Tier 2 standards were designed to significantly reduce ozone-forming pollution and PM emissions from passenger vehicles regardless of the fuel used and the type of vehicle, namely car, light-duty truck or larger passenger vehicle. The Tier 2 standards were implemented along with the gasoline fuel sulfur standards in order to enable emissions reduction technologies necessary to meet the stringent

vehicle emissions standards. The gasoline fuel sulfur standard mandates the refiners and importers to meet a corporate average gasoline sulfur standard of 30 ppm starting from 2006 [6].

The EPA Tier 2 emissions standard requires each LDV/LDT vehicle manufacturer to meet a corporate average $NO_x$ standard of 0.07g/mile (0.04 g/km) for the fleet of vehicles being sold for a given model year. Furthermore, the Tier 2 emissions standard consists of eight sub-bins, each one with a set of standards to which the manufacturer can certify their vehicles provided the corporate sales weighted average $NO_x$ level over the full useful life of the vehicle (10 years/120,000 miles/193,121 km), for a given MY of Tier 2 vehicles, is less than 0.07g/mile (0.04 g/km). The corporate average emission standards are designed to meet the air quality goals allowing manufacturers the flexibility to certify some models above or below the standard, thereby enabling the use of available emissions reduction technologies in a cost-effective manner as opposed to meeting a single set of standards for all vehicles [6]. Final phased-in full and intermediate useful life Tier 2 standards are listed in Table 2.2.

**Table 2.2: Light-duty vehicle, light-duty truck, and medium-duty passenger vehicle - EPA Tier 2 exhaust emissions standards in [g/miles] [6]**

| Bin# | Intermediate life (5 years / 50,000 mi) | | | | | Full useful life (10 years/120,000 mi) | | | | |
|---|---|---|---|---|---|---|---|---|---|---|
| | NMOG* | CO | $NO_x$ | PM | HCHO | NMOG* | CO | $NO_x$† | PM | HCHO |
| Temporary Bins | | | | | | | | | | |
| 11 MDPV[c] | | | | | | 0.28 | 7.3 | 0.90 | 0.12 | 0.032 |
| 10[a,b,d,f] | 0.125 (0.160) | 3.4 (4.4) | 0.40 | - | 0.015 (0.018) | 0.156 (0.230) | 4.2 (6.4) | 0.60 | 0.08 | 0.018 (0.027) |
| 9[a,b,e,f] | 0.075 (0.140) | 3.4 | 0.20 | - | 0.015 | 0.090 (0.180) | 4.2 | 0.30 | 0.06 | 0.018 |
| Permanent Bins | | | | | | | | | | |
| 8[b] | 0.100 (0.125) | 3.4 | 0.14 | - | 0.015 | 0.125 (0.156) | 4.2 | 0.20 | 0.02 | 0.018 |
| 7 | 0.075 | 3.4 | 0.11 | - | 0.015 | 0.09 | 4.2 | 0.15 | 0.02 | 0.018 |
| 6 | 0.075 | 3.4 | 0.08 | - | 0.015 | 0.09 | 4.2 | 0.10 | 0.01 | 0.018 |
| 5 | 0.075 | 3.4 | 0.05 | - | 0.015 | 0.09 | 4.2 | 0.07 | 0.01 | 0.018 |
| 4 | - | - | - | - | - | 0.07 | 2.1 | 0.04 | 0.01 | 0.011 |
| 3 | - | - | - | - | - | 0.055 | 2.1 | 0.03 | 0.01 | 0.011 |
| 2 | - | - | - | - | - | 0.01 | 2.1 | 0.02 | 0.01 | 0.004 |
| 1 | - | - | - | - | - | 0 | 0 | 0 | 0 | 0 |

* *for diesel fueled vehicle, NMOG (non-methane organic gases) means NMHC (non-methane hydrocarbons)*
† *average manufacturer fleet $NO_x$ standard is 0.07 g/mi for Tier 2 vehicles*
***a*** *Bin deleted at end of 2006 model year (2008 for HLDTs)*
***b*** *The higher temporary NMOG, CO and HCHO values apply only to HLDTs and MDPVs and expire after 2008*

*c An additional temporary bin restricted to MDPVs, expires after model year 2008*
*d Optional temporary NMOG standard of 0.195 g/mi (50,000) and 0.280 g/mi (full useful life) applies for qualifying LDT4s and MDPVs only*
*e Optional temporary NMOG standard of 0.100 g/mi (50,000) and 0.130 g/mi (full useful life) applies for qualifying LDT2s only*
*f 50,000 mile standard optional for diesels certified to bins 9 or 10*

All Tier 2 exhaust emissions standards must be met over the FTP-75 chassis dynamometer test cycle. In addition to the above listed emissions standards, Tier 2 vehicles must also satisfy the supplemental FTP (SFTP) standards. The SFTP standards are intended to control emissions from vehicles when operated at high speed and acceleration rates (i.e. aggressive driving, as simulated through the US06 test cycle), as well as when operated under high ambient temperature conditions with vehicle air-conditioning system turned on (simulated through the SC03 test cycle). The SFTP emissions results are determined using the relationship outlined in Equation (1) where individual emissions measured over FTP, US06 and SC03 test cycles are added together with different weighting factors.

$$E_{pollutant} = 0.35 * (FTP) + 0.28 * (US06) + 0.37 * (SC03) \qquad \textbf{Eq. 1}$$

Manufacturers must comply with 4000 mile and full useful life SFTP standards. The 4000 mile SFTP standards are shown in Table 2.3.

**Table 2.3: US-EPA 4000 mile SFTP standards in [g/mi] for Tier 2 vehicles [6]**

| Vehicle Class [1] | US06 | | SC03 | |
|---|---|---|---|---|
| | NMHC + $NO_x$ | CO | NMHC + $NO_x$ | CO |
| LDV/LDT1 | 0.14 | 8.0 | 0.20 | 2.7 |
| LDT2 | 0.25 | 10.5 | 0.27 | 3.5 |
| LDT3 | 0.40 | 10.5 | 0.31 | 3.5 |
| LDT4 | 0.60 | 11.8 | 0.44 | 4.0 |

[1] *Supplemental exhaust emission standards are applicable to gasoline and diesel-fueled LDV/Ts but are not applicable to MDPVs, alternative fueled LDV/Ts, or flexible fueled LDV/Ts when operated on a fuel other than gasoline or diesel*

The full useful life SFTP standards are determined following Equation 2, which is based on Tier 1 SFTP standards, lowered by 35% of the difference between the Tier 2 and Tier 1 exhaust emissions standards. Tier 1 full useful life SFTP standards for different vehicle classes along with CO standards for individual chassis dynamometer test cycles as well as Tier 1 full useful life FTP standards are shown in Table 2.4 and Table 2.5, respectively.

$$Tier\ 2\ SFTP\ Std. = Tier\ 1\ SFTP\ Std. - 0.35 * (Tier\ 1\ FTP\ Std. - Tier\ 2\ FTP\ Std.) \quad \textbf{Eq. 2}$$

**Table 2.4: US-EPA Tier 1 full useful life SFTP standards in [g/mi] [6]**

| Vehicle Class | NMHC + $NO_x$ [a,c] | CO [b,c] | | |
|---|---|---|---|---|
| | | US06 | SC03 | Weighted |
| LDV/LDT1 | 0.91 (0.65) | 11.1 (9.0) | 3.7 (3.0) | 4.2 (3.4) |
| LDT2 | 1.37 (1.02) | 14.6 (11.6) | 4.9 (3.9) | 5.5 (4.4) |
| LDT3 | 1.44 | 16.9 | 5.6 | 6.4 |
| LDT4 | 20.9 | 19.3 | 6.4 | 7.3 |

a) *Weighting for NMHC + $NO_x$ and optional weighting for CO is 0.35*(FTP) + 0.28*(US06) + 0.37*(SC03)*

b) *CO standards are stand alone for US06 and SC03 with option for a weighted standard*

c) *Intermediate life standards are shown in parentheses for diesel LDV/LLDTs opting to calculate intermediate life SFTP standards in lieu of 4,000 mile SFTP standards as permitted.*

**Table 2.5: US-EPA Tier 1 full useful life FTP standards in [g/mi] [6]**

| Vehicle Class | NMHC [a] | $NO_x$ [a] | CO [a] | PM |
|---|---|---|---|---|
| LDV/LDT1 | 0.31 (0.25) | 0.60 (0.40) | 4.2 (3.4) | 0.10 |
| LDT2 | 0.40 (0.32) | 0.97 (0.70) | 5.5 (4.4) | 0.10 |
| LDT3 | 0.46 | 0.98 | 6.4 | 0.10 |
| LDT4 | 0.56 | 1.53 | 7.3 | 0.12 |

a) *Intermediate life standards are shown in parentheses for diesel LDV/LLDTs opting to calculate intermediate life SFTP standards in lieu of 4,000 mile SFTP standards as permitted*

In-use testing of light duty vehicles under the Tier 2 regulation involves testing of vehicles on a chassis dynamometer that have accumulated at least 50,000 miles during in-use operation, to verify compliance with FTP and SFTP emissions standards at intermediate useful life. There has been no regulatory requirement in the United States to verify compliance of Tier 2 vehicles for emissions standards over off-cycle tests such as on road emissions testing with the use of PEMS equipment, similar to what is being mandated for heavy-duty vehicles via the engine in-use compliance requirements (i.e. NTE emissions). Meanwhile, the European Commission (EC) has established a working group to propose modifications to its current vehicle certification procedures in order to better limit and control off-cycle emissions [7]. Over the course of a two-year evaluation process, different approaches were being assessed with two of them believed to be promising for application in a future light-duty emissions regulation, namely; i) emissions testing with random driving cycle generation in the laboratory, and ii) on-road emissions testing with PEMS equipment [7].

Fuel economy and $CO_2$ emission ratings as published by the US-EPA and the US Department of Energy (DOE) are based on laboratory testing of vehicles while being operated over a series of five driving cycles on a chassis dynamometer specified in more detail in Table 2.6 [2]. Originally, only the '*city*' (i.e. FTP-75) and '*highway*' cycles were used to determine vehicle fuel economy, however, starting with model year 2008 vehicles the test procedure has been augmented by three additional driving schedules, specifically, '*high-speed*' (i.e. US06), '*air conditioning*' (i.e. SC03 with air conditioning turned on), and '*cold temperature*' (i.e. FTP-75 at 20°F ambient temperature) driving cycles [2]. Vehicle manufacturer are required to test a number of vehicles representative of all available combinations of engine, transmission and vehicle weight classes being sold in the US. The fuel economy label provides distance-specific fuel consumption and $CO_2$ emissions values for '*city*', and '*highway*' driving as well as a combined value (i.e. Combined MPG) calculated as a weighted average of 55% '*city*' and 45% '*highway*' driving, allowing for a simplified comparison of fuel efficiency across different vehicles [2].

**Table 2.6: Fuel economy and $CO_2$ emissions test characteristics [2]**

| Driving Schedule Attributes | Test Schedule | | | | |
|---|---|---|---|---|---|
| | City | Highway | High Speed | AC | Cold Temp. |
| Trip type | Low speeds in stop-and-go urban traffic | Free-flow traffic at highway speeds | Higher speeds; harder accel. and braking | AC use under hot ambient conditions | City test w/ colder outside temperature |
| Max. speed [mph] | 56 | 60 | 80 | 54.8 | 56 |
| Avg. speed [mph] | 21.2 | 48.3 | 48.4 | 21.2 | 21.2 |
| Max. accl. [mph/s] | 3.3 | 3.2 | 8.46 | 5.1 | 3.3 |
| Distance [miles] | 11 | 10.3 | 8 | 3.6 | 11 |
| Duration [min] | 31.2 | 12.75 | 9.9 | 9.9 | 31.2 |
| Stops [#] | 23 | None | 4 | 5 | 23 |
| Idling time [%] [1)] | 18 | None | 7 | 19 | 18 |
| Engine Startup [2)] | Cold | Warm | Warm | Warm | Cold |
| Lab temperature [°F] | 68 - 86 | 68 - 86 | 68 - 86 | 95 | 20 |
| Vehicle AC | Off | Off | Off | On | Off |

[1)] *Idling time in percent of total test duration*

[2)] *Maximum fuel efficiency is not reached until engine is in warmed up condition*

# 3 METHODOLOGY

The following section of the report will discuss the test vehicles selected for this study, describe the specific test routes and their characteristics, as well as present the emissions sampling setup and instrumentation utilized during this work.

## 3.1 Test Vehicle Selection

The vehicles tested in this study comprise two MY 2012 and one MY 2013, diesel-fueled passenger cars, and will hereinafter be referred to as '*Vehicle A*', '*Vehicle B*', and '*Vehicle C*' in order to anonymize model- and make-specific information for the purpose of this report. *Vehicle A* and *Vehicle B* were equipped with the same 2.0L turbocharged, four cylinder base engine. However, they were equipped with two different $NO_x$ reduction technologies. *Vehicle A* featured a lean $NO_x$ trap (LNT) for $NO_x$ abatement, whereas *Vehicle B* was fitted with an aqueous urea-based selective catalytic reduction system. Both vehicles had a DPF installed for controlling particulate matter emissions. *Vehicle C* was fitted with a 3.0L turbocharged in-line six-cylinder engine in conjunction with an aqueous urea-SCR system and DPF for $NO_x$ and PM control, respectively. The drive-train of both *Vehicles A* and *B* comprised 6-speed automatic transmissions with front wheel drive, whereas *Vehicle C* featured all-wheel drive with a 6-speed automatic transmission.

All three test vehicles were compliant with EPA Tier2-Bin5, as well as California LEV-II ULEV (for *Vehicles A* and *B)* and LEV-II LEV (for *Vehicle C*) emissions standards as per EPA certification documents. *Vehicles A* and *B* are categorized as '*light-duty vehicles*' (LDV) whereas *Vehicle C* as '*light-duty truck 4*' (LDT4). Actual $CO_2$ emissions and fuel economy for city, highway, and combined driving conditions, as advertised by the EPA for new vehicles sold in the US are given in Table 3.1 for all three test vehicles.

*Vehicle A* and *Vehicle C* were rented from two separate rental agencies and had initial odometer readings of 4,710 and 15,031 miles, respectively. *Vehicle B* had 15,226 miles at start of testing and was acquired from a private owner. Furthermore, all three test vehicles were thoroughly checked for possible engine or after-treatment malfunction codes using an ECU scanning tool prior to selecting a vehicle for this on-road measurement campaign, with none of them showing any fault code or other anomalies. The after-treatment system was assumed to be '*de-greened*' as all three vehicles have accumulated more than 3,000 to 4,000 miles, and no

reduction in catalytic activity due to aging was expected as the total mileage was relatively low (< 15,000 miles) for all test vehicles. More specific details for the three test vehicles are presented in Table 3.1.

**Table 3.1: Test vehicles and engine specifications**

| Vehicle | | A | B | C |
|---|---|---|---|---|
| Mileage at test start [miles] | | 4,710 | 15,226 | 15,031 |
| Fuel | | ULSD | ULSD | ULSD |
| Engine displacement [L] | | 2.0 | 2.0 | 3.0 |
| Engine aspiration | | Turbocharged/ Intercooled | Turbocharged/ Intercooled | Turbocharged/ Intercooled |
| Max. engine power [kW] | | 104 @ 4200 rpm | 104 @ 4200 rpm | 198 |
| Max. engine torque [Nm] | | 320 @ 1750 rpm | 320 @ 1750 rpm | - |
| Emission after-treatment technology | | OC, DPF, LNT | OC, DPF, urea-SCR | OC, DPF, urea-SCR |
| Drive train | | 2-wheel drive, front | 2-wheel drive, front | 4-wheel drive |
| Applicable emissions limit | *U.S. EPA* | T2B5 (LDV) | T2B5 (LDV) | T2B5 (LDV) |
| | *CARB* | LEV-II ULEV | LEV-II ULEV | LEV-II LEV |
| EPA Fuel Economy Values [mpg] [1] | *City* | 29 | 30 | 19 |
| | *Highway* | 39 | 40 | 26 |
| | *Combined* | 33 | 34 | 22 |
| EPA $CO_2$ Values [g/km] [1] | | 193 | 186 | 288 |

[1] *EPA advertised fuel economy and $CO_2$ emissions values for new vehicles in the US (www.fueleconomy.gov)*

Table 3.2 lists the individual curb weights, gross vehicle weight ratings (GVWR), and actual test weights while performing the on-road PEMS testing. Actual test weights were calculated as the sum of manufacturer specified vehicle curb weights and physically acquired weights of the payload on a scale. The payload comprised the entire instrumentation and associated equipment, including pressurized gas bottles for the emissions analyzers, as well as the weight of a driver and passenger of 77kg each. The total payload for *Vehicle C* was approximately 200kg heavier than for *Vehicles A* and *B* due to additional instrumentation as will be explained in more detail in Section 3.3. Table 3.2 further allows for a comparison between the actual test weight of the three vehicles during PEMS testing and the respective equivalent test weight (ETW) as applied during emissions certification testing on the chassis dynamometer according to 40 CFR paragraph 86.129-00(f)(1).

The diesel fuel used during this study was commercially available ultra-low diesel fuel (ULSD) in California. Fuel for *Vehicles A* and *B* originated from the same batch and was purchased from a truck stop in Fontana, CA. A fuel analysis showed a sulfur content of 5ppm (via Microcoulometry, ASTM D3120, see Appendix 7.4 for more details). This same batch of diesel fuel was also used for chassis dynamometer testing of *Vehicles A* and *B* at CARB's El Monte, CA, testing facility. The fuel used during on-road testing of *Vehicle C* was purchased from the Quick Gas Valero fuel station in Ontario, CA. ULSD used for the California to Washington State trip with *Vehicle B* was purchased exclusively from Shell fuel stations along highway I-5. Specifically, the test vehicle was refueled six times during the entire trip, namely in Kettleman, CA, Redding, CA, Vancouver, WA, Olympia, WA, Medford, OR and finally Gustine, CA.

**Table 3.2: Test weights for vehicles**

| Vehicle | Curb Weight [kg] | GVWR [kg] | Payload [kg] | Actual Test Weight [kg] | Equiv. Test Weight [kg] |
|---|---|---|---|---|---|
| Vehicle A | 1550 | 2010 | 305 | 1855 | 1701 |
| Vehicle B | 1570 | 2110 | 314 | 1884 | 1701 |
| Vehicle C | 2370 | 3001 | 533 | 2903 | 2495 |

## 3.2 Vehicle Test Routes

On-road PEMS testing was grouped into two main route categories for this study, with one comprising a set of strictly defined test routes that were used for all test vehicles and the other containing predominantly highway driving solely defined by the departure and final destination, specifically, Los Angeles, CA as the starting point and Seattle, WA as the end point, that was only used in conjunction with *Vehicle B*. Section 3.2.1 will describe the pre-defined test routes of category one in more detail, whereas Section 3.2.2 will highlight the characteristics of the multi-state driving route between California and Washington State.

### 3.2.1 Pre-defined Test Routes

Five test routes were defined within the three primary population centers in California, namely, Los Angeles, San Diego, and San Francisco, aimed at reflecting a rich diversity of

topological characteristics, driving patterns, as well as ambient conditions, that are expected to be representative of typical vehicle operation within the given areas. The routes can be split into four categories, including i) *highway operation*, characterized by high speed driving during regular hours and frequent stop/go patterns during rush-hours, ii) *urban driving*, characterized by low vehicle speeds and frequent stop and go, iii) *rural driving*, medium vehicle speed operation with occasional stops in the suburbs of the selected metropolitan areas, and finally iv) *uphill/downhill driving*, characterized by steeper than usual road grades and medium to higher speed vehicle operation. Table 3.3 summarizes the characteristics of the five defined test routes whose driving patterns are described as follows:

1) Route 1: highway driving in Los Angeles
2) Route 2: urban driving in downtown Los Angeles
3) Route 3: rural and uphill/downhill driving in Los Angeles foothills
4) Route 4: urban driving in downtown San Diego
5) Route 5: urban driving in downtown San Francisco

**Table 3.3: Comparison of test route and driving characteristics**

| Route | Route 1[1)] | Route 2[2)] | Route 3 | Route 4[2)] | Route 5[2)] |
|---|---|---|---|---|---|
| Route distance [km] | 70.18 | 25.67 | 59.09 | 21.22 | 26.72 |
| Avg. vehicle speed [km/h] | 77.85 | 24.09 | 52.27 | 26.54 | 24.69 |
| Max. vehicle speed [km/h] | 112.65 | 92.57 | 112.65 | 109.87 | 112.65 |
| Avg. RPA [3)] [m/s$^2$] | 0.24 | 0.27 | 0.26 | 0.30 | 0.33 |
| Characteristic Power [m$^2$/s$^3$] | 2.57 | 2.24 | 3.93 | 2.60 | 2.97 |
| Min. elevation [m a.s.l. [4)]] | 46.0 | 42.1 | 300.1 | 1.1 | 1.0 |
| Max. elevation [m a.s.l] | 360.1 | 123.5 | 1319.7 | 101.4 | 190.9 |
| **Share [%] (*time based*)** | | | | | |
| - idling (≤2 km/h) | 7.0 | 23.8 | 13.5 | 26.8 | 27.9 |
| - low speed (>2≤50 km/h) | 20.5 | 64.2 | 23.9 | 57.0 | 58.9 |
| - medium speed (>50≤90 km/h) | 14.9 | 11.2 | 55.6 | 12.9 | 7.5 |
| - high speed (>90 km/h) | 57.7 | 0.8 | 7.0 | 3.3 | 5.6 |

[1)] *week-day, non-rush-hour driving conditions*
[2)] *typical week-day driving conditions*
[3)] *RPA - relative positive acceleration*
[4)] *a.s.l. - above sea level*

Route and driving characteristics provided in Table 3.4 are representative of typical week-day driving conditions for the urban routes (i.e. Routes 2, 4, and 5), and non-rush-hour, week-day driving conditions for highway driving (i.e. Route 1). Relative positive acceleration (RPA) is

a frequently used metric for analysis of route characteristics [1, 8] and will be described in more detail later in this section (see Eq. 4 and 5). '*Characteristic Power*' is a metric derived by Delgado *et al.* [9, 10] taking kinematic power and grade changes over the driving route into account, and is representative of the positive mechanical energy supplied per unit mass and unit time. Delgado *et al.* [9, 10] described '*Characteristic Power*' as outlined in Equation 3 having units [$m^2/s^3$ or W/kg] with '$T$' being the duration of the route, '$g$' the gravitational acceleration (i.e. 9.81m/$s^2$), '$v_i$' and '$h_i$' being the vehicle speed and altitude at each time step, respectively.

$$P_{ch} = \frac{1}{T} \cdot \sum_{i=2}^{N} \left[ \frac{1}{2} \cdot (v_i^2 - v_{i-1}^2) + g \cdot (h_i - h_{i-1}) \right]^+ \qquad \textbf{Eq. 3}$$

For comparison reason with the five defined test routes, Table 3.4 provides a summary containing the same metrics as shown in Table 3.3 for a set of chassis dynamometer vehicle certification test cycles that are currently used by the US EPA (FTP-75, US06) and the European Union (NEDC). It can be noticed that the US06 cycle shows similar maximum and average speed patterns as the highway (i.e. Route 1) and uphill/downhill (i.e. Route 3) routes, whereas the FTP-75 closer represents maximum and average speed characteristics of the urban test routes (i.e. Route 2, 4, and 5).

**Table 3.4: Comparison of characteristics of light-duty vehicle certification cycles**

| Cycle | FTP-75 | US06 | NEDC |
|---|---|---|---|
| Cycle duration [sec] | 1877 | 596 | 1180 |
| Cycle distance [km] | 17.77 | 12.89 | 10.93 |
| Avg. vehicle speed [km/h] | 34.08 | 77.84 | 33.35 |
| Max. vehicle speed [km/h] | 91.25 | 129.23 | 120.00 |
| Avg. RPA [3] [$m/s^2$] | 0.23 | 0.52 | 0.15 |
| Characteristic Power [$m^2/s^3$] | 1.65 | 4.55 | 1.04 |
| **Share [%] (*time based*)** | | | |
| - idling (≤2 km/h) | 19.6 | 7.2 | 24.8 |
| - low speed (>2≤50 km/h) | 59.3 | 18.8 | 53.9 |
| - medium speed (>50≤90 km/h) | 19.5 | 18.0 | 14.2 |
| - high speed (>90 km/h) | 1.6 | 56.0 | 7.0 |

The topographic map of Route 1 is depicted in Figure 3.1. Route 1 is ~70 kilometers in distance and comprises approximately 95% highway driving between the convention center in Ontario and the main campus of the University of Southern California (USC) South of

downtown LA, following interstate I-10 East and highway 110 South till exit 20B (W. Exposition Blvd.). Average vehicle speed during day-time and outside morning or evening rush-hours was ~ 77.8 km/h.

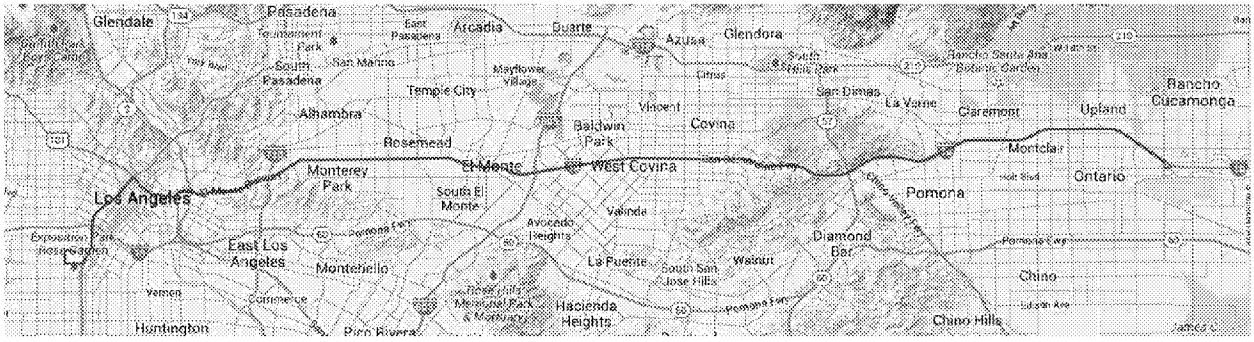


**Figure 3.1: Topographic map of Route 1, highway driving between Ontario and downtown LA**


**Figure 3.2: Topographic map of Route 2, urban driving downtown Los Angeles**

Figure 3.2 shows the topographic map of Route 2, representative of urban driving downtown Los Angeles. This route essentially represents the "*Los Angeles Route Four*" (i.e. LA4) which was ultimately used in developing the original FTP vehicle certification cycle [11], with some minor modifications at locations where the traffic pattern or roads have changed since the FTP's development. The route is ~25.6 km long, and started and terminated at USC's main campus on

Jefferson Blvd. From USC the route followed westwards on W. Exposition Blvd., then North on S. Western Ave. till W. Olympic Blvd. From there it turned eastwards and followed W. Olympic Blvd. till S. San Pedro Street, then North on S. San Pedro St., and again West on W. Temple Street before merging onto highway 110 South leading back to the USC campus (Exit 20B, W. Exposition Blvd.). Even though the route contains ~5.3 km or 20% of highway driving on Hwy 110-S, the average vehicle speed is only marginally affected due to highly dense traffic on this portion of Hwy 110-S with many roads intersecting or merging.

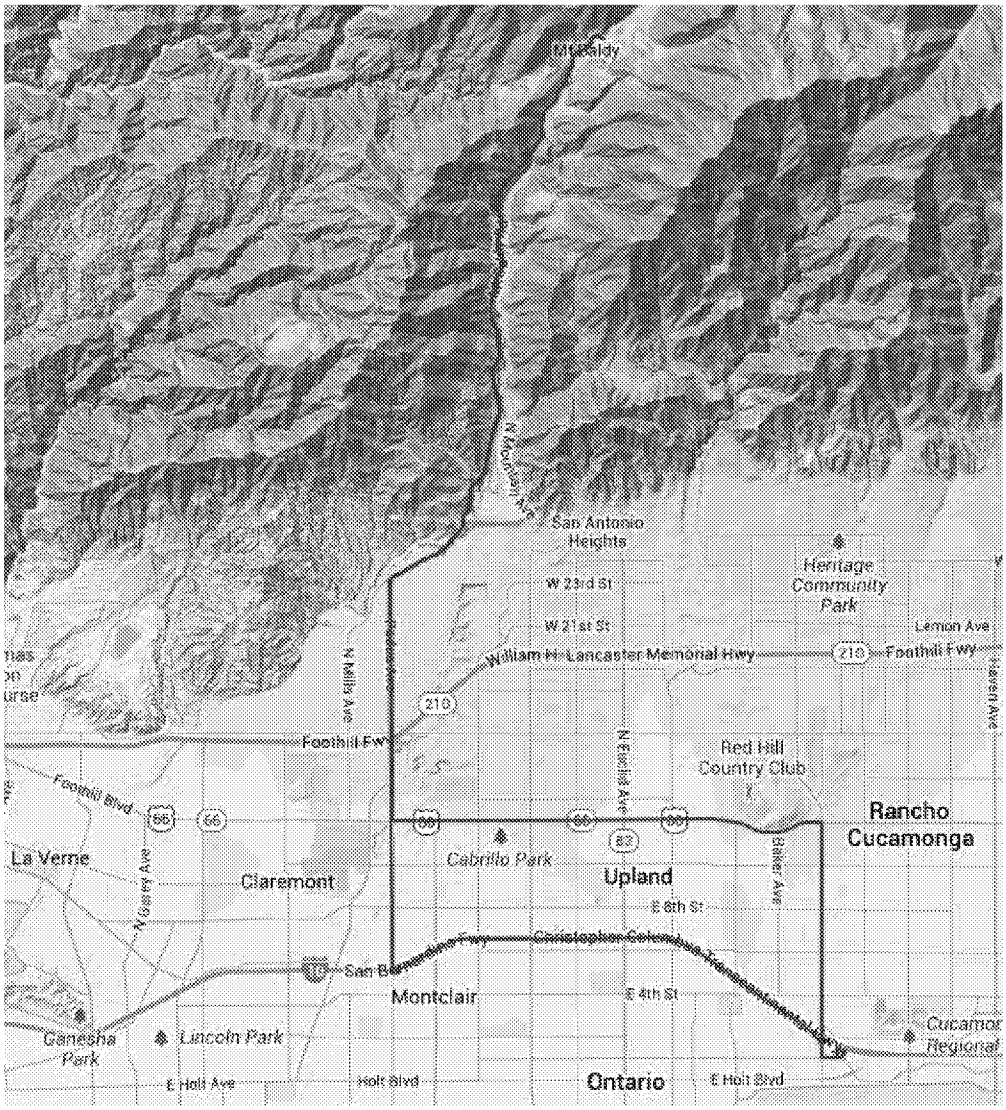


**Figure 3.3: Topographic map of Route 3, rural-up/downhill driving between Ontario and Mt. Baldy**

The topographic map of Route 3, representative of rural and uphill/downhill driving is shown in Figure 3.3. The route is ~59 kilometers in distance and experiences an elevation change

of approximately 1000 meters between the lowest and highest points of the route. The route starts and terminates at the convention center in Ontario, CA and follows Foothill Blvd. eastwards till the intersection with Mt. Baldy Rd. From there the route climbs up a windy road to Mt. Baldy and back. On the return the route follows for ~9km on interstate I-10 East, which represents 15% of the total route's distance. The average vehicle speed for Route 3 is 52.3 km/h.

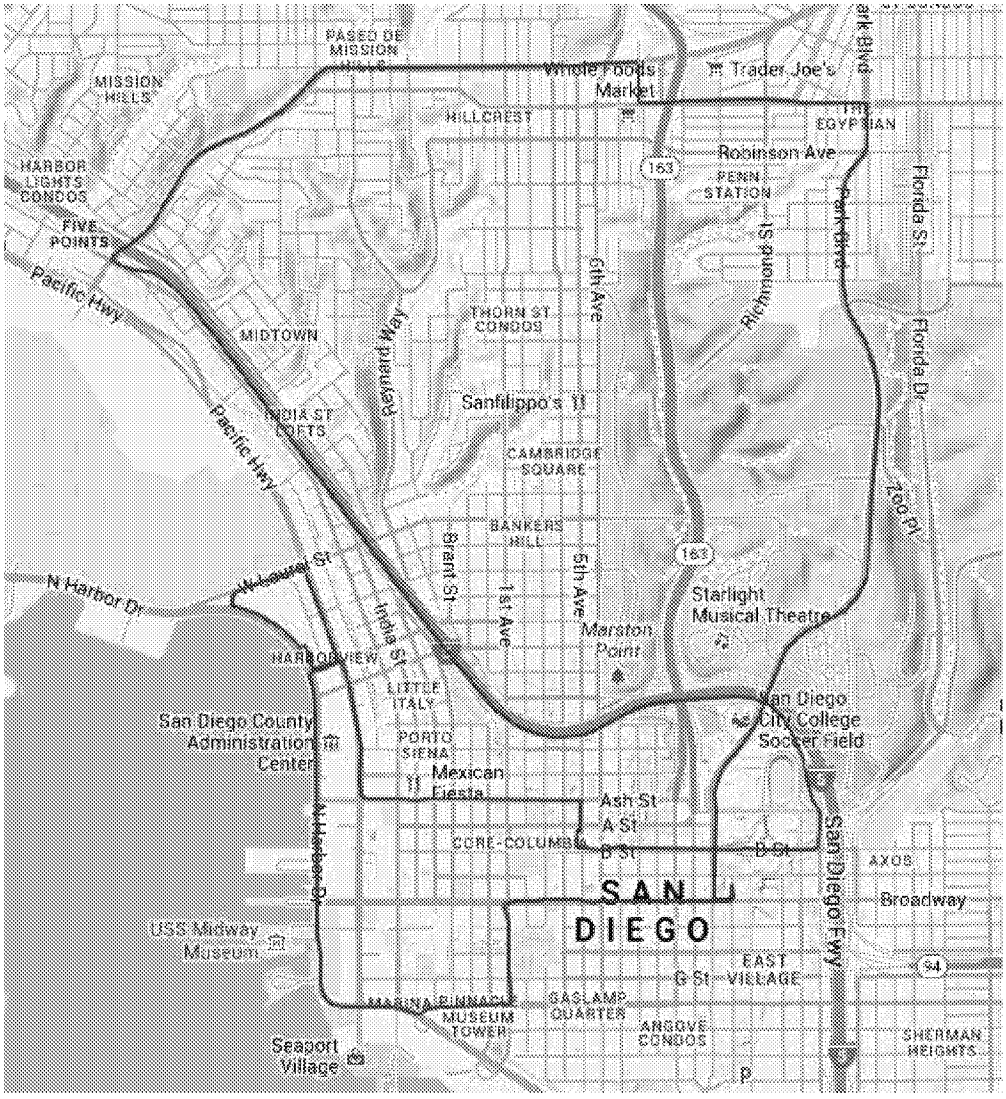


**Figure 3.4: Topographic map of Route 4, urban driving downtown San Diego**

Figure 3.4 depicts the topographic map of the urban driving route, Route 4, in downtown San Diego. Route 4 is slightly shorter when compared to Route 2, approximately 21 km in length; however, it experiences more elevation changes than the downtown LA route. The route starts and terminates at the harbor at sea level (N. Harbor Drive). It first follows along the harbor then leads through downtown before climbing up on Park Blvd. to the Bridgeview and Hillcrest

neighborhood. From there the route follows W. Washington St. to San Diego airport where it merges onto interstate I-5 South till Exit B St., and then going back through downtown to the harbor again. Route 4 comprises roughly 20% or 4.2 km of highway driving on interstate I-5 South. However, similar to Route 2, this portion of I-5 is heavily congested throughout the day, thus not significantly affecting the average vehicle speed of Route 4 which was measured as ~26.5 km/h.


**Figure 3.5: Topographic map of Route 5, urban driving downtown San Francisco**

Finally, the topographic map of Route 5 is shown in Figure 3.5. Route 5 is located in and around downtown San Francisco and is specifically characterized by faster speed changes of the

traffic flow and steep inclines and declines of the road when compared to the two other urban routes in LA and San Diego. In terms of average vehicle speeds Route 5 is similar to Routes 2 and 4; however, it exhibited highest average relative positive acceleration of all three urban routes. The route is ~26.7 km in distance and starts as well as terminates in the Marina District on Marina Blvd. From there the route goes southwards to Eureka Valley area and climbs over Diamond Heights neighborhood before merging onto highway 280 North and descending back to downtown and the Financial District. Approximately 28% of the entire route or 7.4 km are driven on highway 280.

Figure 3.6 presents a comparison of vehicle speed distributions for all five test routes and three regulatory vehicle certification cycles over four distinct vehicle speed bins defined as i) *idle*, speeds at or below 2 km/h, ii) *low speed*, speeds higher than 2 km/h and lower or at 50 km/h, iii) *medium speed*, speeds higher than 50 km/h and lower or at 90 km/h, and finally iv) *high speed*, speeds higher than 90 km/h. Vehicle speed bins ii, iii and iv can alternatively be described as urban, rural, and highway operation, respectively, following the notation used by Weiss *et al.* [1]. It can be noticed from Figure 3.6 that highway driving (i.e. Route 1, week-day non-rush-hour) is similar to the US06 chassis dynamometer schedule as both show the same vehicle speed distribution pattern. A similar conclusion can be drawn between the three urban routes and two certification cycles FTP-75 and NEDC. Route 3, the rural and up/downhill route on the other hand is not well represented by any of the three certification cycles as they all lack significant medium speed operation. At vehicle speeds below 50 km/h Route 3 shows similar speed distributions as the US06 cycle. One observation from Figure 3.6 is that the introduction of the US06 test cycle to the US light-duty vehicle certification process has led to a better representation of high-speed vehicle operation as compared to the FTP-75.

It has to be noted that data presented in Figure 3.6 are representative of week-day, non-rush-hour driving conditions for highway driving (i.e. Route 1) and typical week-day traffic conditions for the urban routes (i.e. Route 2, 4, and 5). Changing traffic densities, for example during morning or evening rush-hours as opposed to regular day-time traffic conditions can lead to significant alterations in driving characteristics for a given test route.

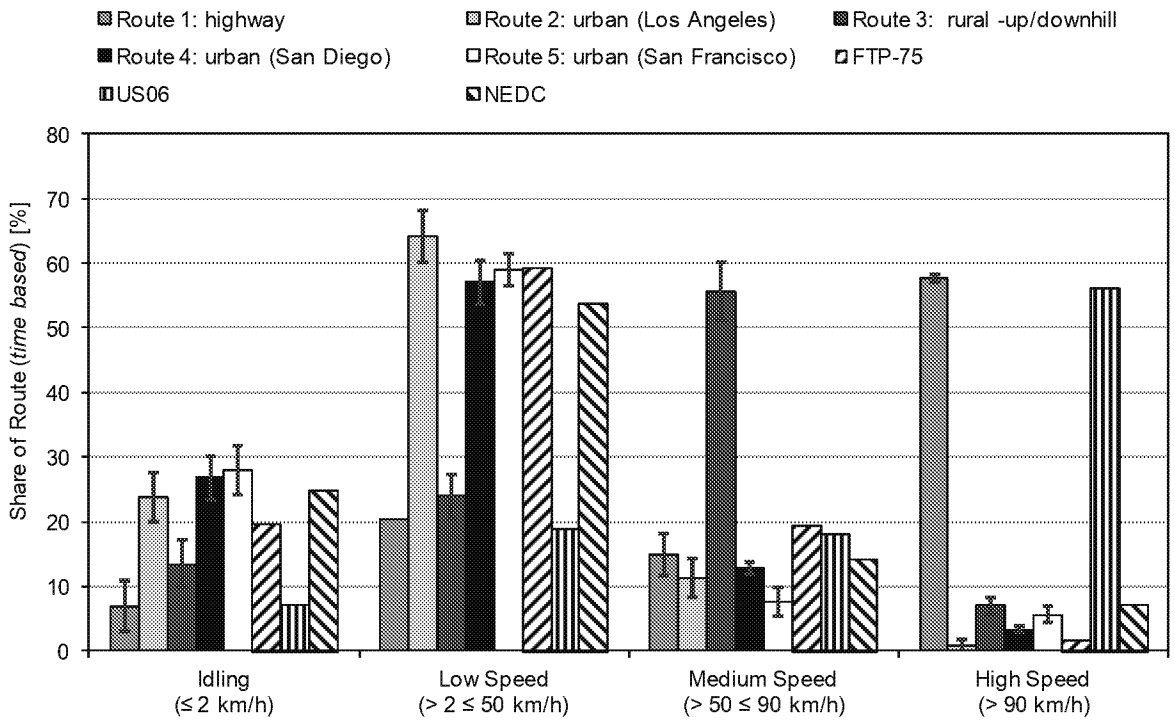


**Figure 3.6: Comparison of vehicle speed distribution (*time based*) over the test routes and certification cycles, red bars represent ±1σ**

**Table 3.5: Comparison of test route and driving characteristics with low and high traffic densities**

| Route | Route 1 low traffic [1] | Route 1 high traffic [2] | Diff [%] | Route 2 low traffic [3] | Route 2 high traffic [4] | Diff [%] |
|---|---|---|---|---|---|---|
| Route distance [km] | 70.18 | 71.11 | *-1.3* [5] | 25.67 | 25.67 | *0.0* |
| Avg. vehicle speed [km/h] | 77.85 | 42.41 | *45.5* | 37.70 | 24.09 | *36.1* |
| Max. vehicle speed [km/h] | 112.65 | 112.65 | *0.0* | 110.27 | 92.57 | *16.1* |
| Avg. RPA [3] [m/s$^2$] | 0.24 | 0.21 | *11.3* | 0.31 | 0.27 | *11.8* |
| Characteristic Power [m$^2$/s$^3$] | 2.57 | 2.50 | *2.7* | 3.27 | 2.24 | *31.4* |
| **Share [%] (*time based*)** | | | | | | |
| - idling (≤2 km/h) | 7.0 | 7.8 | *-11.9* | 15.8 | 23.8 | *-50.3* |
| - low speed (>2≤50 km/h) | 20.5 | 59.0 | *-188.1* | 48.7 | 64.2 | *-31.9* |
| - medium speed (>50≤90 km/h) | 14.9 | 19.7 | *-32.3* | 29.9 | 11.2 | *62.6* |
| - high speed (>90 km/h) | 57.7 | 13.5 | *76.6* | 5.6 | 0.8 | *85.8* |

[1] *week-day, non-rush-hour driving conditions*
[2] *week-day, evening-rush-hour driving conditions*
[3] *typical week-day driving conditions*
[4] *weekend (holiday) driving conditions*
[5] *low traffic route: inbound (Ontario to LA), high traffic route: outbound (LA to Ontario)*

Table 3.5 compares the route characteristics of Route 1 and 2 between low and high traffic densities. In case of Route 2, urban driving downtown LA, the traffic densities during weekdays were usually high with an average vehicle speed of ~24 km/h and frequent stop/go patterns. This

can be underlined by the fact that both *Vehicles A* and *B* were tested on two random and regular working weekdays in the afternoon between 13:00 and 16:00 and both experienced the same route characteristics. On the other hand, the low traffic characteristics for Route 2, shown in Table 3.5, were measured during testing of *Vehicle C* which happened to fall on Memorial Day Monday (May 27, 2013) in the afternoon between 14:00 and 18:00. Due to the holiday, downtown traffic was greatly reduced and average vehicle speeds rose by 36% from ~24 to 37.7 km/h. Overall, the share of medium speeds increased by 62% while the idling portion dropped significantly by 50%. Another example of the strong influence of traffic densities onto route characteristics is given for Route 1, the highway operation. Table 3.5 shows a comparison for *Vehicle A* between low traffic conditions while driving from Ontario to downtown LA during regular daytime traffic (around 11:30), and high traffic densities going from downtown LA towards Ontario (same route, opposite direction) during evening rush-hours (around 16:30) when a large number of people were leaving their offices/workplaces and driving back to their suburban homes. As a result, the average speed dropped by 46% from 77.9 to 42.4 km/h, while the time to cover the same distance nearly doubled from 54min to 1h 41min. Figure 3.7 shows how the speed distributions changed and the low speed bin's share increased from 20% to nearly 60% while at the same time the share of speeds above 90 km/h dropped by 77% from 58% to merely 14% of the entire route.

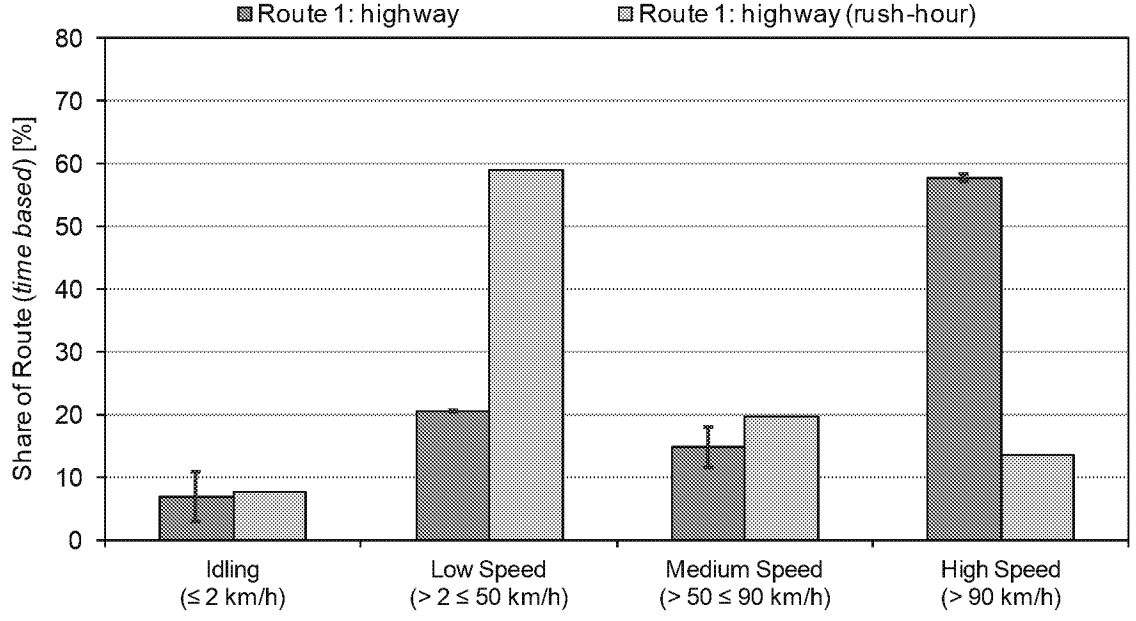


**Figure 3.7: Comparison of vehicle speed distribution (*time based*) over Route 1 during low traffic and rush-hour, red bars represent ±1σ**

Figure 3.8 summarizes the cumulative frequencies of the vehicle speeds for all three test vehicles and Routes 1 through 4 in comparison to three chassis dynamometer certification cycles. It has to be noted that for comparison purposes, vehicle speed data presented herein for chassis dynamometer cycles is based on vehicle speed set-point rather than actually measured data. As already concluded from Figure 3.6 and Table 3.3, the top left graph in Figure 3.8 confirms again the representativeness of the US06 cycle of highway driving during non-rush-hour vehicle operation. In stark contrast are cumulative frequency pattern for vehicle operation during rush-hours (i.e. high traffic densities) as shown by one *Vehicle A* and one *Vehicle B* test run. Highway speed patterns during rush-hours seem to be close to FTP-75 or NEDC vehicle operation characteristics.

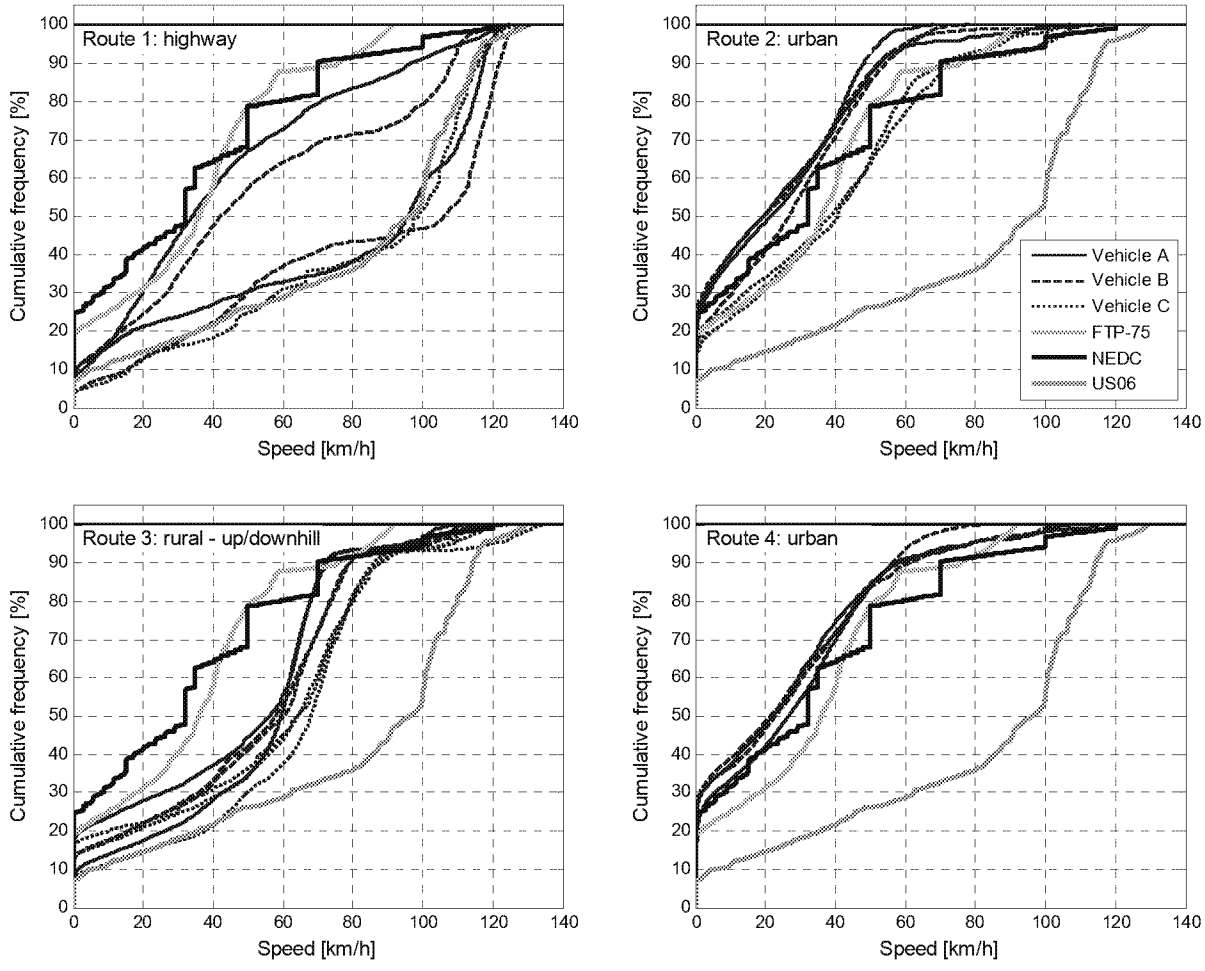


**Figure 3.8: Vehicle speed distributions of test routes 1 through 4 in comparison to certification test cycles (FTP-75, US06, and NEDC, based on speed set-point data)**

Urban driving in downtown LA and San Diego are shown to exhibit cumulative frequencies of vehicle speeds close to the frequencies of FTP-75 and NEDC certification cycles, although mostly slightly on the slower side compared to the certification cycles (top right and bottom right graphs). Route 2 driving for Vehicle C shows a noticeable difference when compared to both *Vehicles A* and *B* (top right graph) as previously discussed. The bottom left graph in Figure 3.8 shows rural and uphill/downhill driving, emphasizing again its significant contribution to the medium speed range, which is poorly represented by any of the three light-duty certification cycles depicted herein.

The altitude profiles for all five test routes are compared in Figure 3.9 in terms of elevation above sea level (i.e. meter a.s.l.). The majority of urban routes varied between sea level and 100 meters, with the San Francisco route (Route 5) being the only one exhibiting elevation changes more frequently with a range of ~200 meters from lowest to highest point.

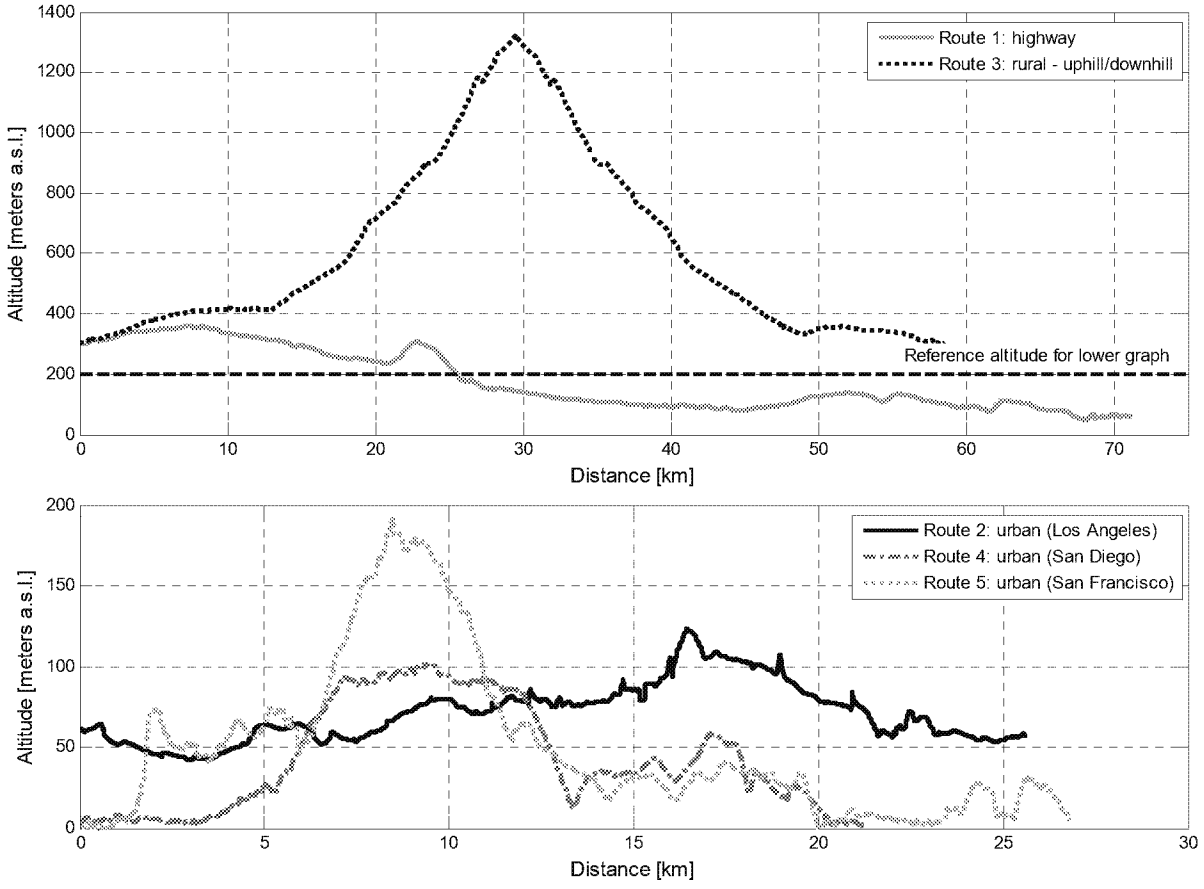


**Figure 3.9: Altitude profiles of test routes given in meters above sea level (a.s.l.)**

The uphill/downhill driving route experienced an elevation change of approximately 1000 meters, starting at about 300 meters a.s.l. with a turning point at 1300 meters a.s.l. The road grade was on the order of 5.5 to 6% over a distance of ~16 km (between distance marker 14 and 30km). The same road grade applied for the downhill portion of the route, as the same road was chosen to drive back from Mt. Baldy. The primary measure of altitude during the course of this study was the GPS signal. However, due to sporadically deteriorating GPS reception, caused by a multitude of factors, including but not limited to heavy cloud overcast, road tunnels and underpasses (e.g. bridges), as well as high buildings in downtown areas, an alternative backup method to calculate altitude was employed by means of measuring changes in barometric pressure as a function of altitude using a high resolution pressure transducer. The latter method has proven, during previous studies at WVU [9, 12], to be more accurate for the purpose of calculating road grade changes, however, it is plagued by the requirement to consider local weather conditions as changes in environmental conditions will lead to changing barometric pressures, hence, offset the altitude calculation.

Equation 3 shows a simplified version of the formula used to calculate altitude '$H$' as a function of reference temperature '$T_0$' and pressure '$p_0$' at ground level as well as the actually measured barometric pressure '$p_{baro}$'. With '$L$' being the temperature lapse rate, 0.0065K/m, and $g$, $M$, $R$ being the gravitational acceleration, molar mass of dry air and universal gas constant, respectively [12]. Equation 3 is derived from the International Standard Atmosphere (ISA) model which has been formulated by the International Civil Aviation Organization (ICAO) and is based on assuming ideal gas, gravity independence of altitude, hydrostatic equilibrium, and a constant lapse rate [9].

$$H = f(T_0, p_0, p_{baro}) = \left(\frac{T_0}{L}\right) \cdot \left[1 - \left(\frac{p_{baro}}{p_0}\right)^{\left[\frac{R \cdot L}{g \cdot M_{air}}\right]}\right] \qquad \textbf{Eq. 3}$$

Figure 3.10 shows a sample of the individual vehicle speed profiles for all five test routes as a function of driving time during week-day, non-rush-hour conditions for highway driving (i.e. Route 1) and typical week-day traffic conditions for the urban routes (i.e. Route 2, 4, and 5).

Figure 3.11 depicts ambient conditions, including temperature, barometric pressure, and relative humidity experienced during the five test routes for *Vehicles A* through *C*. The variation

intervals (red bars) represent minimum and maximum values encountered over the test route. An increase in the observed range of barometric pressure (i.e. minimum to maximum value) is indicative of larger elevation changes experienced over a given test route (see Figure 3.9 for altitude profiles).

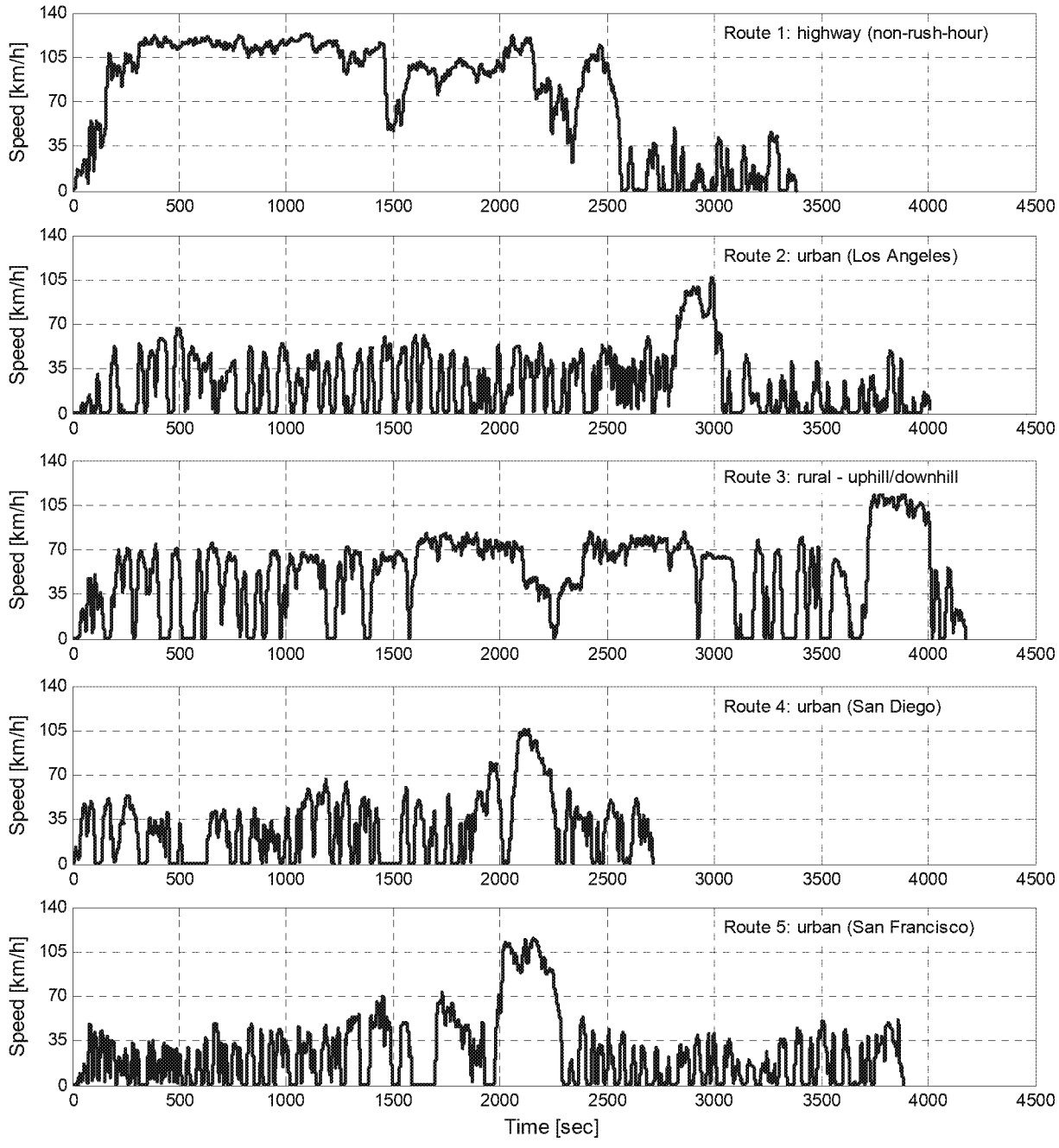


**Figure 3.10: Characteristic vehicle speed vs. time for five test routes during typical week-day non-rush-hour traffic densities for highway and urban driving**

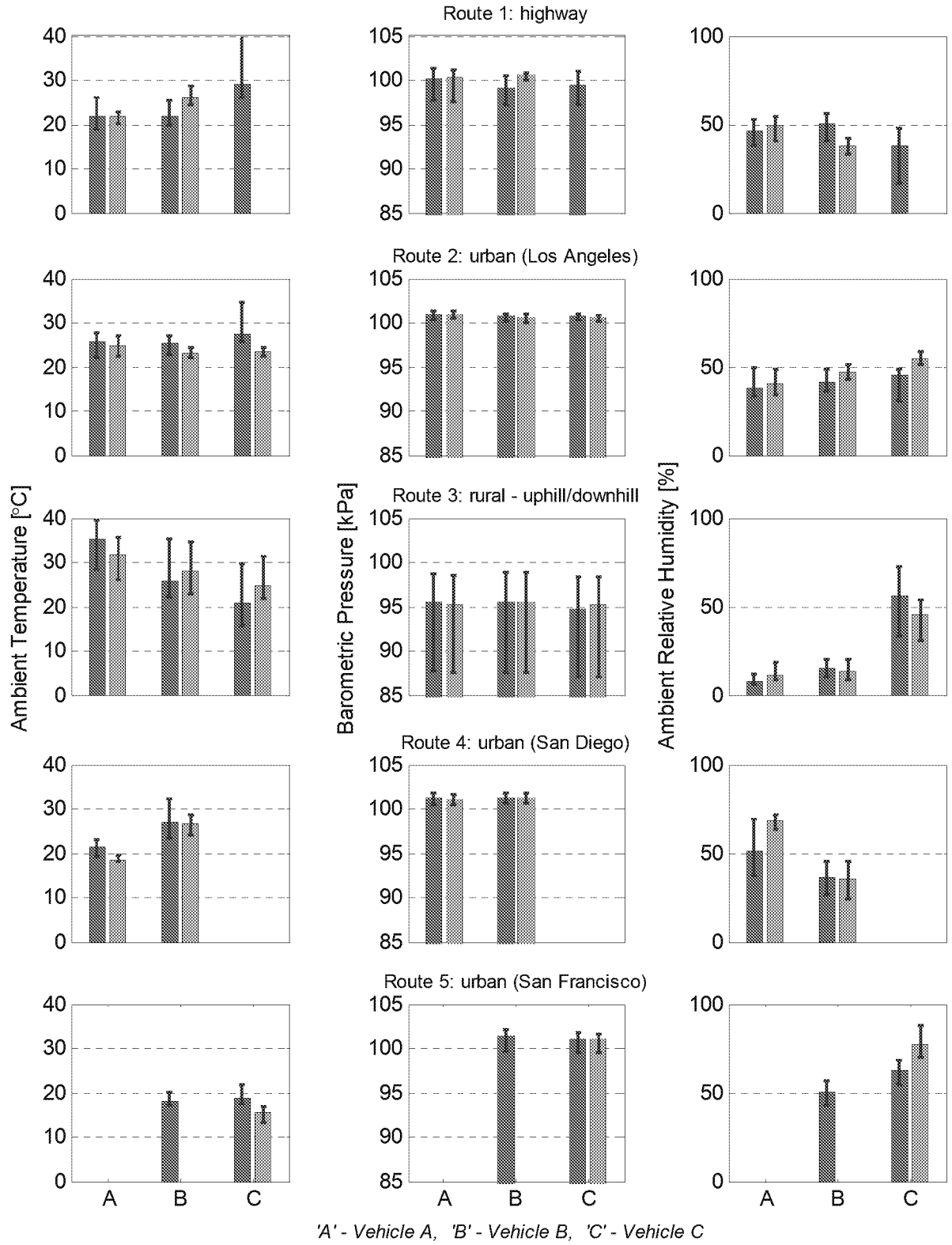


**Figure 3.11: Average ambient conditions (temperature, barometric pressure, and relative humidity) experienced over five test routes for all three vehicles. Note: variation intervals (red bars) refer to minimum and maximum values experienced over the test route**

Relative positive acceleration (RPA) is a frequently used metric [1, 8] for the analysis of driving patterns and as input parameter to aid in developing chassis dynamometer test cycles representative of real-world driving. The RPA is calculated as the integral of the product of vehicle speed and positive acceleration for each instance in time, over a given '*micro-trip*' of the test route under investigation as shown by Equation 4. For this study a '*micro-trip*' was defined following the same convention as proposed by Weiss *et al.* [1] as any portion of the test route, where the vehicle speed is equal or larger than 2 km/h for a duration of at least 5 seconds or more. Instantaneous vehicle acceleration was calculated according to Equation 5 by means of differentiating vehicle speed data collected via GPS, and subsequently filtered with negative values being forced to zero.

$$RPA = \frac{\int_0^{t_j}(v_i \cdot a_i)dt}{x_j} \qquad \textbf{Eq. 4}$$

where: $t_j$ duration of micro-trip $j$

$x_j$ distance of micro-trip $j$

$v_i$ speed during each time increment $i$

$a_i$ instantaneous positive acceleration during each time increment $i$ contained in the micro-trip $j$

$$a_i = \begin{cases} \frac{(v_2 - v_1)}{(t_2 - t_1)} & if\ i = 1 \\ \frac{(v_{i+1} - v_{i-1})}{(t_{i+1} - t_{i-1})} & if\ 2 \le i \le n-1 \\ \frac{(v_n - v_{n-1})}{(t_n - t_{n-1})} & if\ i = n \end{cases} \qquad \textbf{Eq. 5}$$

Figure 3.12 and Figure 3.13 depict the relative positive accelerations for routes 1 through 4, and 5, respectively, in comparison to RPAs for three chassis dynamometer vehicle certification test cycles (note: using vehicle speed set-point data for calculations). A distinct pattern can be recognized between the highway, rural, and urban test routes. The urban routes show a predominant cluster in the range of 15 to 40 km/h with RPA values between 0.2 and 0.6 m/s$^2$, and up to 0.8 m/s$^2$ for the San Francisco route. The latter was characterized by more pronounced grade changes (i.e. increased '*hilliness*') and '*aggressiveness*' of the driving pattern (i.e. increased stop-go). Furthermore, RPA values for the urban routes show similarity to RPA values calculated for the FTP-75 certification cycle. Average RPA values are shown in Table 3.3.

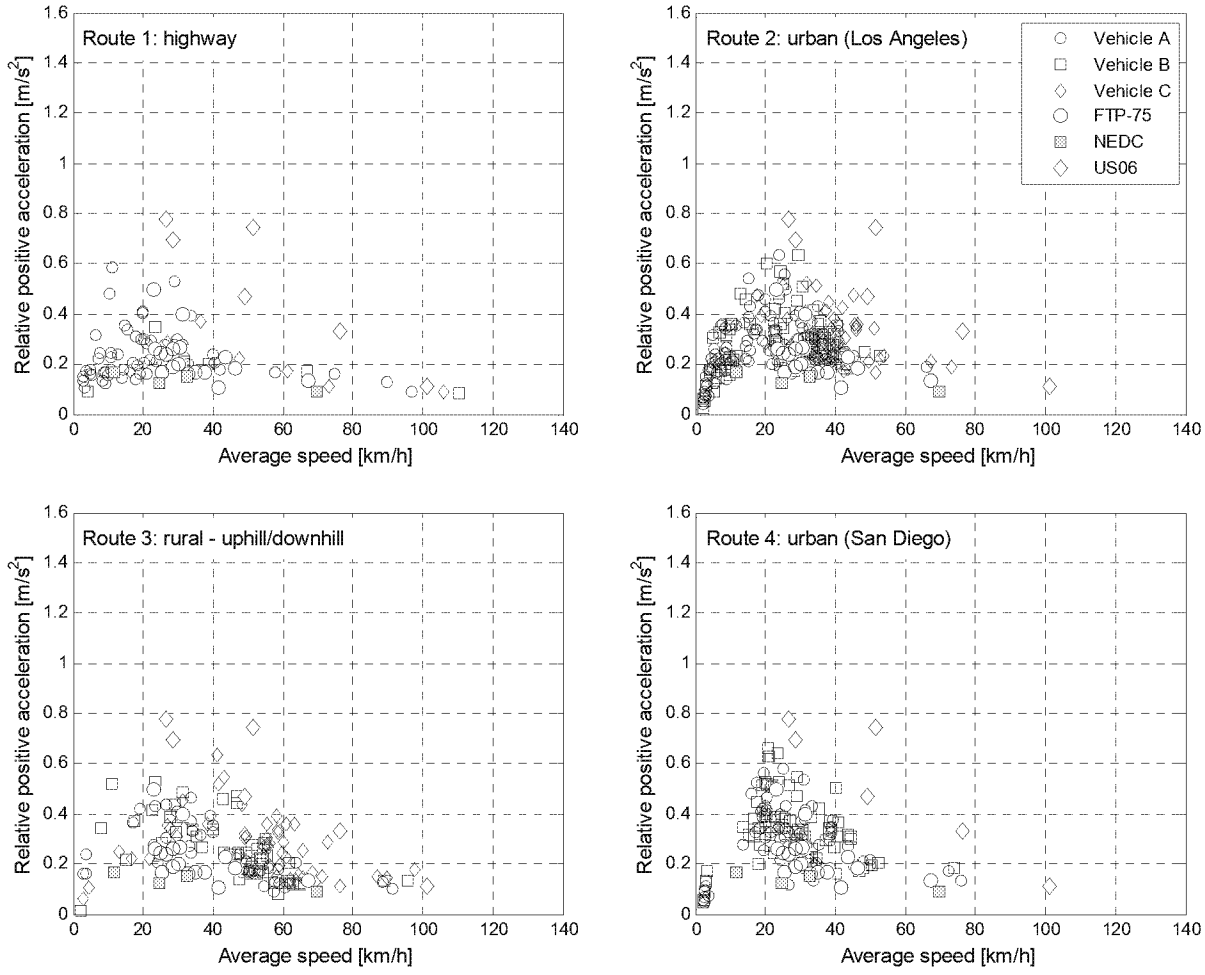


**Figure 3.12: Relative positive acceleration of sub-trips composing test routes 1 through 4 in comparison to certification cycles (FTP-75, US06, and NEDC)**

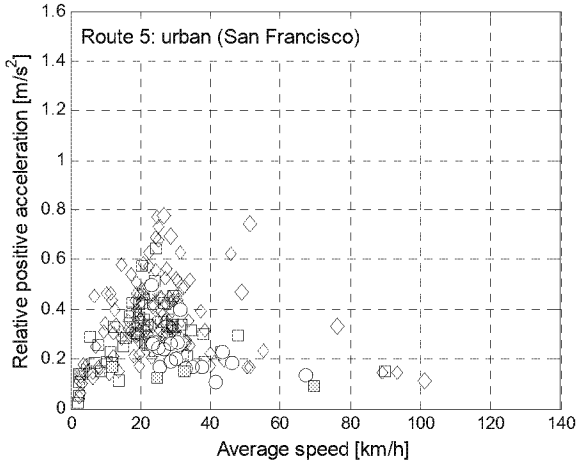


**Figure 3.13: Relative positive acceleration of sub-trips composing test Route 5 in comparison to certification cycles (FTP-75, US06, and NEDC)**

Interestingly, the relative positive acceleration values for highway driving, Route 1 (top left graph), were not well represented by the US06 certification cycle even though vehicle speed distributions were in good agreement with each other as previously shown in Figure 3.6 and Figure 3.8. There are only a few matching RPA values at the upper end of the vehicle speed range (around 100 km/h). However, it has to be noted that the US06 certification cycle was not developed with the intention to be a representative test cycle but rather to address shortcomings of the FTP-75 cycle in representing high-speed driving and increased acceleration behavior (i.e. aggressive driving) [13, 14], thereby accounting for '*off-cycle*' emissions not reflected in the standard FTP-75 certification cycle [14]. The US06 cycle was adopted by the US-EPA in 1997 as part of the '*Supplemental Federal Test Procedure*' (SFTP) (see Section 2) [13]. The RPA values for the European certification cycle NEDC are well below the majority of RPA values calculated for all five test routes, whereas the US certification cycles (i.e. FTP-75, US06) appear to be more representative of real-world driving for a wide range of vehicle operating conditions for this test program.

### 3.2.2 Cross-Multi-State Driving Route

*Vehicle B* was driven over a total distance of 3968 miles between Los Angeles, CA and Seattle, WA in order to characterize after-treatment performance and emissions rates over an extended time of in-use operation. The route, hereinafter referred to as the '*cross-multi-state driving route*' comprises out/inbound Los Angeles to Seattle driving as well as urban/suburban vehicle operation in Seattle, WA and Sacramento, CA, and is dominated by a majority of 83.5% highway driving at speeds above 90 km/h. The average vehicle speed over the entire route was ~100 km/h with maximum speeds of up to ~140 km/h. Table 3.6 lists additional characteristics for the cross-multi-state driving route including highway and urban/suburban vehicle operation (i.e. highway, Route 6, and Route 7).

Figure 3.14 shows the topographic maps for the LA to Seattle route on the left following interstate I-5 North as well as the Seattle to LA route on the right. The return route from Seattle to LA included additional urban driving in Seattle, Sacramento and San Francisco (i.e. Route 5). Figure 3.15 and Figure 3.16 depict the topographical maps for the urban/suburban route in Seattle (referred to as '*Route 6*') and urban route in Sacramento (referred to as '*Route 7*'), respectively. Route 6 was driven in the morning, thus included rush-hour traffic from the

surrounding residential suburban towns into downtown Seattle. Furthermore, Seattle is located in a hilly costal area, whereas Sacramento lies in the relatively flat San Joaquin valley.

**Table 3.6: Overall cross-multi-state route and driving characteristics**

| Parameters | Value |
|---|---|
| Route duration [hr] | 39.31 |
| Route distance [km] | 3968.10 |
| Avg. vehicle speed [km/h] | 100.95 |
| Max. vehicle speed [km/h] | 120.00 |
| Avg. RPA [1)] [$m/s^2$] | 0.23 |
| Characteristic Power [$m^2/s^3$] | 2.63 |
| Min. elevation [m a.s.l. [2)]] | 1.0 |
| Max. elevation [m a.s.l.] | 1320.1 |
| **Share [%] (*time based*)** | |
| - idling (≤2 km/h) | 3.4 |
| - low speed (>2≤50 km/h) | 8.1 |
| - medium speed (>50≤90 km/h) | 5.0 |
| - high speed (>90 km/h) | 83.5 |

[1)] *RPA - relative positive acceleration*
[2)] *a.s.l. - above sea level*

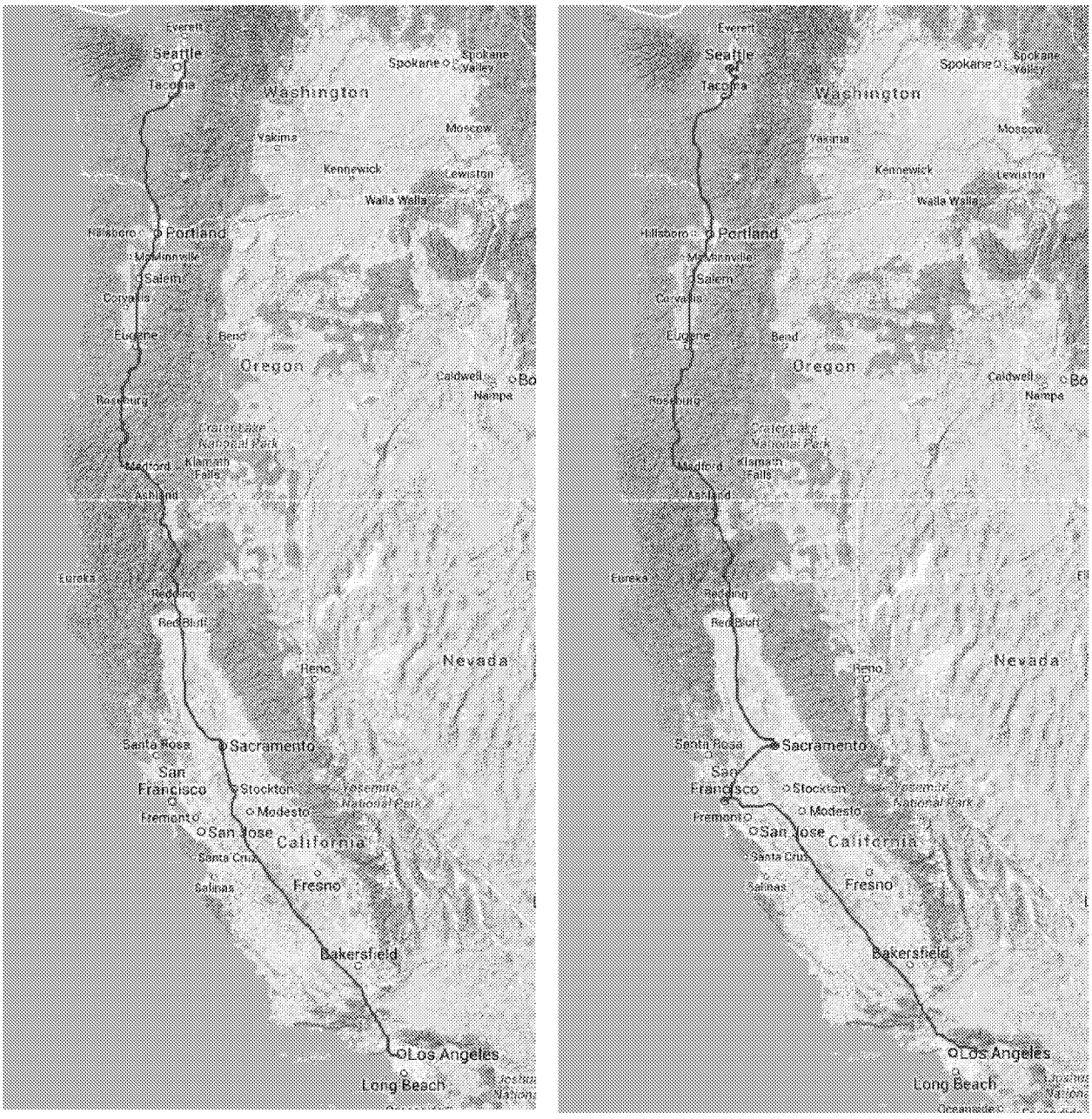


**Figure 3.14: Topographic map of *left)* Los Angeles to Seattle, and *right)* Seattle to Los Angeles cross-multi-state driving route**

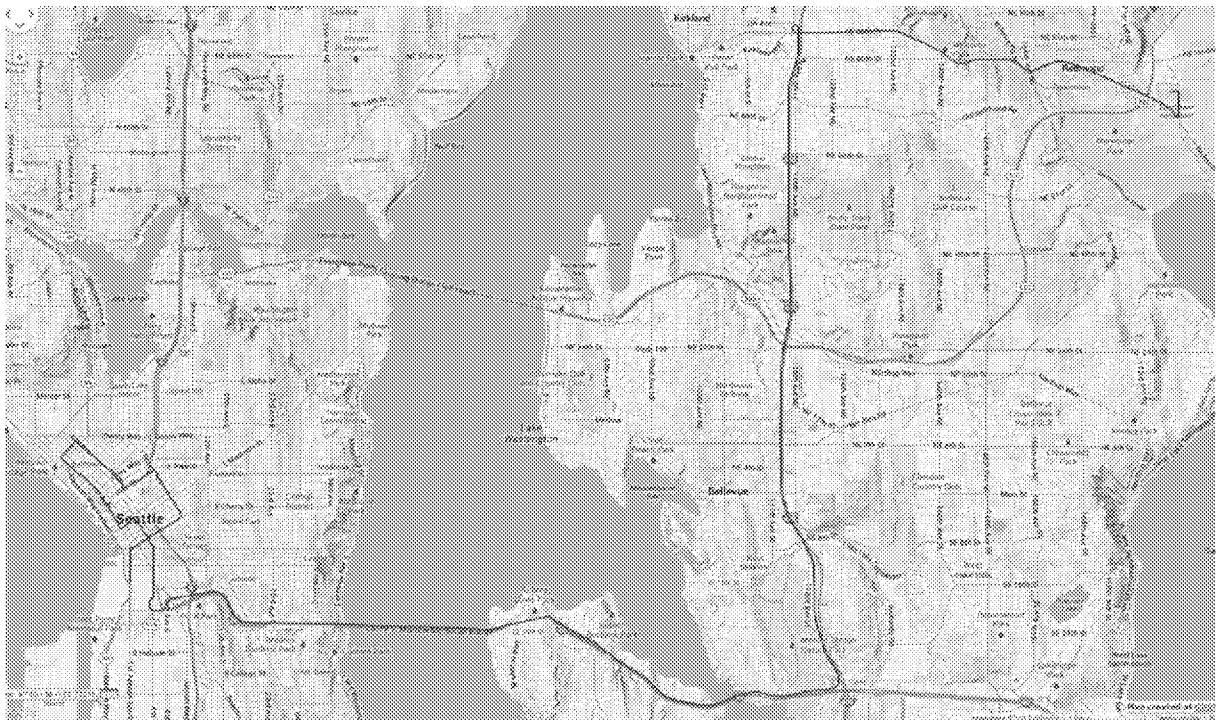


**Figure 3.15: Topographic map of Route 6, urban and suburban driving around Seattle, WA**

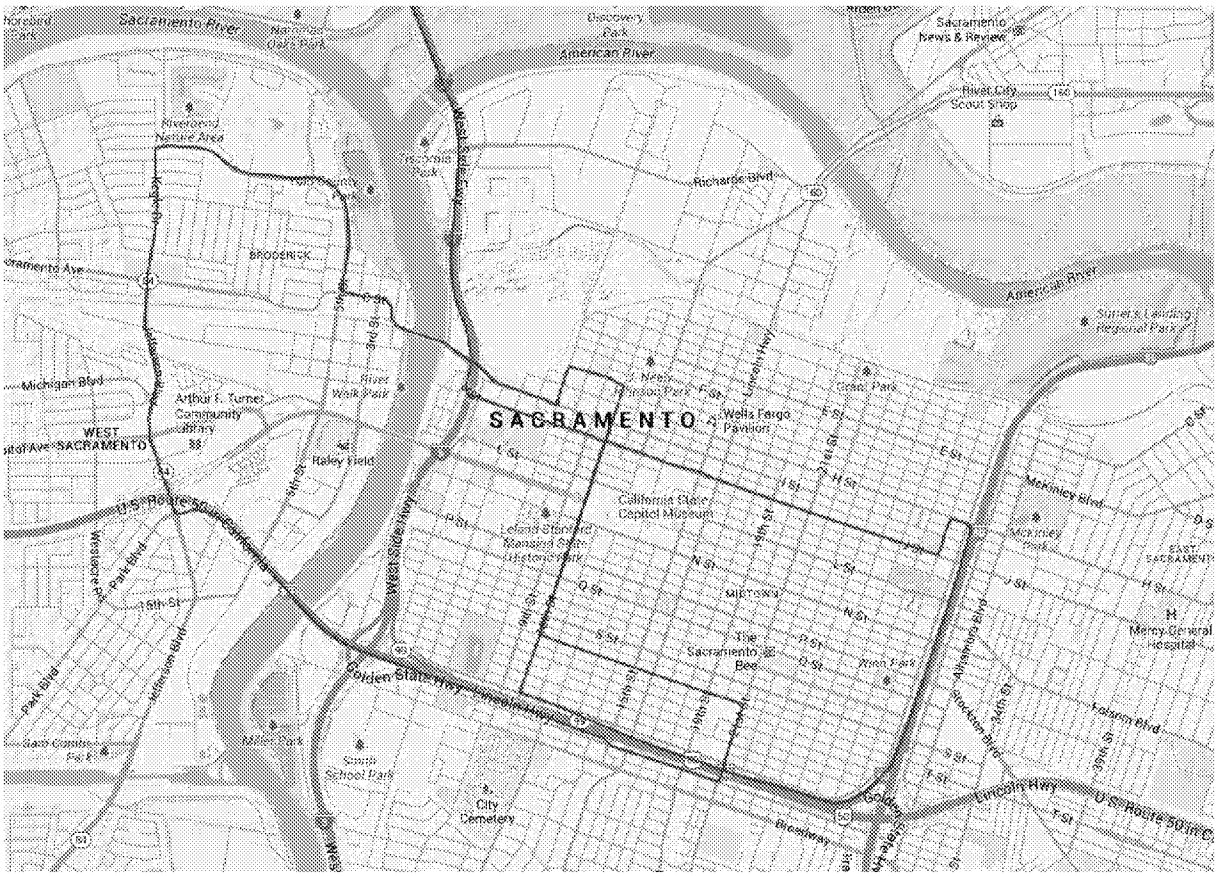


**Figure 3.16: Topographic map of Route 7, urban driving downtown Sacramento, CA**

Figure 3.17 b) depicts the vehicle speed distribution for the entire cross-multi state driving route against standard chassis dynamometer test cycles. It can be noticed that even though 85% of the vehicle speeds are in excess of 90 km/h, and thereby significantly exceeding the high-speed (>90 km/h) contribution in the US06 cycle (i.e. 56%), the shape of the two vehicle speed distributions are comparable. The relative positive acceleration for the cross-multi state driving route is plotted in Figure 3.17 a), with urban/suburban driving (i.e. Seattle and Sacramento) contributing to the high RPA values at lower speeds (towards lower left corner), and highway driving predominantly to the low RPA values at high vehicle speeds (towards right corner). Furthermore, comparing RPA values in Figure 3.17 a) with values presented in Figure 3.12 and Figure 3.13 it is possible to identify the individual contributions of urban/suburban as well as high speed highway driving.

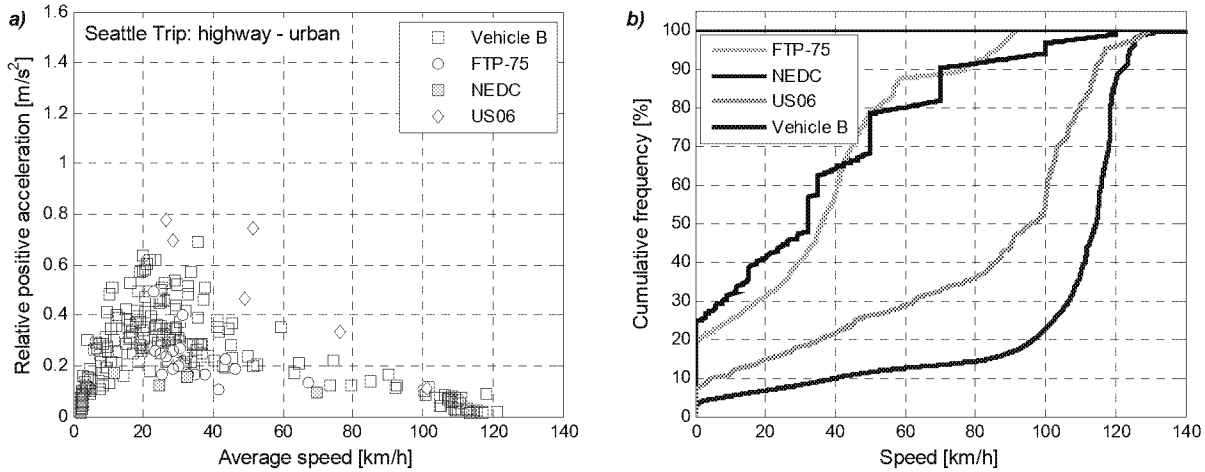


**Figure 3.17: *a)* Relative positive acceleration of sub-trips composing cross-multi-state route in comparison to certification cycles (FTP-75, US06, and NEDC); *b)* vehicle speed distributions of cross-multi-state route in comparison to certification test cycles**

Figure 3.18 a) and Figure 3.18 b) shows the vehicle speed and altitude, respectively, for the entire cross-multi state driving route as a function of distance traveled. From the altitude graph (see Figure 3.18 b)), one can recognize the symmetry of the driving route predominantly following Interstate I-5 North and South. The reduced vehicle speeds at around 1800km and 3100km into the route mark the urban/suburban driving portions in Seattle, WA and Sacramento, CA, respectively. Furthermore, from the vehicle speed trace one can distinguish portions of the route where the vehicle was driven in cruise control mode (i.e. constant vehicle speeds), from parts where vehicle speed was manually governed by the pedal position of the driver.

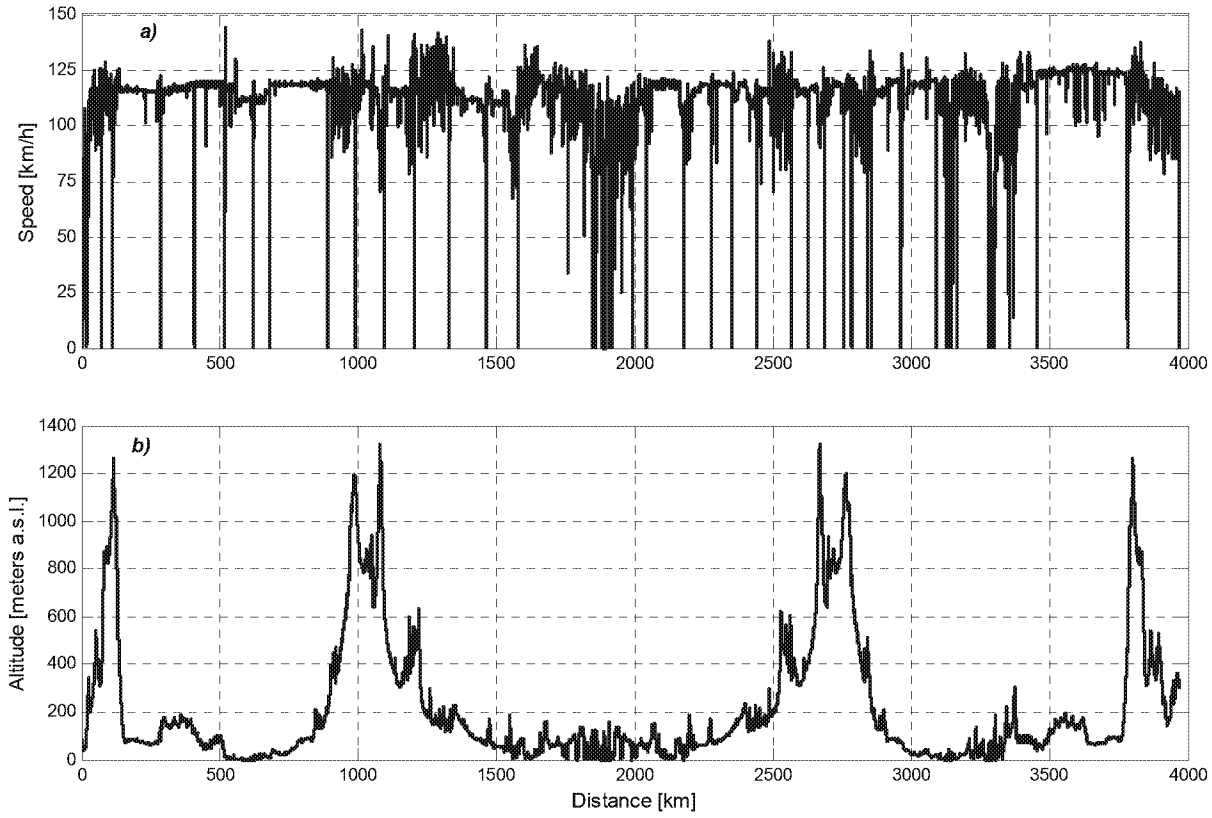


**Figure 3.18: *a)* Characteristic vehicle speed and, *b)* altitude profile of cross-multi-state route given in meters above sea level (a.s.l.)**

Finally, Table 3.7 lists the individual readiness of the primary instruments and data acquisition components, namely for i) gaseous, ii) particle, and iii) vehicle parameters, that have been utilized to collect data during the cross-multi state driving route. It can be noticed that gaseous and particle matter emissions were collected for ~60% of the entire route, corresponding to approximately 2300km. Instrument operation got primarily limited due to i) cold temperature conditions during late night driving (e.g. sample condensation issues inside analyzer units), and ii) rain fall during portions of the route between Seattle and Sacramento. It has to be noted that instrument readiness was 100% for vehicle testing over the pre-defined test routes (Route 1 to 5).

**Table 3.7: Instrumentation readiness during cross-multi state driving route**

| Instrument | Total time of operation [hr] | Fraction of total trip duration [%] | Total distance of operation [km] | Fraction of total trip distance [%] |
|---|---|---|---|---|
| OBS (gaseous emissions) | 23.6 | 60.1 | 2352.0 | 59.3 |
| ECU (engine parameter) | 31.2 | 79.4 | 3143.3 | 79.2 |
| PPS (particle emissions) | 22.7 | 57.8 | 2304.6 | 58.1 |

Figure 3.1 along with Table 3.8 provide ambient air conditions, including barometric pressure, temperature, and relative humidity encountered during the entire cross-multi-state route as a function of distance traveled. Ambient temperatures ranged from below freezing to ~+30°C with an average temperature of around 13°C as seen from Table 3.8.

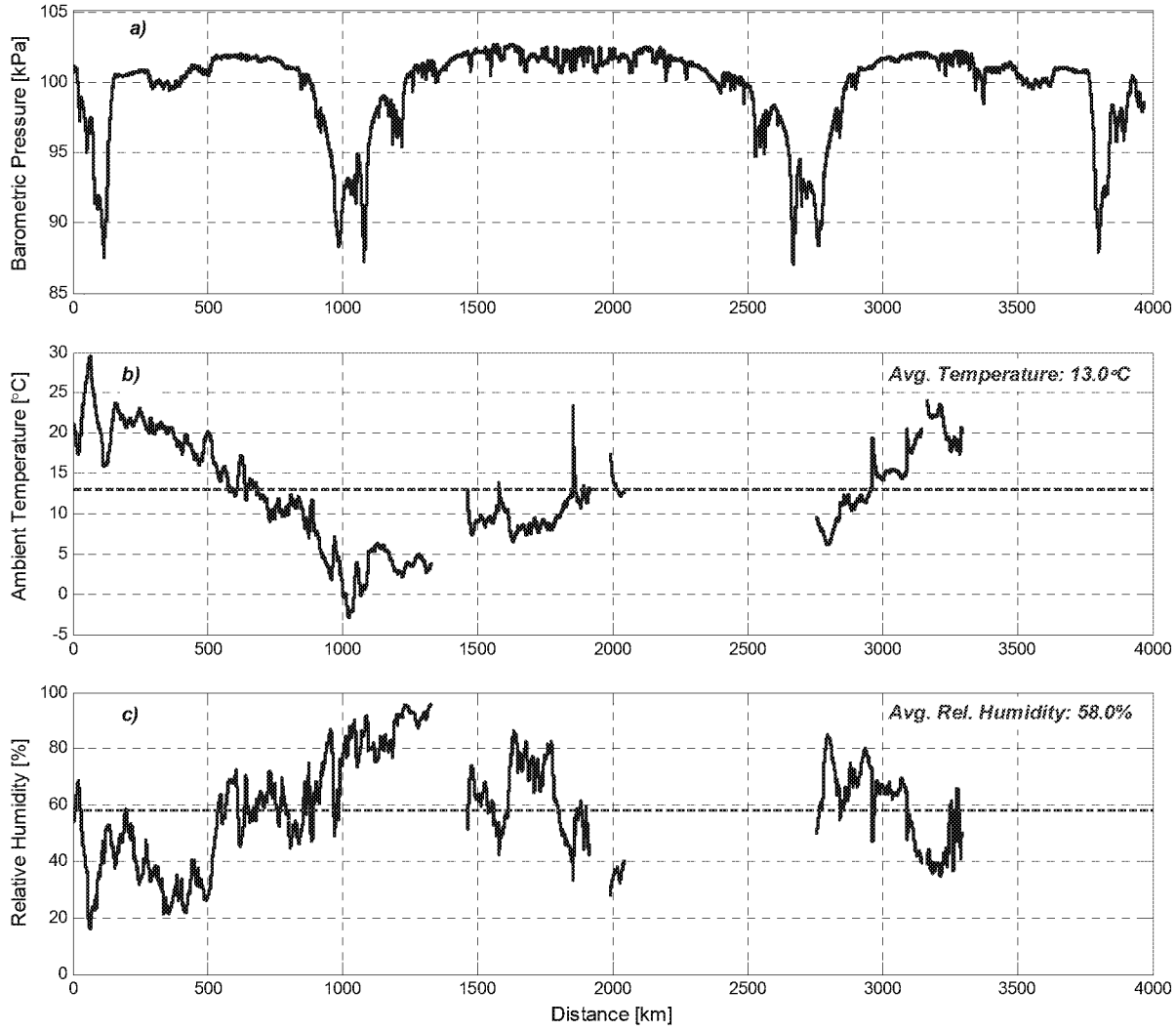


**Figure 3.19: a) Barometric pressure, b) ambient temperature, and c) relative humidity experienced during cross-multi-state route as a function of distance traveled (Note: missing data for b) and c) is due to non-operational ambient sensor)**

**Table 3.8: Range of ambient conditions experienced during cross-multi state route**

| | Temperature [C] | Baro. Pressure [kPa] | Rel. Humidity [%] |
|---|---|---|---|
| Average | 12.97 | 99.63 | 57.95 |
| Minimum | -2.87 | 86.97 | 15.84 |
| Maximum | 29.65 | 102.43 | 96.02 |

## 3.3 Emissions Testing Procedure and PEMS Equipment

The emissions sampling setup employed during the course of this study comprised three measurement sub-systems as shown in the schematic in Figure 3.20. Gaseous exhaust emissions were quantified using the on-board measurement system, OBS-2200, from Horiba described in more detail in Section 3.3.1. Real-time particle number concentration measurements were performed using the Pegasor particle sensor (PPS), model PPS-M from Pegasor Ltd. discussed in Section 3.3.2.2, while particle mass measurements were made with the OBS-TRPM system from Horiba as described in Section 3.3.2.1. The Horiba OBS-2200 PEMS system was chosen for this study as it is an approved device under the US EPA heavy-duty in-use emissions compliance program and complies to the EU 582/2011 in-use emissions measurement requirements as well.

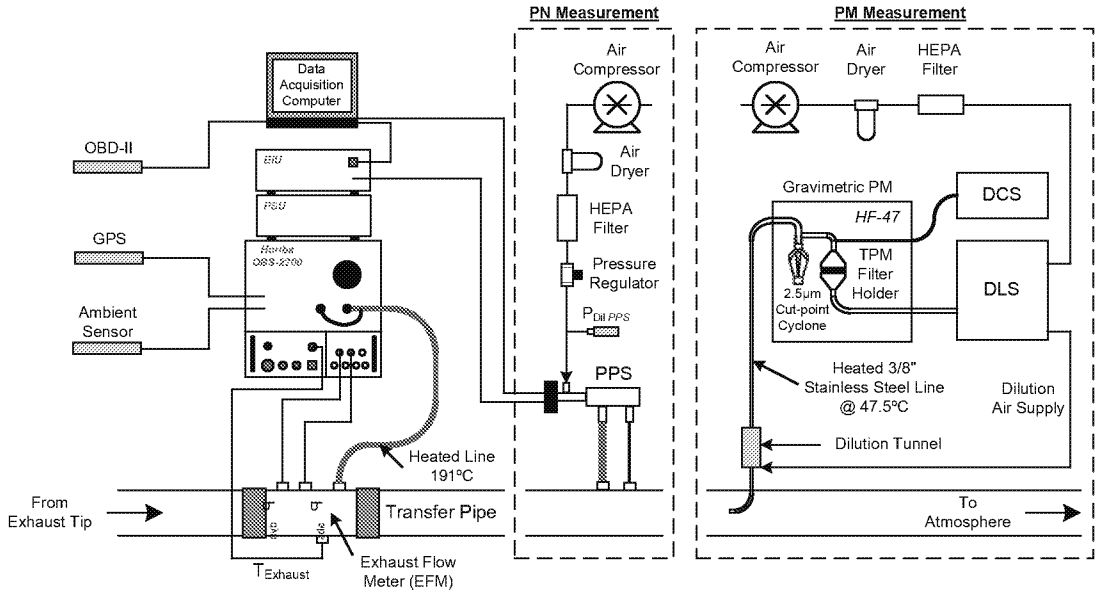


**Figure 3.20: Schematic of measurement setup, PN measurement for Vehicles A and B, PM measurement for Vehicle C**

Table 3.9 lists all the parameters and emissions constituents collected during on-road testing for this study. Emissions parameters were sampled and stored continuously at 10 Hz frequency, whereas GPS and ECU data were updated at 1 Hz, but stored at the same frequency as emissions data (i.e 10 Hz) by the data acquisition system. An external sensor was used to measure ambient conditions, including temperature, barometric pressure and relative humidity, feeding data directly to the OBS data acquisition software. Vehicle position (i.e. longitude, latitude and altitude) and relative speed were measured by means of a GPS receiver, allowing for subsequent calculation of instantaneous vehicle acceleration and distance traveled. An additional high-

resolution barometric pressure sensor was used to calculate road grade changes and altitude as an alternative to the GPS signal based on Equation 3 as presented in Section 3.2.1.

Engine specific parameters were recorded from publicly broadcasted ECU signals through the vehicles OBD-II port using a commercially available CAN logging software called AutoTap® from B&B Electronics Manufacturing Company Inc. Logged parameters included engine speed and load, intake air mass flow rate and exhaust temperatures. *Vehicle A* broadcasted DPF outlet temperature, whereas *Vehicle B* broadcasted two exhaust temperatures, namely the DPF inlet and SCR inlet temperatures.

**Table 3.9: Overview of measured parameters and respective instruments/analyzers**

| Category | Parameter | Measurement Technique |
|---|---|---|
| **Exhaust gas pollutants** | THC [ppm] | FID (Horiba OBS-2200) |
| | CO [%] | NDIR (Horiba OBS-2200) |
| | $CO_2$ [%] | NDIR (Horiba OBS-2200) |
| | $NO_x$ [ppm] | CLD (Horiba OBS-2200) |
| | $H_2O$ [%] | NDIR (Horiba OBS-2200) |
| **Exhaust flow** | Exhaust flow rate [$m^3$/min] | EFM (Horiba OBS-2200) |
| | Exhaust temperature [°C] | EFM, K-type thermocouple |
| | Exhaust absolute pressure [kPa] | EFM (Horiba OBS-2200) |
| **Exhaust PN/PM emissions** | PN concentration [#/$cm^3$] | Pegasor Particle Sensor |
| | PM (gravimetric) [mg] | Horiba OBS-TRPM |
| **Ambient conditions** | Ambient temperature [°C] | Temp. Sensor (OBS-2200) |
| | Ambient humidity [%] | Humidity Sensor (OBS-2200) |
| | Barometric pressure [kPa] | Pressure Sensor (OBS-2200) |
| **Vehicle/route characteristics** | Vehicle speed [km/h] | GPS |
| | Vehicle position [°] | GPS |
| | Vehicle altitude [m a.s.l.] | GPS |
| | Vehicle acceleration [$m/s^2$] | Derived from GPS data |
| | Vehicle distance traveled [km] | Derived from GPS data |
| **Engine characteristics** | Engine speed [rpm] | ECU OBD-II |
| | Engine load [%] | ECU OBD-II |
| | Engine coolant temperature [°C] | ECU OBD-II |
| | Engine intake air flow [kg/min] | ECU OBD-II |
| | Exhaust temperature [°C] | ECU OBD-II |

Table 3.10 gives the combination of measurement sub-systems employed for the individual test vehicles. Gaseous emissions of CO, $CO_2$, THC, and $NO_x$ were measured for all three

vehicles, whereas particle number concentration measurements via the PPS were only performed for *Vehicles A* and *B* and particle mass quantification via the OBS-TRPM only for *Vehicle C*.

**Table 3.10: Emissions constituent measurement matrix**

| Component | Vehicle A | Vehicle B | Vehicle C |
|---|---|---|---|
| Gaseous emissions | X | X | X |
| Particle number (*PPS*) | X | X | |
| Particle mass (*OBS-TRPM*) | | | X |

**Figure 3.21: Vehicle A instrumentation setup**

Figure 3.21 through Figure 3.23 depict the experimental setup and instrument arrangement inside the test vehicles, *Vehicle A*, *B*, and *C*, respectively. For on-road testing with both *Vehicles A* and *B*, a 2kW Honda generator (gasoline fueled) was utilized to supply the necessary electrical power to operate the OBS, PPS and ancillary systems. The power requirements for the OBS-TRPM however, required the addition of a second 2kW Honda generator to support the power demand for the entire sampling setup during testing of *Vehicle C*. Using a vehicle independent power generator had the advantage of not having to draw any current from the test vehicles power system; hence, no additional load was added to the engine which might have skewed the emissions production rate and therefore the results of this study. On the other hand, it has to be

noted that the addition of measurement equipment was increasing the actual vehicle weight, thereby possibly influencing the engine's load demand and resulting emissions rates. The payload of *Vehicles A* and *B* was representative of four adult passengers totaling 300kg when assuming 75kg per individual passenger (i.e. *Vehicle A*: 305kg, *Vehicle B*: 314kg), whereas *Vehicle C*'s payload had to account for additional 230kg (i.e. 533kg).

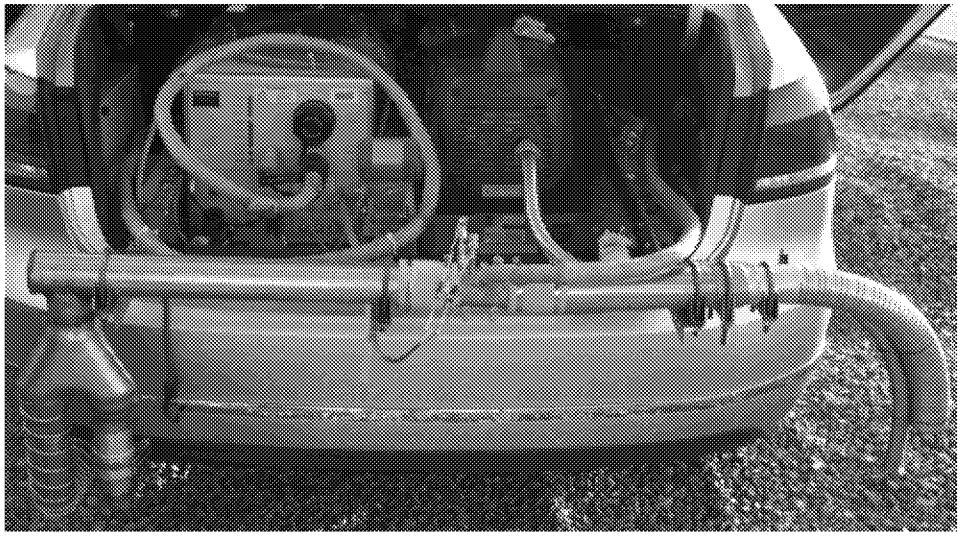

**Figure 3.22: Vehicle B instrumentation setup**

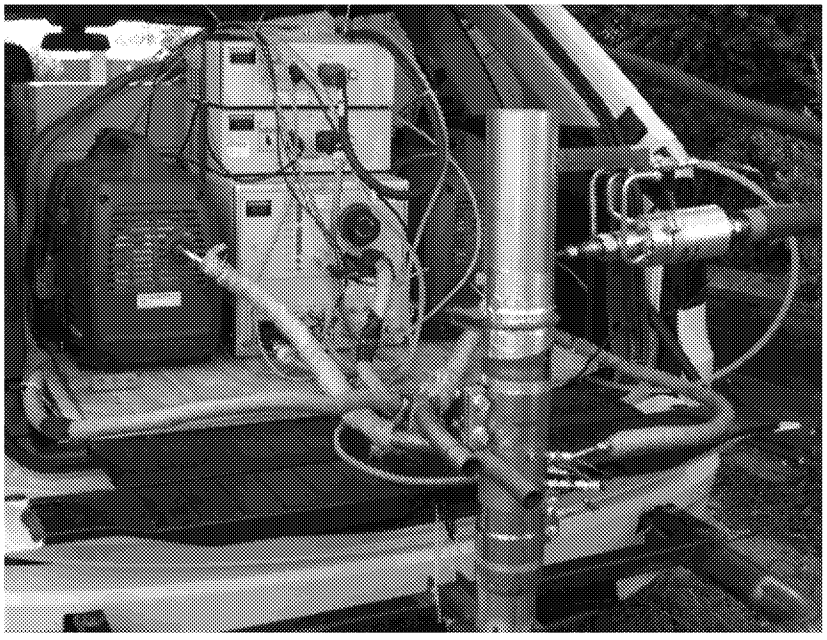

**Figure 3.23: Vehicle C instrumentation setup**

### 3.3.1 Gaseous Emissions Sampling – Horiba OBS-2200

Gaseous raw emissions, including CO, $NO_x$, THC as well as $CO_2$ were measured on a continuous basis using the Horiba OBS-2200 on-board emissions measurement system which has been specifically developed with regard to PEMS requirements for on-road vehicle emissions testing according to recommendations outlined in CFR, Title 40, Part 1065. The emissions of CO and $CO_2$ were measured using a non-dispersive infrared (NDIR) spectrometer (heated wet sample), THC using a flame ionization detector (FID) (heated wet sample), and total $NO_x$ using a chemiluminescence detector (CLD) in conjunction with an $NO_2$-to-NO converter (heated wet sample). The Horiba OBS system gives the option to either sample in $NO_x$ mode ($NO_2$-to-NO converter on) or NO mode ($NO_2$-to-NO converter off), however, for the entire duration of this study the instrument was solely operated in $NO_x$ mode (total $NO_x$ measurement). Detailed information regarding the chosen measurement ranges, span values to which the analyzers were calibrated to, as well as analyzer linearity, accuracy and repeatability of the Horiba OBS-2200 system are given in Table 3.11.

Gaseous emissions were extracted by means of an averaging sample probe through a ½" NPT port installed on the exhaust flow meter adapter that was mounted to the exhaust end pipe. The exhaust sample was directed through a heated line, maintained at a nominal temperature of 191°C using a PID-type controller, to the analyzer inlet port.

**Table 3.11: Horiba OBS-2200, Gaseous analyzer specifications [15]**

| Comp. | Range | Span | Linearity | Accuracy | Repeatability |
|---|---|---|---|---|---|
| CO | 0.1 vol.% | 0.099% | within ±1.0% of full scale | within ±2.5% of full scale | Zero: within ±1.0% of full scale<br>Span: within ±1.0% of readings |
| $CO_2$ | 12 vol.% | 11.9% | within ±1.0% of full scale | within ±2.5% of full scale | Zero: within ±1.0% of full scale<br>Span: within ±1.0% of readings |
| $NO_x$ | 1600 ppm | 1492ppm | within ±1.0% of full scale | within ±2.5% of full scale | Zero: within ±1.0% of full scale<br>Span: within ±1.0% of readings |
| THC | 350 ppm | 303ppm | within ±1.0% of full scale | within ±2.5% of full scale | Zero: within ±1.0% of full scale<br>Span: within ±1.0% of readings |

The exhaust flow meter (EFM), used in conjunction with the OBS-2200 instrument is a Pitot-tube type flow meter involving the measurement of dynamic and static pressure heads by means of differential and absolute pressure transducers. The fluid temperature (exhaust gas) is measured via a K-type thermocouple allowing to adjust the exhaust gas flow measurement to

EPA defined standard conditions (i.e. 293.15K and 101.325 kPa). Additional to pressure and thermocouple ports the EFM adapter features a port for connecting the exhaust gas sampling probe. An averaging type probe with multiple holes spanning the entire EFM adapter's diameter was used to extract continuous exhaust samples. Depending on the vehicle tested two differently sized EFM units were utilized for this study. An EFM adapter with 2" diameter (ID) was installed for testing *Vehicles A* and *B* as shown in Figure 3.24 and Figure 3.25, respectively, whereas a 3.5" diameter EFM was employed during *Vehicle C* testing as depicted in Figure 3.26.

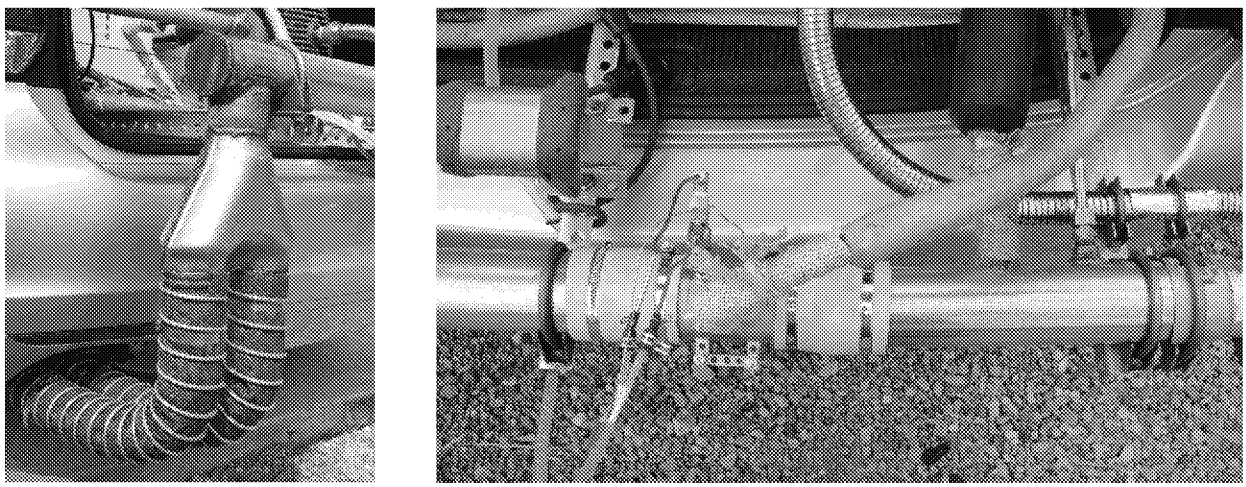

**Figure 3.24: Exhaust adapter setup for Vehicle A, *left*: flexible high temperature exhaust hose connecting double vehicle exhaust tip to exhaust transfer pipe, *right*: 2" exhaust flow meter (EFM)**

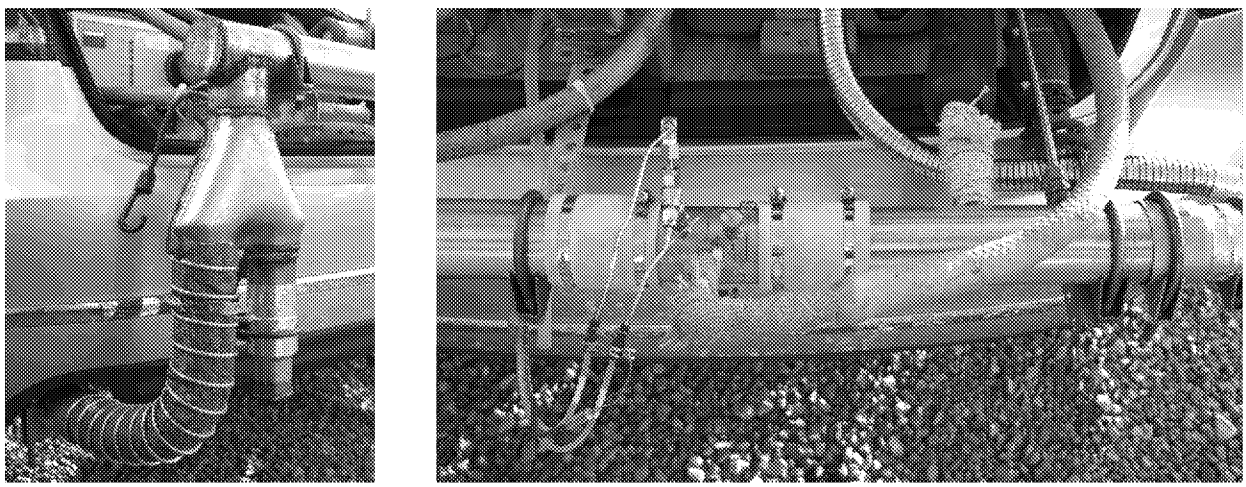

**Figure 3.25: Exhaust adapter setup for Vehicle B, *left*: flexible high temperature exhaust hose connecting single vehicle exhaust tip to exhaust transfer pipe, *right*: 2" exhaust flow meter (EFM)**

Prior to vehicle testing, the exhaust flow meter units were verified against a NIST traceable laminar flow element (LFE) installed on a flow bench at WVU's on-campus laboratory (i.e. EERL). A least-square regression analysis between the LFE and the EFM measurements resulted in a coefficient of determination ($R^2$) of 0.9986 and 0.9989 for the 2" and 3.5" EFM adapter, respectively.

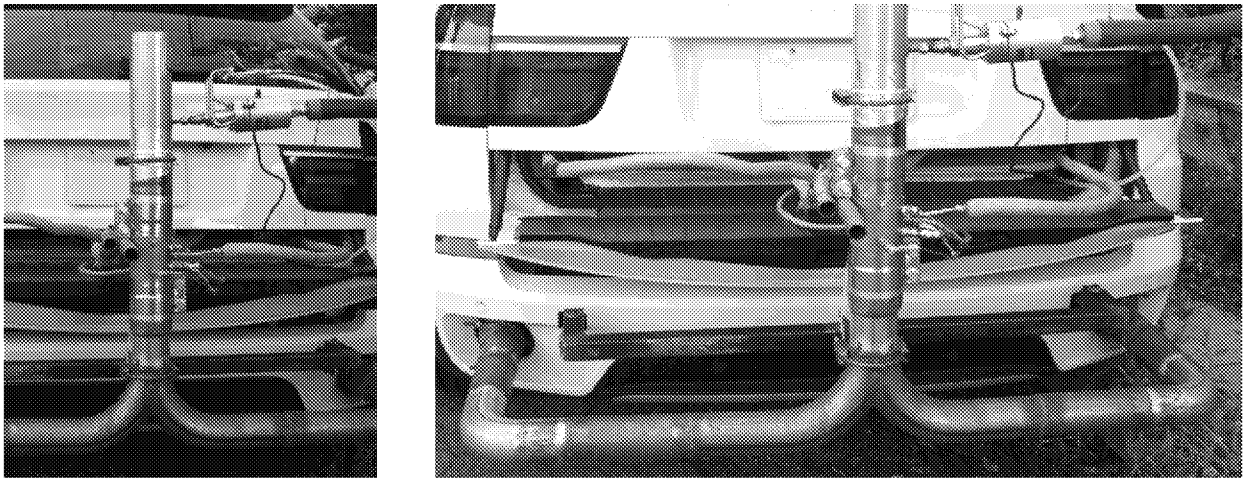

**Figure 3.26: Exhaust adapter setup for Vehicle C, *left*: 3.5" exhaust flow meter (EFM), *right*: joining double vehicle exhaust stack into exhaust transfer pipe**

### 3.3.2 PEMS Particle Mass/Number Measurements

PEMS development for PM quantification (PM-PEMS) during on-road operation has been primarily driven by the heavy-duty diesel sector in recent years. Numerous studies were performed within the US [16] and Europe [17, 18, and 19] aimed at evaluating the sensitivity and accuracy of different PM-PEMS, their comparability to the standard engine certification method (i.e. gravimetric sampling via CVS) as well as the feasibility and practicality of their application in a harsh environment such as on-road emissions measurement. Giechaskiel et al. [20] recently performed a comprehensive study comparing commercially available PM-PEMS and PM sensors to the standard gravimetric PM sampling method used for engine certification and type-approval, with regard to particle mass and number concentration measurements during in-use testing. The authors specifically highlighted the advantage of particle number (PN) measurement approaches, due to their possible applicability to future PN emissions standards as will be introduced in the EURO VI heavy-duty regulation by 2014. Based on the positive performance of the Horiba

OBS-TRPM system during the aforementioned studies [16, 17, 18, 19, and 20] and due to the fact that this system is currently the only commercially available system with approval from the European Union for heavy-duty on-road PM measurement, Horiba's PM-PEMS system was chosen to conduct PM sampling during this study. On the other hand the, Pegasor particle sensor model PPS-M from Pegasor Ltd. was selected for on-line particle number concentration measurements directly from the raw exhaust stream.

#### *3.3.2.1 Gravimetric PM Measurement with Horiba OBS-TRPM*

As described earlier Horiba's OBS-TRPM (On-Board System for Transient PM Mass Measurement) system was selected to perform in-use particle mass quantification. This instrument has been specifically developed for the primary purpose of in-use certification of on-road heavy-duty diesel vehicles, as mandated by the US Environmental Protection Agency (US-EPA) [21] and is designed to be used in conjunction with Horiba's OBS-2200 gaseous system. The OBS-TRPM is a combination of a proportional diluted sampling system for gravimetric PM sampling on 47mm filter media and real-time measurements of particle length [$mm/cm^3$] (including soot, sulfates and volatile particles), which can be defined as the product of total number concentration and average particle diameter, by means of a diffusion charging type sensor called Electrical Aerosol Detector (EAD) from TSI Inc. The underlying assumption is that the mass accumulated on the filter is proportional to the PM length parameter as measured by the EAD, therefore, making the OBS-TRPM ultimately capable of calculating a quasi "real-time" PM mass concentration rate. However, the gravimetric sampling component of the OBS-TRPM, requiring physical weighing of the filter media on a microbalance, makes "real-time" PM mass concentration information only available after post-processing of the measured data.

A proportional sample was extracted through a 3/8" stainless steel J-type probe located downstream the OBS exhaust flow meter unit. Proportionality was calculated based on the EFM signal and controlled by a series of fast acting piezo-valves and mass-flow controllers (MFC). Close-coupled to the sampling probe was a dilution unit (i.e. "*dilution tunnel*") that uniformly introduced HEPA filtered dilution air. A ½" heated stainless steel line connected the dilution unit to the temperature controlled filter holder compartment (called "*HF-47*", see Figure 3.27) where the exhaust sample was first directed through a $PM_{2.5}$ cut-point cyclone separator to remove particles bigger than 2.5μm (50% efficiency at cut-point), and then through the filter media

holder where PM was retained on 47mm Pallflex® Quartz-fiber filter (TX40) membranes (Pall Corporation) for subsequent gravimetric analysis. All components, including, dilution tunnel, transfer line and HF-47 filter box were heated in order to maintain the filter-face temperature at constant 47±5°C. A constant slip stream was extracted from the sample flow before entering the filter media holder and routed to the diffusion-charger (i.e. EAD) for quantification of the particle length parameter. Dilution and sample flows for the entire system were controlled by the flow control unit (called "*DLS*").

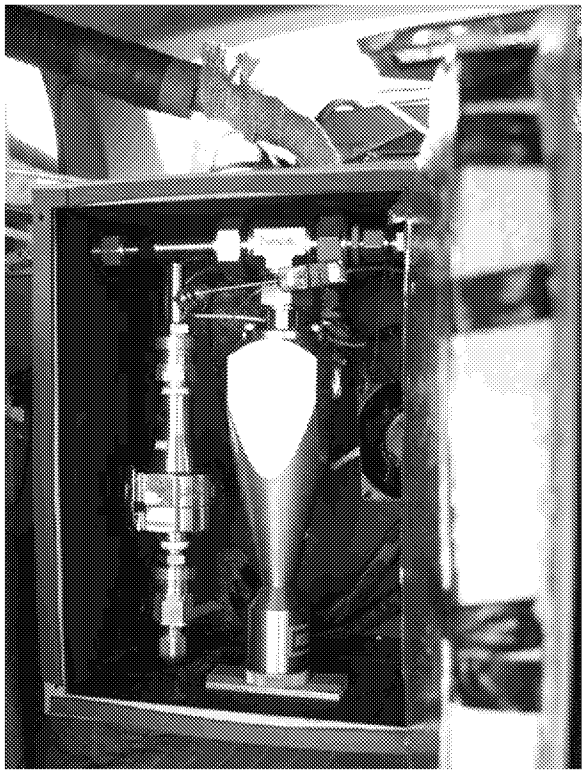

**Figure 3.27: Horiba OBS-TRPM heated filter holder box for gravimetric PM quantification, sample is introduced from the top, *left*: 47mm filter holder, *right*: 2.5 cut-point cyclone**

All filter media (i.e. TX40 membranes) used during the course of this study were pre and post-weighed at CAFEE's on-campus clean room facility and shipped (overnight) to and back from the vehicle testing location in California. The clean room is environmentally controlled (Class 1000, maintained at 21°C and 50% RH), thus allowing for stable conditions for PM filter media handling, storage and weighting procedures. A Sartorius microbalance with a minimum detection limit of 10 µg and an accuracy of 0.1µg was utilized to pre and post-weigh filter media. The measurement system was operated with in-house developed software to calibrate the scale, perform measurements, as well as to monitor the history of individual filter membranes.

### 3.3.2.2 *Real-Time PM Measurement with Pegasor Particle Sensor*

Particle number concentration measurements were performed using the Pegasor particle sensor, model PPS-M from Pegasor Ltd. (Finland) [22] which is capable of performing continuous measurements directly in the exhaust stack and providing a real-time signal with a frequency response of up to 100Hz (see Figure 3.28). The sensor operates as diffusion-charging (DC) type device and measures PM based on the current induced by the charged particles leaving the sensor. Figure 3.29 shows the PPS as well as the sample gas flow paths. Dry, HEPA filtered dilution air is supplied at about 22psi and subsequently charged by a unipolar corona discharge charger using a tungsten wire at ~2kV and 5μA. The pressurized dilution air, carrying the unipolar ions, then draws raw exhaust gas through an ejector-type diluter into a mixing chamber, where the ions are turbulently mixed with exhaust aerosol particles for diffusion charging. The sample gas flow is controlled by means of a critical flow orifice and is a function of the supplied dilution air pressure. An electrostatic precipitator (ion trap), installed downstream of the mixing chamber and operating at a moderate voltage of approximately 100V, traps excess ions that escaped the charging zone. Finally, the charge of the out-flowing particles is measured using a built-in electrometer. The measured current signal is amplified and filtered by the internal electronic control unit of the sensor and outputted either as a voltage or current value. The sensors output can be subsequently correlated to other aerosol instruments by means of linear regression in order to measure the concentration of the mass, surface or number of the exhaust particles, depending on the chosen reference instrument.

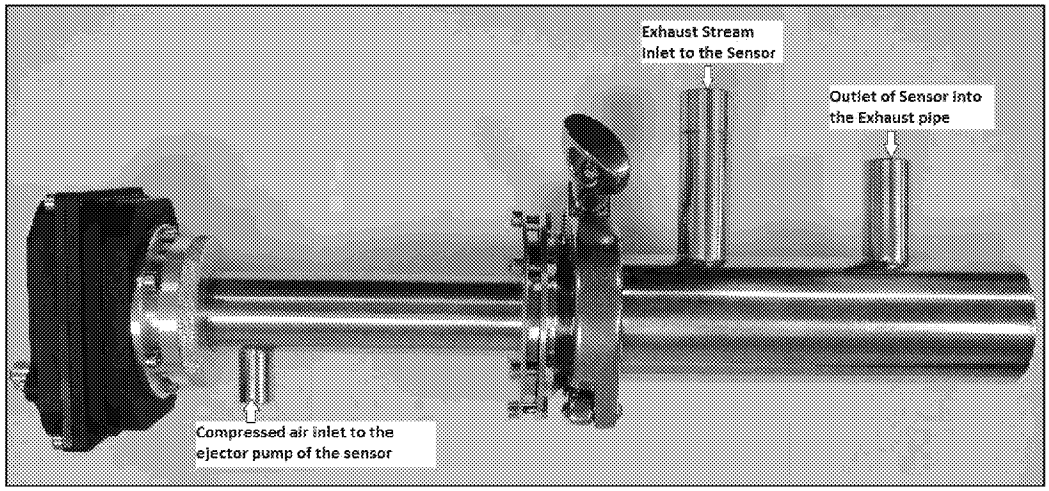


**Figure 3.28: Pegasor particle sensor, model PPS-M from Pegasor Ltd. (Finland)**

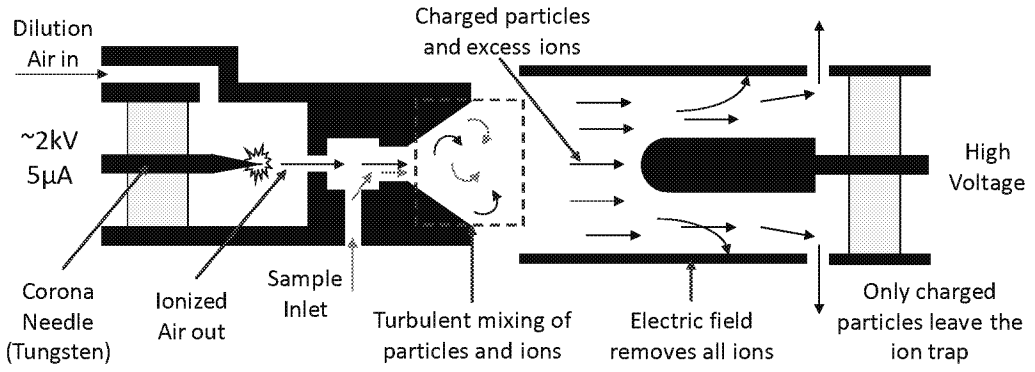


**Figure 3.29: PPS measurement principle with sample gas and dilution air flow paths [23, 24]**

Extensive testing of this sensor at the engine testing facility at WVU, has shown the capability of this sensor to accurately measure the total PM concentration in comparison to other standard aerosol instruments such as the Ultrafine Condensation Particle Counter (TSI UCPC, Model 3025), the Engine Exhaust Particle Sizer spectrometer (TSI EEPS™, Model 3090) as well as the Micro-Soot Sensor (MSS) from AVL (Model 483) [24]. The sensor was designed as a flow through device and therefore does not involve collection or contact with particles in the exhaust stream, which is especially advantageous for long-term stability and operation without frequent maintenance; hence, best suited for in-use application.

Figure 3.30 shows the positioning of the PPS within the test vehicle. The sensor was enclosed in a compartment (green box seen in Figure 3.30) that provided thermal insulation from the surroundings. Additionally, the sensor was wrapped in insulation material and a resistive heater, in conjunction with a PID controller, maintained the sensor core at a nominal 200°C in order to prevent condensation of volatile components within the sensors. A three-foot heated sampling line (maintained at 200°C) was used to transfer the extracted exhaust sample from the exhaust transfer pipe to the PPS inlet, whereas a non-heated, but thermally insulated stainless steel line was used to direct the sample exiting the PPS back to the exhaust transfer pipe.

Pressurized air supply for the PPS was provided by a small electrical air compressor (Blue Hawk, 0.3hp with 2 gallon reservoir). Prior to the sensor inlet, the pressurized air was dried and HEPA filtered as can be seen in the top left corner of Figure 3.30. A manually adjustable pressure control value was used to maintain the dilution air supply pressure at constant 22 psi (~ 1.5bar). As the PPS draws and dilutes the exhaust sample via an ejector type diluter/pump and controls the sample and dilution air flows, and thus, the internal dilution ratio, by means of a

critical flow orifice, knowledge of the dilution air pressure is required to calculate particle number concentrations in the exhaust stream. An absolute pressure transducer (Omega, model PX602, range 30psi) was used to continuously measure the dilution air pressure.

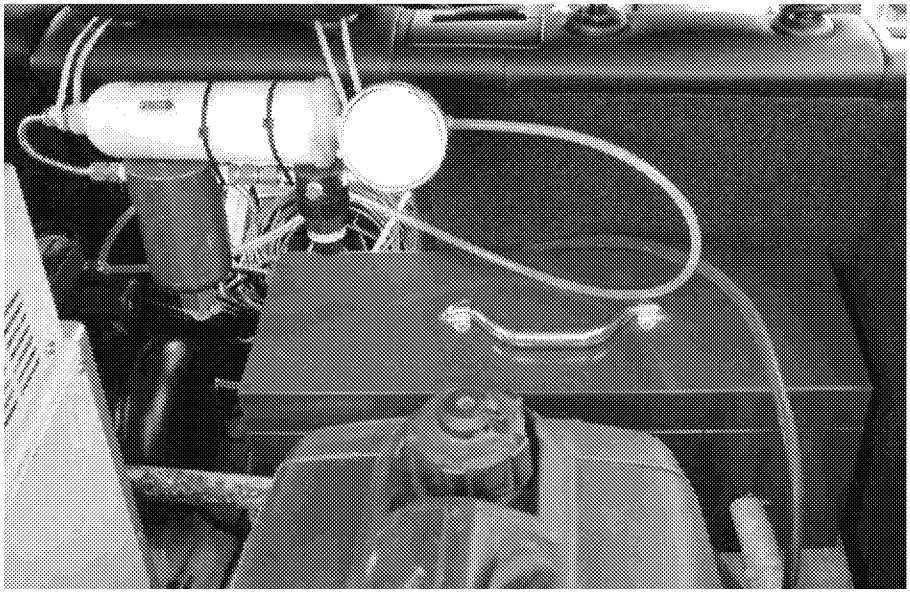

**Figure 3.30: PPS setup, the sensor is housed within the green box, *top left*: pressurized, dried and HEPA filtered air supply for PPS**

Using the dilution air pressure as input to linear Equation 6 the sample flow rate can be calculated as a function of constant coefficients $\beta_0$ and $\beta_1$ only. These coefficients depend on the internal configuration (i.e. orifice dimensions) of the PPS and were evaluated as $\beta_0 \approx 3.668$ and $\beta_1 \approx 0.105$ for the sensor used during the course of this study.

$$\dot{V}_{sample}[slpm] = \beta_1 \cdot P_{Dil}[psi] + \beta_0 \qquad \textbf{Eq. 6}$$

For the purpose of this study the raw sensor signal was calibrated for both particle number concentration in [#/cm$^3$] as well as particle mass concentration in [mg/m$^3$] by means of the linear calibration coefficients developed by Ntziachristos et al. [25, 26], and given by Equations 7 through 10 with constant $C_1 = 3333.33$.

$$PN\ [\#/cm^3] = f_N\left(\dot{V}, C_{N-calib}\right) \cdot PPS_{Signal}[mV] \qquad \textbf{Eq. 7}$$

$$PM\ [mg/m^3] = f_M\left(\dot{V}, C_{M-calib}\right) \cdot PPS_{Signal}[mV] \qquad \textbf{Eq. 8}$$

$$f_N = \frac{288}{\dot{V}_{sample}[slpm]} \cdot C_1 \qquad \textbf{Eq. 9}$$

$$f_M = \frac{6.3 \cdot 10^{-5}}{\dot{V}_{sample}[slpm]} \cdot C_1 \qquad \textbf{Eq. 10}$$

The particle number concentration measurement setup (i.e. PPS) used in this study was designed and configured to follow the spirit of the Particle Measurement Program (PMP) method as mandated by the European Union [3, 27] for regulatory particle number concentration quantification. The three foot sample transfer line and the PPS sensor itself were heated and maintained at a nominal temperature of 200°C, thereby reducing the probability for volatile and semi-volatile components to condensate and possibly nucleate and form measurement artifacts. Even though the PPS temperature of 200°C is below the recommended temperature for the first stage dilution (150 to 400°C) and evaporation tube (300 to 400°C) it has to be considered that the PMP method is designed to sample from an already diluted, and therefore '*cooled*', sample stream from either a constant volume sampling (CVS) or partial dilution system [27] as opposed to the PPS sampling from the raw exhaust at elevated gas temperatures. Particle nucleation phenomena are strongly driven by exhaust gas dilution and cooling which does not occur when the sample is extracted directly from the exhaust stack (or transfer line). As described earlier, the PPS requires a small amount of pressurized dry air to drive the sample flow via an internal ejector diluter, however, the dilution process is assumed to be rapid and without the necessary residence time required to form artifacts before particle charging and measurement occurs. It is therefore believed that the measurement setup used in this study mainly detects solid particles as required by the PMP method.

The electrostatic precipitator (ion trap) installed downstream the mixing chamber of the PPS allows, depending on the voltage applied, not only to remove excess ions but also to trap particle of a certain mobility diameter. Increasing the voltage on the center electrode leads to a stronger electrical field causing particles to deflect and impact inside the PPS, and thereby escape from being counted. This particle removal mechanism can be utilized towards inducing a lower particle cut-point similar to the 50% counting efficiency for particles of 23nm in an ultrafine particle counter as recommended by the PMP method [27].

Based on the above discussion it can be concluded that, even though the PPS method for particle number concentration measurements does not comply with recommendations outlined in the European regulation for PN measurements [3, 27], it follows the spirit of the PMP method of counting '*only solid particles of size larger than 23nm*' (and smaller than 2.5μm). Tikkanen *et al.* [28] found good agreement between a PPS measuring directly from the exhaust stack and a second PPS, equipped with a catalytic stripper (CS) to remove volatile and semi-volatile particles, sampling from the diluted exhaust gas in a CVS system for both light and heavy-duty engines. Finally, it has to be emphasized again that the PPS does not directly measure particle number concentrations but rather infers PN counts from a charge measurement as opposed to the ultrafine particle counters required by the PMP method [27] that are based on optical counting of individual particles after they were allowed to grow to a detectable size in a saturated Butanol or water environment.

Therefore, the reader is cautioned when directly comparing the particle number concentration results presented in this report (see Results and Discussion, Section 4) with European PN limits (i.e. Euro 5b/b+ [4]) for light-duty diesel vehicles as the measurement method used during this study differs from the measurement protocol set forth by the European Union [3, 27]. An additional and more detailed discussion about the PMP method required for PN measurements according to the European regulation is given in Appendix 7.2.

### 3.3.3 PEMS Verification and Pre-test Checks

#### *3.3.3.1 PEMS Verification and Analyzer Checks*

All PEMS instruments employed during the course of this study were calibrated, verified and operated according to manufacturer's recommendations and requirements outlined in CFR, Title 40, Part 1065, Subparts D and J [29]. Individual analyzers of the OBS system were calibrated and verified prior to deployment of the instrument to the field at WVU's on-campus laboratory. The following discussion will briefly outline the verification and system checks performed on the OBS-2200 instrument.

As recommended by the manufacturer, "*amplifier zero*" and "*detector gain*" adjustments for flame ionization detector and chemiluminescence detector, and "*amplifier gain*" adjustments for the FID were performed prior to analyzer linearization as these adjustments affect the sensitivity

of the FID and CLD analyzers. Following this, analyzer "*linearity*" verifications were performed for each individual analyzer (i.e. CO, $CO_2$, THC, and $NO_x$) by flooding the instruments inlet port with a calibration gas mixture, blended at 10 different ratios equally spaced across the selected measurement range for a given analyzer. A least-squares regression analysis was subsequently performed between the analyzer's response and the theoretical calibration gas blend concentrations and verified to comply with linearization criterions as per 40 CFR §1065.307.

After "*linearity*" verifications a set of interference checks was performed in order to quantify the amount of interference between the component being measured and any other components that are known to interfere with its measurement and that are ordinarily present in the exhaust gas sample. These include, $CO_2$ and water ($H_2O$) quench checks on $NO_x$, $CO_2$, propane ($C_3H_8$), and $H_2O$ interference checks on CO, oxygen ($O_2$) interference check on THC, as well as CO, $C_3H_8$, and $H_2O$ interference checks on $CO_2$. The Horiba OBS-2200 system automated these procedures to help guide the operator through the respective processes with a routine that compares interference results against pre-determined limits based on 40 CFR 1065 Subpart D and J. Additionally, $NO_x$ converter efficiency and THC hang-up checks were performed to ensure proper analyzer response.

The heated sample lines for gaseous (OBS-2200) and PM (OBS-TRPM) samples were checked for any leaks, and for proper control of the heated surfaces. Leak checks were performed via a vacuum-side leak verification (40 CFR §1065.345), using a pressure calibration device, and temperature traces were established with a thermocouple and thermocouple calibrator.

The OBS-TRPM system was verified according to manufacturer recommendations, involving various leak checks and sample flow checks using calibrated reference mass flow meters.

#### *3.3.3.2 PEMS Installation and Testing*

After initial installation of the PEMS on the test vehicle and prior to start of each test day, the PEMS was warmed-up and allowed to thermally stabilize for at least one hour. After warm-up and prior to start of each test route "*zero*" and "*span*" checks and adjustments were performed for each analyzer, followed by an automated internal system check.

Prior to start of testing, the PEMS equipment was validated by placing all systems in sample mode with the test vehicle's engine turned on and set to idle operation. During this time, each measurement was checked for consistency, using good engineering judgment.

"Zero" and "span" checks and adjustments were performed before and immediately after completion of each test route and analyzer drift values were automatically recorded by the OBS software for subsequent drift correction of measurement results.

#### *3.3.3.3 PEMS Comparison with CVS System*

One out of the three test vehicles, specifically the *Vehicle B*, was selected for a cross-correlation evaluation between the OBS-2200 PEMS and laboratory grade instruments while the vehicle was operated over standardized test cycles on a chassis dynamometer at CARB's light-duty constant volume sampling (CVS) test facility in El Monte (CA). This allowed to establish confidence in the measurement results of the PEMS, as well as to identify possible issues with the on-road measurement setup.

The same 2" diameter (ID) EFM adapter as used during on-road testing of *Vehicles A* and *B* (see Figure 3.24 and Figure 3.25) was installed into the exhaust transfer line leading from the vehicles exhaust tip to the CVS tunnel as shown in Figure 3.31 (see right side of figure). The OBS-2200 PEMS was setup and configured in the same manner as it was used during on-road testing, measuring raw exhaust gas concentrations of $CO_2$, $NO_x$, CO, and THC, volumetric exhaust flow, and ambient air conditions inside the test cell. Also, the Pegasor particle sensor was installed downstream the EFM using the same sample extraction configuration as during on-road testing. Upstream of the OBS-2200 sampling location, CARB personnel installed a Semtech-DS PEMS unit from Sensors Inc. along with an exhaust flow meter allowing for additional cross-correlation of between two different PEMS instruments. Furthermore, an AVL SESAM FTIR multi-component measurement system sampling raw exhaust gas as well as an AVL Particle Counter (APC) and an Engine Exhaust Particle Sizer (EEPS®) spectrometer (model 3090) from TSI Inc. quantifying particle number concentrations and size distributions from diluted exhaust (CVS) were being operated during chassis dynamometer testing of *Vehicle B*.

However, this report will only present and discuss cross-correlation analysis performed between regulated exhaust gas constituents measured with the OBS-2200 PEMS and the CVS system, including $CO_2$, $NO_x$, CO, and THC.

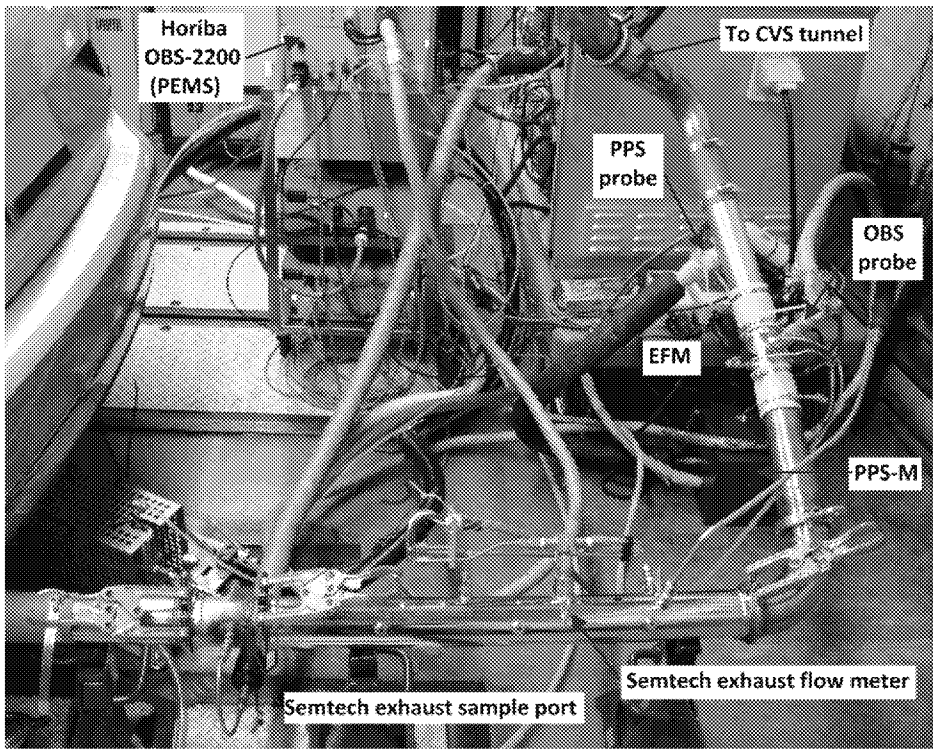


**Figure 3.31: Experimental setup and exhaust sample extraction during chassis dynamometer testing of Vehicle B at CARB's El Monte, CA, vehicle test facility**

Experiments were performed over three certification test cycles, namely the FTP-75, US06, and the European NEDC as shown in Table 3.12 using the same test fuel as has been used during the on-road emissions testing (see Appendix 7.4 for fuel specifications). Figure 3.32 depicts the continuous emissions mass rates of both PEMS and CVS system in [g/s] over the three bags of the FTP-75 cycle, where '*Bag 1*' is a cold start and transient phase, '*Bag 2*' the stabilized phase followed by a 10min hot soak, and finally '*Bag 3*' a hot start and transient phase (same vehicle speed as '*Bag1*'). It has to be noted that the scale of the y-axis in Figure 3.32 for '*Bags 2* and *3*' for $NO_x$, CO and THC is being reduced by up to one order of magnitude compared to '*Bag 1*' (i.e. cold start).

**Table 3.12: Chassis dynamometer test matrix for Vehicle B**

| Test Cycle | Condition | CVS | PEMS | Comment |
|---|---|---|---|---|
| NEDC | Cold | X | X | w/ DPF regen. event |
| US06 | Warm | X | X | |
| FTP-75 | Cold/Hot | X | X | |
| US06 | Warm | X | X | |
| NEDC | Cold | X | X | |

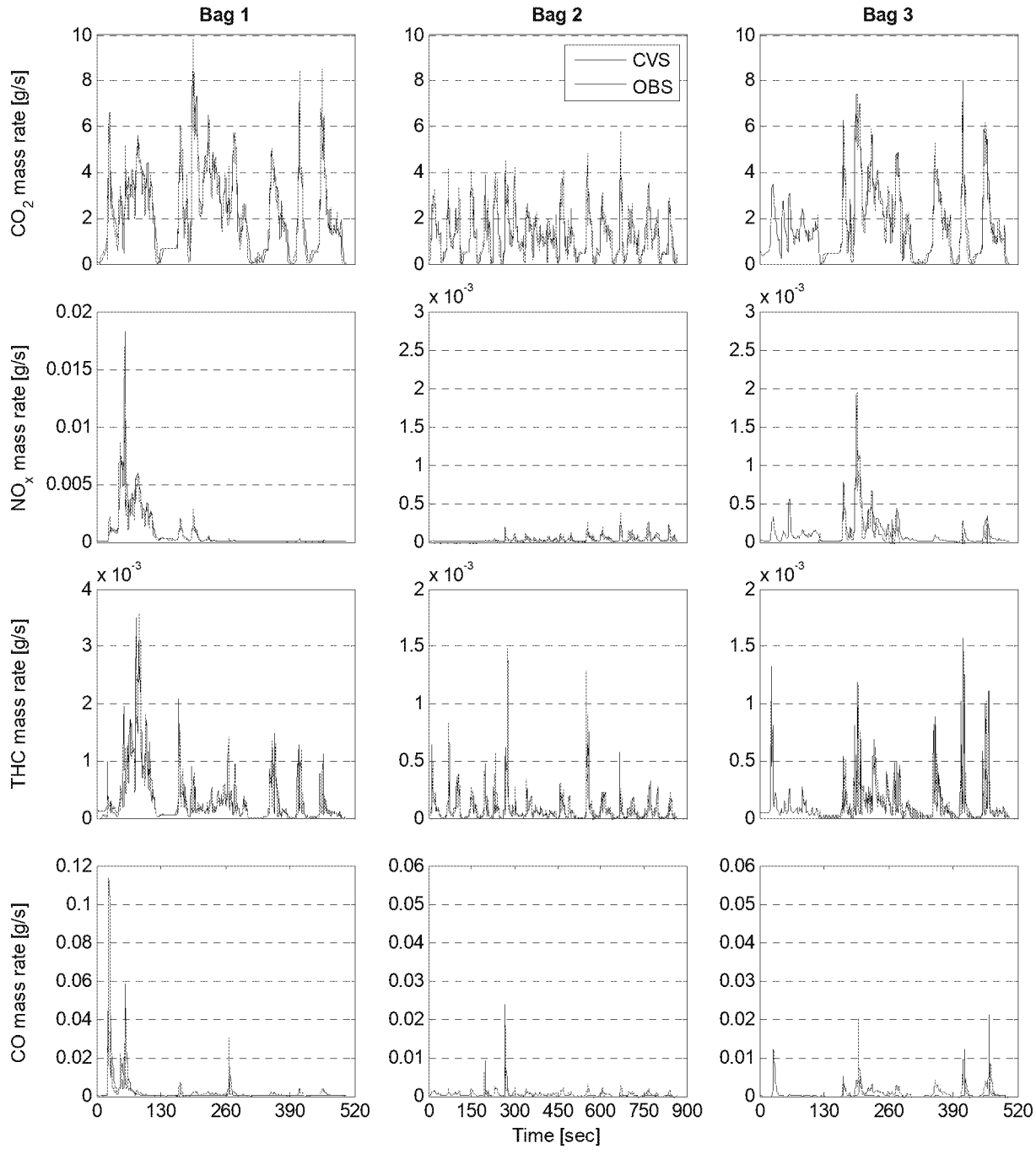


**Figure 3.32: Emissions rate comparison between CVS laboratory (CARB, El Monte CA) and Horiba OBS-2200 PEMS measurements over the FTP-75 standard chassis dynamometer test cycle**

Furthermore, as seen from the continuous mass rates in Figure 3.32, '*Bag 3*' data collection with the PEMS only started after 130 seconds, thus, data points for the first 130 seconds of '*Bag 3*' were not considered for the emissions mass rate calculation and PEMS evaluation presented in this chapter. In addition, Figure 7.1 in Appendix 7.3 provides a linear regression analysis between the emissions mass rates as measured by the two different systems.

As can be seen from Figure 3.32 the PEMS shows fairly good overall correlation with the CVS for $CO_2$ and $NO_x$ over all three bags of the FTP-75. For $NO_x$ emissions the PEMS fails to adequately capture the full magnitude of some of the larger emissions spikes during acceleration events (see e.g. $NO_x$ spike during initial acceleration for '*Bag 1*' (~30sec) being larger for CVS as compared to PEMS, Figure 3.32). However, one has to keep the low concentrations in mind when interpreting the data, especially with '*Bag 2*' and '*Bag 3*' $NO_x$ emissions being up to two orders of magnitude lower than for '*Bag 1*'. The latter is primarily due to the SCR system becoming effective in reducing $NO_x$ only after achieving a certain threshold temperature, while not being active during cold-start conditions.

Total hydrocarbons and CO both exhibit low emissions rates, as is typical for diesel combustion engines, thus, regression analysis between the two measurement methods shows reduced correlation on an instantaneous basis. Especially CO emissions were observed to be near zero as measured by the CVS system once the after-treatment system was warmed up, while the PEMS captured occasional emissions spikes during acceleration events.

However, when comparing continuous emissions mass rates calculated from diluted CVS and raw PEMS concentration measurements one has to consider the different transport phenomena such as transport times and possible '*smearing*' effects (i.e. especially for CVS), amongst others, between the two systems that might significantly affect the instantaneous concentration measurements. Also, the different flow rate quantification methods, namely subsonic venturi (SSV) or critical flow orifice for CVS and Pitot-tube type flow measurement for the PEMS will additionally impact the instantaneous calculated emissions mass rates.

Regardless of the instantaneous correlation of the signals, it is important to point out that the PEMS follows overall mass emissions with good accuracy for all pollutants. This is shown in Figure 3.33, which depicts the distance-specific emissions in [g/km] of regulated emissions as measured by the PEMS and CVS system over the three bags of the FTP-75 chassis dynamometer test cycle. The integrated values for all three bags do correlate to within ~6% for $CO_2$, ~10% for $NO_x$, ~10% for THC and ~30% for CO. The dotted red and dashed blue lines (see Figure 3.33) indicate the weighted average emissions factors calculated from the CVS and PEMS results, respectively, whereas the dotted green lines (see Figure 3.33) represent the US-EPA Tier2-Bin5 standards for $NO_x$, CO, and THC, and the EPA advertised label value for $CO_2$, respectively. A

significant reduction in emissions factors for criteria pollutants can be noticed between '*Bag 1*' versus '*Bag 2 & 3*' which is attributed to the change in conversion efficiencies as the after-treatment system is being warmed-up after the cold-start. It takes approximately 2 minutes to warm-up the after-treatment system as can be concluded from the drastic drop in emissions rates in Figure 3.32. $NO_x$, CO, and THC emissions are reduced by 92%, 61% and 94%, respectively, between '*Bag 1*' (cold start) and '*Bag 2*' (stabilized phase). Table 3.13 lists the weighted emissions factors for the criteria pollutants and $CO_2$ as calculated from CVS system and PEMS measurements along with the US-EPA Tier2-Bin5 (at full useful life) standards. It can be noticed that weighted $NO_x$ emissions are approximately 60% below the applicable standard. Note that although the CO difference between the CVS and PEMS is large, these measurements are two orders of magnitude lower than the Tier2-Bin5 regulatory limit.

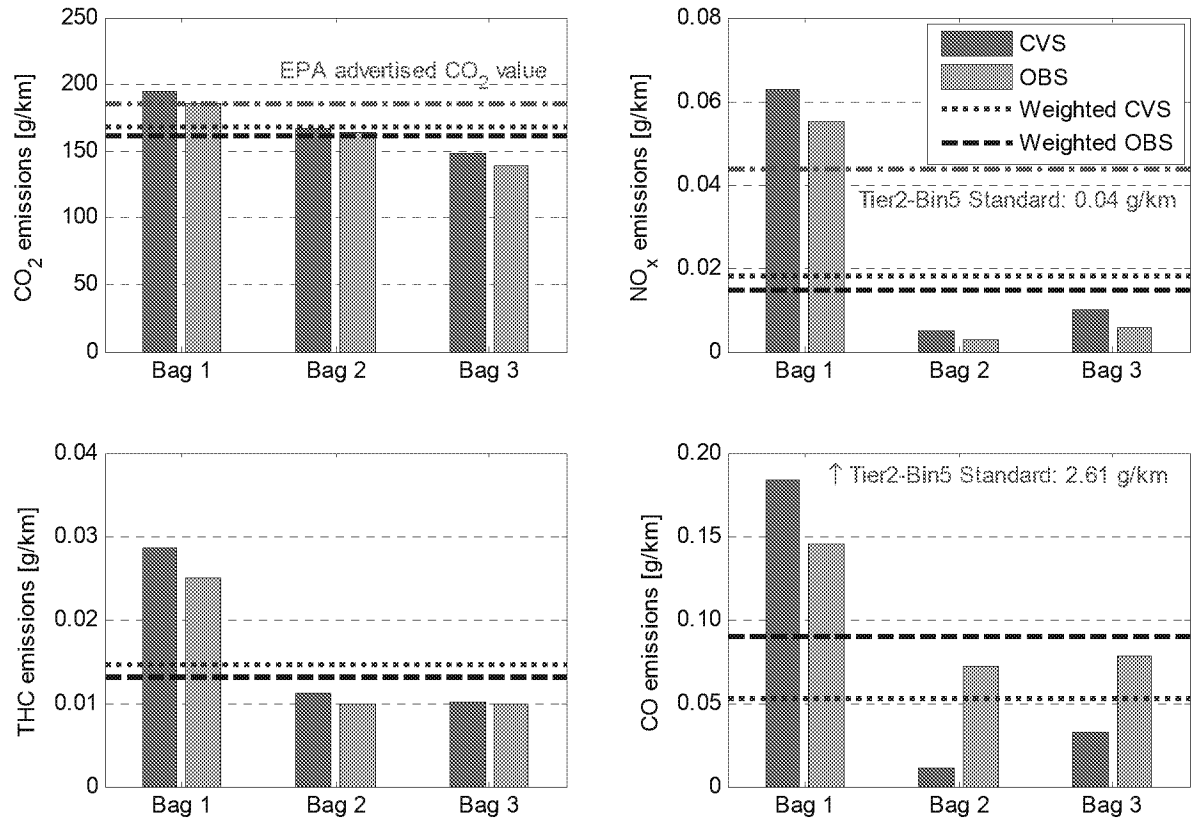


**Figure 3.33: Comparison of integrated emissions rates between CVS laboratory (CARB, El Monte, CA) and Horiba OBS-2200 PEMS for bags 1 through 3 of the FTP-75 standard chassis dynamometer test cycle. Note: red dotted and blue dashed lines represent weighted emission rates from the CVS and PEMS; green dotted lines are US-EPA Tier2-Bin5 standards (@ full useful life)**

**Table 3.13: Weighted emissions factors over FTP-75 test cycle measured by CVS system and PEMS vs. US-EPA Tier2-Bin5 standard (at full useful life) and EPA advertised $CO_2$ values for *Vehicle B*; along with relative differences between measurement systems**

| Category | $CO_2$ [g/km] | $NO_x$ [g/km] | THC [g/km] | CO [g/km] |
|---|---|---|---|---|
| Tier2-Bin5 | 186 [1)] | 0.043 | 0.056 [3)] | 2.610 |
| Weighted CVS | 167.69 | 0.018 | 0.014 | 0.053 |
| Weighted PEMS | 161.59 | 0.015 | 0.013 | 0.089 |
| **Difference** | **[%]** | **[%]** | **[%]** | **[%]** |
| Tier2-Bin5 vs. CVS | 9.8 [2)] | 58.0 | 74.1 | 98.0 |
| Tier2-Bin5 vs. PEMS | 13.1 [2)] | 65.9 | 76.5 | 96.6 |
| CVS vs. PEMS | 3.6 | 18.8 | 9.4 | -69.8 |

[1)] *EPA advertised $CO_2$ emissions value for Vehicle B (www.fueleconomy.gov) [2]*
[2)] *CVS and PEMS vs. EPA advertised $CO_2$ emissions value for Vehicle B*
[3)] *NMOG standards taken for THC limit*

Similarly, Figure 3.34 depicts the emissions factors for the criteria pollutants and $CO_2$ over the two bags of the NEDC, where '*Bag 1*' refers to urban driving including cold-start during the first portion (i.e. four repeats of ECE) and '*Bag 2*' to high-speed highway driving conditions during the second portion (i.e. one repeat of EUDC) of the cycle. The significant reduction in $NO_x$, CO, and THC emissions of 65%, 99%, and 95% between '*Bag 1*' and '*Bag 2*' is attributed to the fully warmed up after-treatment system during the second portion of the test cycle, thus, leading to improved emissions conversion efficiencies.

Additionally, Figure 3.34 shows a 40% reduction in $CO_2$ emissions factor between urban and highway driving conditions that translates into an approximately 67% improvement in fuel economy from ~28mpg to ~48mpg, respectively.

Table 3.14 summarizes the emissions factors over the NEDC for both CVS system and PEMS along with the relative differences. As seen in this table, there is good correlation between the CVS and PEMS unit for $CO_2$ and $NO_x$ while a relatively large variation in THC and CO was observed (i.e. especially for '*Bag 2*'). The relative error in the THC and CO emissions should be kept in perspective with the relatively low levels as compared to the regulatory emissions limits.

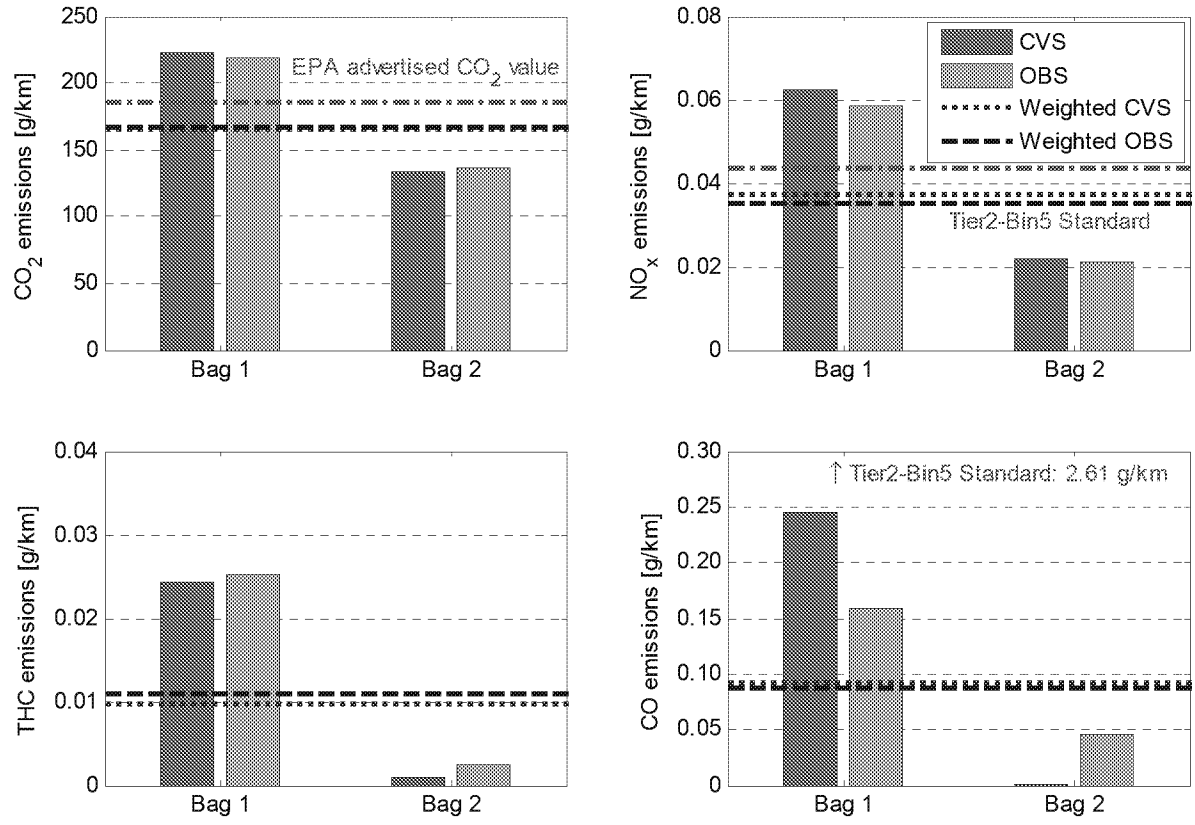


**Figure 3.34: Comparison of integrated emissions rates between CVS laboratory (CARB, El Monte, CA) and Horiba OBS-2200 PEMS over the NEDC standard chassis dynamometer test cycle. Note: red dotted and blue dashed lines represent weighted emission rates from the CVS and PEMS; green dotted lines are US-EPA Tier2-Bin5 standards (@ full useful life)**

**Table 3.14: Emissions factors over the NEDC test cycle as measured by CVS system and PEMS; along with relative differences between measurement systems**

| Category | $CO_2$ [g/km] | $NO_x$ [g/km] | THC [g/km] | CO [g/km] |
|---|---|---|---|---|
| CVS '*Bag 1*' | 222.28 | 0.063 | 0.024 | 0.246 |
| CVS '*Bag 2*' | 133.09 | 0.022 | 0.001 | 0.001 |
| PEMS '*Bag 1*' | 218.42 | 0.059 | 0.025 | 0.159 |
| PEMS '*Bag 2*' | 136.73 | 0.021 | 0.003 | 0.045 |
| Total CVS | 166.10 | 0.037 | 0.010 | 0.092 |
| Total PEMS | 166.96 | 0.035 | 0.011 | 0.087 |
| **Difference** | **[%]** | **[%]** | **[%]** | **[%]** |
| CVS vs. PEMS '*Bag 1*' | 1.7 | 6.1 | -3.5 | 35.2 |
| CVS vs. PEMS '*Bag 2*' | -2.7 | 4.2 | -151.6 | -3688.8 |
| CVS vs. PEMS '*Total*' | -0.5 | 5.4 | -13.1 | 5.0 |

## 3.4 Vehicle Test Matrix

The test matrix followed during this study is given in Table 3.15. *Vehicle A* was tested over routes 1 through 4, performing two repeats of each route. *Vehicle B* was tested over routes 1 through 5, and additionally over a total distance of ~3968 km between Los Angeles, CA and Seattle, WA. Testing of *Vehicle C* involved driving over routes 1 through 3 as well as route 5. Test routes that were repeated twice were driven with alternating drivers in order to make emissions results independent from a specific driver, hence, driving style. All test routes (i.e. Route 1 through 5) for all three vehicles were performed with the engine and aftertreatment system in warmed-up condition.

**Table 3.15: Vehicle test matrix**

| Route | Vehicle A | Vehicle B | Vehicle C |
|---|---|---|---|
| Route 1: highway | 2 | 2 | 1 |
| Route 2: urban (Los Angeles) | 2 | 2 | 2 |
| Route 3: rural - uphill/downhill | 2 | 2 | 3 |
| Route 4: urban (San Diego) | 2 | 2 | |
| Route 5: urban (San Francisco) | | 1 | 2 |
| Cross-State Trip CA to WA | | X | |

## 3.5 Data Analysis and Emissions Calculations

All data analysis and data quality assurance as well as emissions calculations presented herein are following recommendations outline in CFR, Title 40, Subpart 1065 D, G, and J [29] as well as WVU CAFEE internal and publicly available standard operating procedures (SOP). Drift correction for measured exhaust concentrations, emissions mass rates and distance or work-specific emissions factors are calculated according to CFR, Title 40, Subpart G [29], while moving averaging window method (AWM) calculations follow Annex B of the European draft on PEMS measurement for light-duty vehicles as well as guidelines prescribed in the European Regulations No. 582/2011 for in-use emissions from heavy-duty vehicles [3]. The integrated emissions results and averaging window emissions factors presented in this report are based on total emissions emitted over a given test route and are not corrected for any exclusion conditions such as exhaust temperature limits, altitude, DPF regeneration events or similar. Also, all averaging windows were considered for calculation and none were invalidated based on the 20% minimum power condition as outlined in the European Regulations No. 582/2011 [3]. Additional

information about specific emissions calculating procedures applied to data presented in this report is given in Appendix 7.1.

# 4 RESULTS AND DISCUSSION

The results chapter will discuss the average on-road emissions for the criteria pollutants and $CO_2$ from all three test vehicles in Section 4.1 for the pre-defined test routes (see Section 4.1.1) as well as the cross-multi state driving route (see Section 4.1.2), followed by an in depth analysis of the $NO_x$ emissions using the averaging window method in Section 4.2. Finally, individual results for particle number concentrations and PM mass will be presented and discussed in Section 4.3 of this chapter.

This report presents gaseous emissions mass rates in [g/s] and emissions factors in [g/km], while particle number and mass concentrations are reported in [#/cm$^3$] and [mg/m$^3$], respectively, and particle number and mass emissions factors in [#/km] and [mg/km], respectively. Along with distance-specific emissions, dimensionless deviation ratios (DR) are reported for each emissions constituent as a measure of how much the actual on-road emissions are deviating from the regulatory limit. The calculation of deviation ratios is given by Equation 11 and follows the European regulation for emissions from heavy-duty vehicles [3] and recommendations made by Weiss *et al.* [1], where $m_{x_i}$ and $[s(t_{end}) - s(t_{start})]_i$ are the emissions mass and distance traveled for a given averaging window or test route, respectively. $EF_{x\ stand}$ was selected to be the regulatory limit for the respective pollutant as given by Table 4.1.

$$DR_i = \frac{\frac{m_{x_i}}{[s(t_{end}) - s(t_{start})]_i}}{EF_{x_{standard}}} \qquad \textbf{Eq. 11}$$

**Table 4.1: Applicable regulatory emissions limits and other relevant vehicle emission reference values; US-EPA Tier2-Bin5 at full useful life (10years/ 120,000 mi) for $NO_x$, CO, THC (eq. to NMOG), and PM [6]; EPA advertised $CO_2$ values for each vehicle [2]; Euro 5b/b+ for PN [4]**

| $NO_x$ [g/km] | CO [g/km] | THC [g/km] | $CO_2$ [g/km] | PM [g/km] | PN [#/km] |
|---|---|---|---|---|---|
| 0.043 | 2.610 | 0.056 | 193 (*Vehicle A*)<br>186 (*Vehicle B*)<br>288 (*Vehicle C*) | 0.006 | $6.0 \times 10^{11}$ |

DPF regeneration events occurring during on-road operation of the test vehicles were identified by a simultaneous increase in particle number concentrations as measured with the Pegasor particle sensor and exhaust gas temperatures measured downstream of the DPF. For test runs with DPF regeneration events exhaust gas temperatures were observed to increase to

approximately 600°C which is required to initiate the periodic soot oxidation from the surface of the filter substrate. Table 4.2 lists the individual test runs for each route and vehicle that exhibited a DPF regeneration event.

**Table 4.2: Identified DPF regeneration events during vehicle operation over the five test routes**

| Route | Vehicle A | Vehicle B | Vehicle C |
|---|---|---|---|
| Route 1: highway | Run 2 | - | - |
| Route 2: urban (Los Angeles) | - | Run 1 | - |
| Route 3: rural - uphill/downhill | Run 1 | Run 1 & 2 | - |
| Route 4: urban (San Diego) | Run 2 | - | (*nd*) |
| Route 5: urban (San Francisco) | (*nd*) | - | - |

*nd - vehicle not tested over this specific route*

For comparison purposes with on-road emissions presented hereinafter, Figure 4.1 and Figure 4.2 show average $CO_2$ and $NO_x$ emissions factors, respectively, for *Vehicles A* and *B* as measured over three standard vehicle certification test cycles while operated on CARB's El Monte chassis dynamometer. The test cycles include i) the FTP-75 (presented as individual '*Bags*' and weighted average), ii) the US06, and iii) the European NEDC (presented as individual ECU and EUDC as well as weighted average).

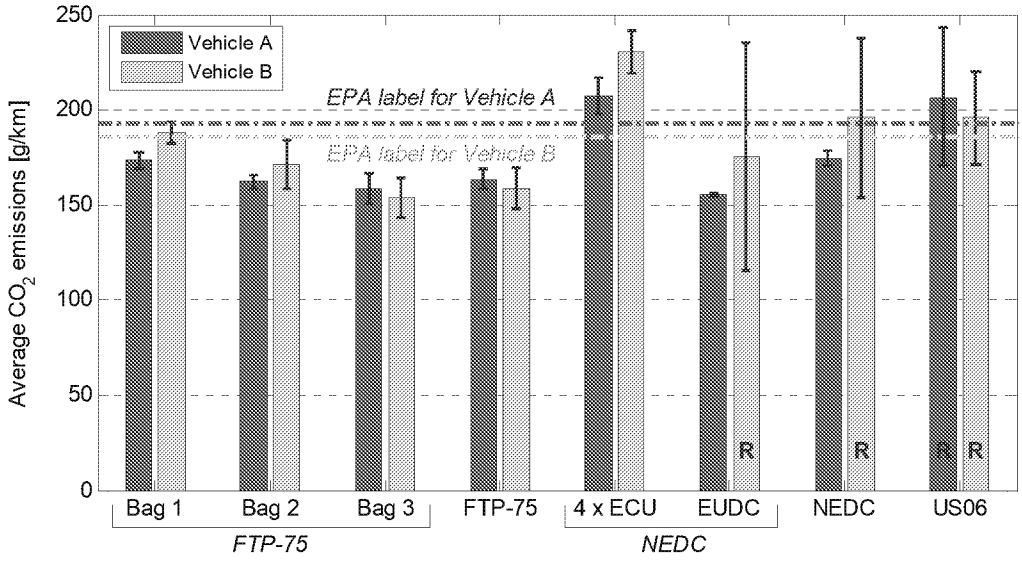


**Figure 4.1: Average $CO_2$ emissions of test vehicles A and B over three standard chassis dynamometer test cycles (FTP-75, NEDC, and US06) measured by the vehicle certification CVS laboratory (CARB, El Monte, CA) compared to EPA advertised $CO_2$ values; repeat test variation intervals are presented as ±1σ; '*R*' designates cycles including a test with DPF regeneration event**

Emissions factors presented in Figure 4.1 and Figure 4.2 were measured with CARB's CVS laboratory that is designed and operated for vehicle certification, and are compared against EPA advertised $CO_2$ values for $CO_2$ and US-EPA Tier2-Bin5, Euro 5b/b+, and Euro 6b/6c emissions standards for $NO_x$. It can be noticed that test cycles exhibiting DPF regeneration events (marked with '*R*' in Figure 4.1 and Figure 4.2) show a significant increase in both $CO_2$ and $NO_x$ emissions. $NO_x$ emissions increase by ~91% for *Vehicle A* over the US06 cycle and by ~88% to 89% for *Vehicle B* over both EUDC and US06 for test cycles with DPF regeneration events. At the same time, $CO_2$ emissions were observed to increase by ~25% for *Vehicle A* over the US06 cycle and by ~39% and ~18% for *Vehicle B* over the US06 and NEDC, respectively.

Most importantly, it can be concluded from Figure 4.2 that both *Vehicles A* and *B* are compliant with US-EPA Tier2-Bin5 emissions standards exhibiting $NO_x$ emissions at levels (i.e. weighted average) 50.4% and 64.1% below the regulatory limit (at full useful life, 10years/ 120,000 mi) over the certification FTP-75 cycle for *Vehicle A* and *B*, respectively. $NO_x$ emissions over the US06 are ~97.% below the US-EPA Tier2-Bin5 standard for the SCR equipped *Vehicle B* and approximately ~58% above the standard for *Vehicle A*, during test runs without DPF regeneration event for both vehicles.

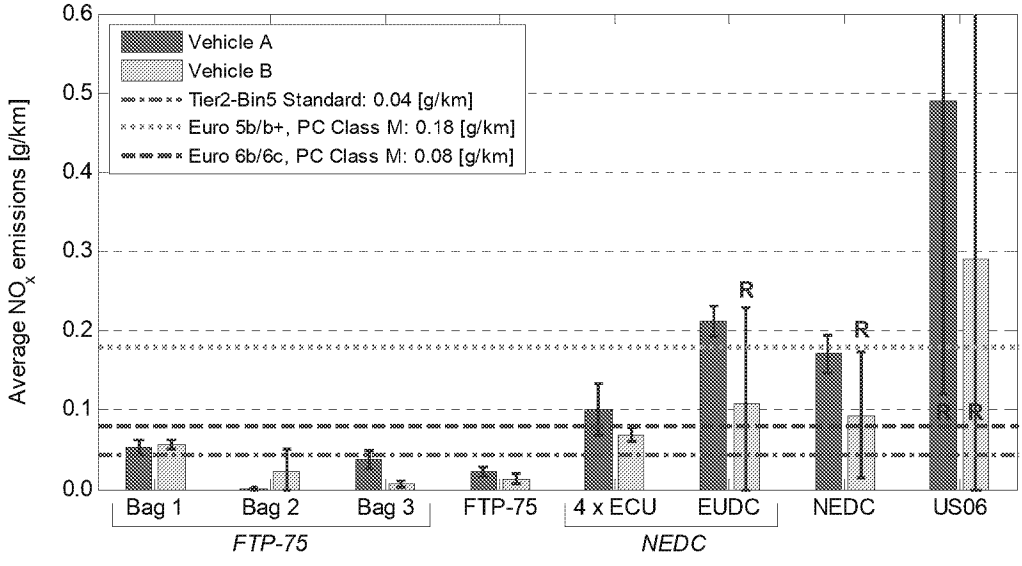


**Figure 4.2: Average $NO_x$ emissions of test vehicles A and B over three standard chassis dynamometer test cycles (FTP-75, NEDC, and US06) measured by the vehicle certification CVS laboratory (CARB, El Monte, CA) compared to US-EPA Tier2-Bin5 (at full useful life, 10years/ 120,000 mi), Euro 5b/b+, and Euro 6b/6c emissions standards; repeat test variation intervals are presented as ±1σ; '*R*' designates cycles including a test with DPF regeneration event**

## 4.1 Average On-Road Emissions of Light-Duty Vehicles

This chapter will present average on-road emissions factors for gaseous, including $NO_x$, CO, THC, and $CO_2$ as well as particle number and mass emissions as measured over pre-defined test routes for all three vehicles (see Section 4.1.1) and over the cross-multi state driving route for *Vehicle B* (see Section 4.1.2). Results presented in this chapter are reported as total emissions over the respective routes and are not corrected for any data exclusion conditions. All three test vehicles exhibited warmed-up engine and after-treatment conditions before being operated over a test route, thus, average emissions results presented in this chapter will be compared to '*Bag-3*' emissions levels as measured over the FTP-75 chassis dynamometer test cycle.

### 4.1.1 Emissions over Pre-Defined Test Routes

Figure 4.3 along with Figure 4.4 show average $NO_x$ emissions factors and their respective deviation ratio from the US-EPA Tier2-Bin5 standard, respectively, over the five pre-defined test routes for vehicles A through C. Additionally, Table 4.3 summarizes the average values and standard deviation (1σ) computed over two consecutive repetitions of a given test route.

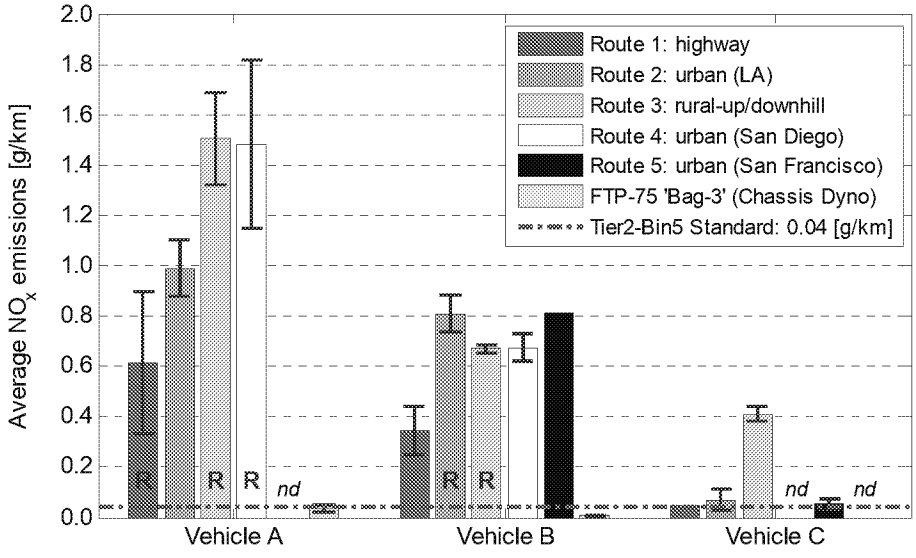


**Figure 4.3: Average $NO_x$ emissions of test vehicles over the five test routes compared to US-EPA Tier2-Bin5 emissions standard; repeat test variation intervals are presented as ±1σ; Route 1 for Vehicle A includes rush-hour/non rush-hour driving, '*R*' designates routes including a test with DPF regeneration event, '*nd*' - no data available**

In general, $NO_x$ emissions factors are highest for rural-up/downhill and lowest for high-speed highway driving conditions. All three test vehicles show distinct $NO_x$ emissions patterns, with the LNT equipped *Vehicle A* exhibiting $NO_x$ values 15 to 35, and the urea-SCR equipped

*Vehicle B* $NO_x$ values 5 to 20 times the Tier2-Bin5 standard depending on test route. *Vehicle C* was observed to emit $NO_x$ emissions around or below the Tier2-Bin5 standard except during the rural-up/downhill route (Route 3), where emissions averaged 0.41 g/km or ~10 times the Tier2-Bin5 standard.

*Vehicle A* and *B* are outfitted with the same engine model. However, they also feature different after-treatment systems allowing to conclude, based on the available data, that the LNT shows deficiencies over the urea-SCR system in efficiently reducing $NO_x$ in-use, especially during highly transient, low-speed urban driving as well as high-load uphill driving. On the other hand, *Vehicles B* and *C* are both equipped with a similar after-treatment technology, namely urea-SCR, but show significantly different $NO_x$ emissions factors for the same test routes. This could be caused by i) different after-treatment control strategies, ii) a difference in catalytic substrate between the two vehicles (different SCR type), iii) under-sized SCR catalyst for *Vehicle B*, or iv) different diesel exhaust fluid (DEF) injection strategy in case of *Vehicle B* to reduce DEF consumption, hence, increasing DEF re-filling intervals.

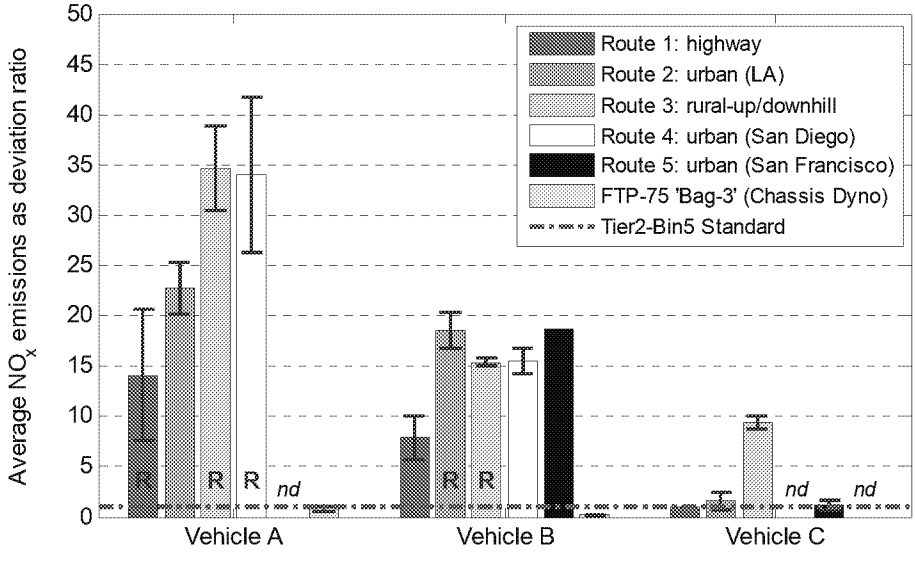


**Figure 4.4: Average $NO_x$ emissions of test vehicles over the five test routes expressed as deviation ratio; repeat test variation intervals are presented as ±1σ, '*R*' designates routes including a test with DPF regeneration event, '*nd*' - no data available**

It has to be noted that all three vehicles were checked for possible engine or after-treatment malfunction codes using an ECU scanning tool prior to selecting each vehicle for this on-road measurement campaign, with none of them showing any fault code or other anomalies. The after-

treatment system was assumed to be '*de-greened*' as all three vehicles had accumulated more than 3,000 to 4,000 miles, and no reduction in catalytic activity due to aging was expected as the total mileage was relatively low (< 15,000 miles) for all test vehicles.

Interestingly, $NO_x$ emissions for *Vehicles A* and *B* were below the US-EPA Tier2-Bin5 standard for the weighted average over the FTP-75 during chassis dynamometer testing at CARB's El Monte facility. $NO_x$ emissions were 0.022g/km ±0.006g/km (±1σ, 2 repeats) and 0.016g/km ±0.002g/km (±1σ, 3 repeats) for *Vehicle A* and *B*, respectively, during chassis dynamometer testing (i.e. weighted FTP-75 results). This is further confirmation that *Vehicles A* and *B* were operating as intended and did not have any malfunctions.

The LNT equipped *Vehicle A* shows increased variability between two consecutive test runs, especially for Routes 1, 3, and 4. This behavior coincides with DPF regeneration events (see Figure 4.45 through Figure 4.52) that are occurring during one of the repeats for the above listed routes. $NO_x$ emissions factors increase by 97% (0.41 g/km to 0.81g/km), 19% (1.38g/km to 1.63g/km), and 38% (1.24g/km to 1.72g/km) for Routes 1, 3, and 4, respectively, between test runs with and without DPF regeneration events. It has to be mentioned that the same test run exhibiting the DPF regeneration event for Route 1 also experienced increased stop-and-go traffic conditions during evening rush-hours, thereby confounding the factors leading to the 97% increase in $NO_x$ compared to the test run without DPF regeneration event. Referring to reference [31] presenting a detailed discussion of DPF regeneration as well as LNT $D_eNO_x$ and $D_eSO_x$ regeneration strategies and control mechanisms, it can be noted (from Figure 12 in [31]) that during an ongoing DPF regeneration event no cyclic $D_eNO_x$ regeneration of the LNT occurs. As described by [31], DPF regeneration happens under oxygen surplus conditions ($\lambda > 1$) and is on the order of up to 15min in duration. Therefore, it is speculated that due to a lack of frequent enrichment of the exhaust gas ($\lambda < 1$) while DPF regeneration is ongoing, necessary LNT regeneration is inhibited, and thus, the $NO_x$ storage catalyst becomes saturated with $NO_x$ emissions starting to break through. Indeed, increased $NO_x$ mass rates were observed from continuous data coinciding with DPF regeneration events during Routes 1, 3, and 4.

Furthermore, when comparing THC emissions factors shown in Figure 4.7 with $NO_x$ emissions factors in Figure 4.3 for *Vehicle A*, it can be noticed that highest THC emissions are exhibited during test routes with lowest $NO_x$ emissions, specifically, for Routes 1 and 2.

Increased THC values could point towards an increased frequency of rich mode operation, thus, leading to an improved $NO_x$ reduction over the LNT catalyst. However, no conclusive explanation can be presented herein for why this behavior is observed, especially considering the vastly different driving conditions experienced between Routes 1 and 2, with Route 1 being representative of highway and Route 2 of urban driving. Additionally, Route 1 included a test run with a DPF regeneration event which normally leads to increased THC emissions, however, appears to have been masked by the order of magnitude increase in THC emissions (see Figure 4.7) caused by this unexplained event.

**Table 4.3: Average $NO_x$ emissions in [g/km] of test vehicles over the five test routes; σ is standard deviation over two consecutive test runs, Route 1 for Vehicle A includes rush-hour/non rush-hour**

| Route | | Vehicle A | Vehicle B | Vehicle C |
|---|---|---|---|---|
| Route 1: highway | μ | **0.614** | **0.344** | **0.048** |
| | σ | *0.283* | *0.096* | - |
| Route 2: urban (LA) | μ | **0.989** | **0.809** | **0.070** |
| | σ | *0.114* | *0.075* | *0.041* |
| Route 3: rural-up/downhill | μ | **1.505** | **0.671** | **0.409** |
| | σ | *0.181* | *0.016* | *0.029* |
| Route 4: urban (San Diego) | μ | **1.480** | **0.675** | - |
| | σ | *0.335* | *0.057* | - |
| Route 5: urban (San Francisco) | μ | - | **0.815** | **0.053** |
| | σ | - | - | *0.021* |

Figure 4.5 along with Figure 4.6 show average CO emissions factors and their respective deviation ratio from the US-EPA Tier2-Bin5 standard, respectively, over the five pre-defined test routes for *Vehicles A* through *C*. Additionally, Table 4.4 summarizes the average values and standard deviations (1σ) computed over two consecutive repetitions of a given test route.

In general, CO emissions factors are close to two orders of magnitude lower than the applicable US-EPA Tier2-Bin5 standard for all three vehicles and no particular pattern in CO emissions rates can be found as a function of driving and/or route conditions. For *Vehicles A* and *B*, highest CO emissions factors were exhibited during urban driving in Los Angeles (i.e. Route 2), whereas *Vehicle C* showed highest CO for rural-up/downhill driving (i.e. Route 3), which however, is accompanied by a significant variation (of same order than mean value) between repeated test runs. The increased variation in CO emissions factor for *Vehicle B* over Route 2

coincides with a regeneration event during one of the test runs leading to an order of magnitude increase in CO emissions from 0.02g/km to 0.26g/km.

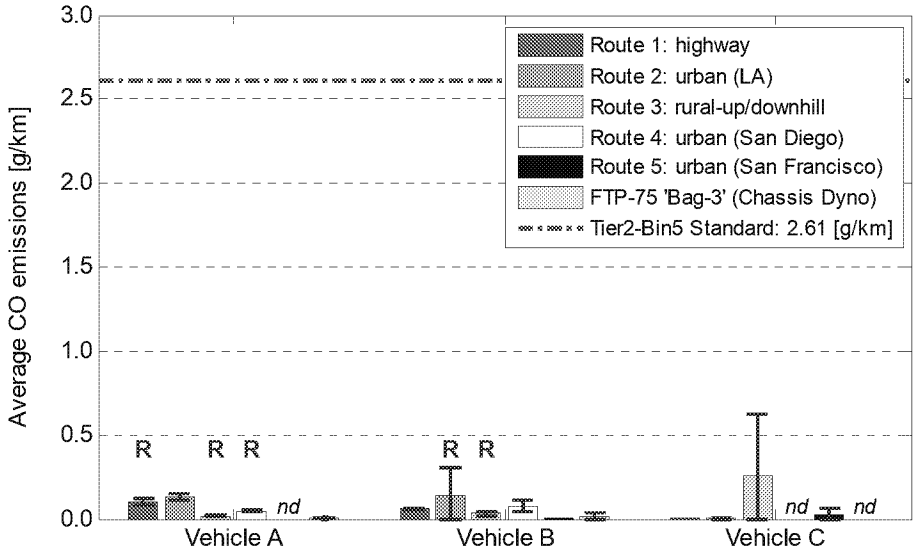


**Figure 4.5: Average CO emissions of test vehicles over the five test routes compared to US-EPA Tier2-Bin5 emissions standard; repeat test variation intervals are presented as ±1σ; Route 1 for Vehicle A includes rush-hour/non rush-hour driving, '*R*' designates routes including a test with DPF regeneration event, '*nd*' - no data available**

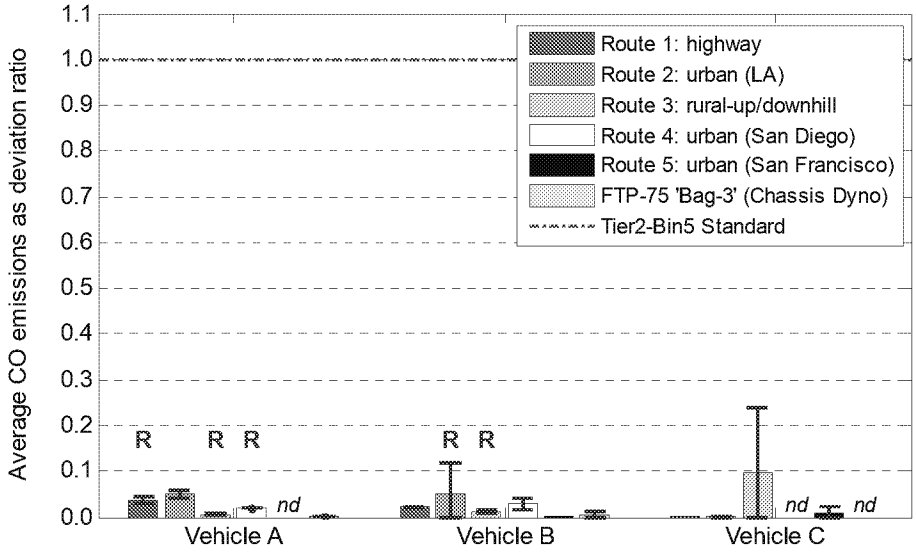


**Figure 4.6: Average CO emissions of test vehicles over the five test routes expressed as deviation ratio; repeat test variation intervals are presented as ±1σ, '*R*' designates routes including a test with DPF regeneration event, '*nd*' - no data available**

**Table 4.4: Average CO emissions in [g/km] of test vehicles over the five test routes; σ is standard deviation over two consecutive test runs, Route 1 for Vehicle A includes rush-hour/non rush-hour**

| Route | | Vehicle A | Vehicle B | Vehicle C |
|---|---|---|---|---|
| Route 1: highway | μ | **0.100** | **0.059** | **0.000** |
| | σ | 0.019 | 0.004 | - |
| Route 2: urban (LA) | μ | **0.130** | **0.138** | **0.004** |
| | σ | 0.021 | 0.169 | 0.005 |
| Route 3: rural-up/downhill | μ | **0.018** | **0.029** | **0.256** |
| | σ | 0.005 | 0.010 | 0.369 |
| Route 4: urban (San Diego) | μ | **0.048** | **0.076** | - |
| | σ | 0.001 | 0.033 | - |
| Route 5: urban (San Francisco) | μ | - | **0.007** | **0.027** |
| | σ | - | - | 0.038 |

Figure 4.7 along with Figure 4.8 show average THC emissions factors and their respective deviation ratio from the US-EPA Tier2-Bin5 standard, respectively, over the five pre-defined test routes for *Vehicles A* through *C*. Additionally, Table 4.5 summarizes the average values and standard deviations (1σ) computed over two consecutive repetitions of a given test route.

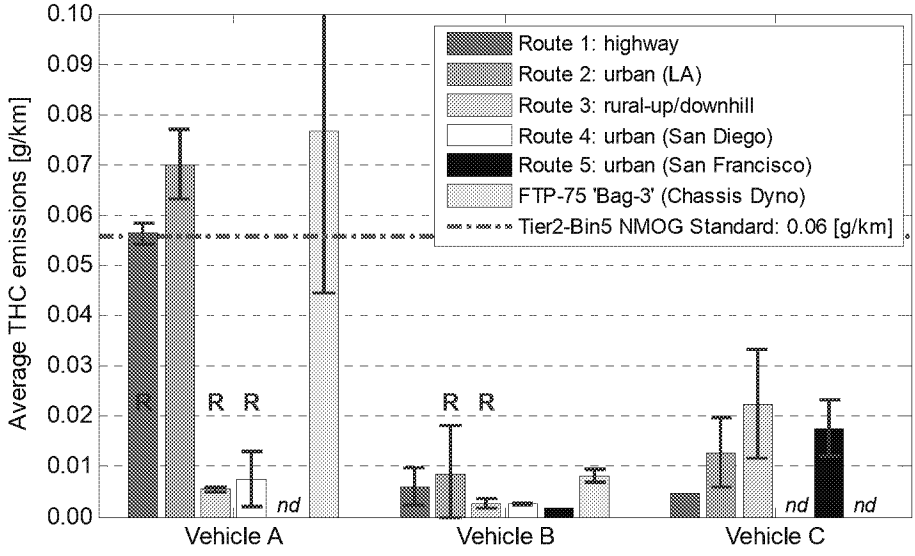


**Figure 4.7: Average THC emissions of test vehicles over the five test routes compared to US-EPA Tier2-Bin5 emissions standard; repeat test variation intervals are presented as ±1σ; Route 1 for Vehicle A includes rush-hour/non rush-hour driving, '*R*' includes DPF regeneration events**

It has to be noted that chassis dynamometer testing of *Vehicle A* and *B* indicated that 95 - 98% of the total hydrocarbons emitted were measured as methane ($CH_4$) which is somewhat surprising for diesel fueled vehicles, however, could be attributed to reactions over the catalytic

surface of the oxidation catalyst or the LNT in case of *Vehicle A*. The NMOG Tier2-Bin5 standard was chosen for comparison as it is currently the only applicable standard for hydrocarbons for Tier 2 light-duty vehicles in the US and since NMOG primarily comprises NMHC for diesel and gasoline fueled vehicles. However, in light of the large $CH_4$/THC ratio observed during chassis dynamometer testing, conclusions between the measured THC emissions during on-road operation and the NMOG standard have to be drawn with caution.

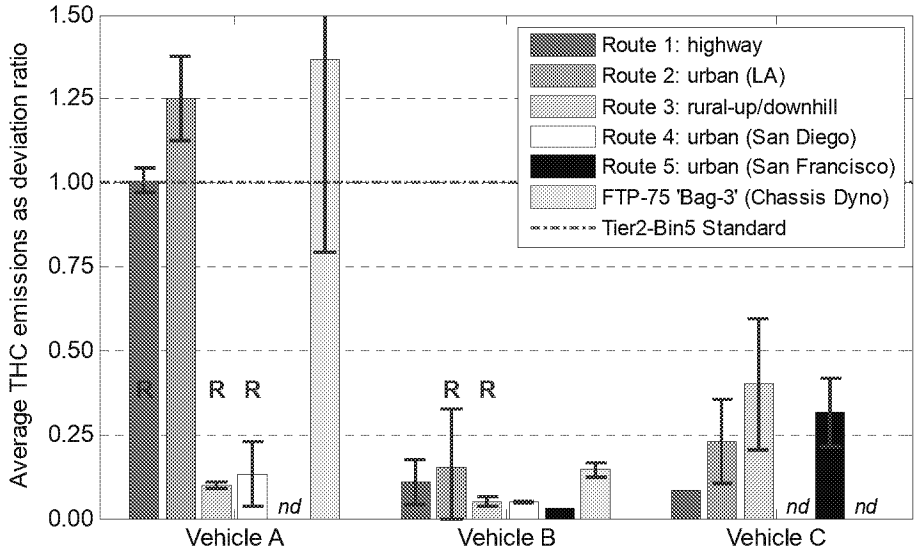


**Figure 4.8: Average THC emissions of test vehicles over the five test routes expressed as deviation ratio; repeat test variation intervals are presented as ±1σ, '*R*' designates routes including a test with DPF regeneration event, '*nd*' - no data available**

**Table 4.5: Average THC emissions in [g/km] of test vehicles over the five test routes; σ is standard deviation over two consecutive test runs, Route 1 for Vehicle A includes rush-hour/non rush-hour**

| Route | | Vehicle A | Vehicle B | Vehicle C |
|---|---|---|---|---|
| Route 1: highway | **μ** | **0.056** | **0.006** | **0.005** |
| | *σ* | *0.002* | *0.004* | - |
| Route 2: urban (LA) | **μ** | **0.070** | **0.009** | **0.013** |
| | *σ* | *0.007* | *0.010* | *0.007* |
| Route 3: rural-up/downhill | **μ** | **0.005** | **0.003** | **0.022** |
| | *σ* | *0.000* | *0.001* | *0.011* |
| Route 4: urban (San Diego) | **μ** | **0.007** | **0.003** | - |
| | *σ* | *0.005* | *0.000* | - |
| Route 5: urban (San Francisco) | **μ** | - | **0.002** | **0.018** |
| | *σ* | - | - | *0.006* |

In general, THC emissions factors are well below the US-EPA Tier2-Bin5 NMOG standard for *Vehicles B* and *C* as well as over Routes 3 and 4 for *Vehicle A*. Only for *Vehicle A* and Routes 1 and 2, THC emissions were observed at (i.e. Route 1, highway) or exceeding (i.e. Route 2, urban Los Angeles, by 1.25) the NMOG standard. However, this has already been discussed in more detail along with the average $NO_x$ results above. *Vehicle A* and *B* showed a tendency for increased THC emissions during test runs with DPF regeneration events compared to tests without such events, however, the same has not been observed for *Vehicle C*.

Figure 4.9 along with Figure 4.10 show average $CO_2$ emissions factors and their respective deviation ratio from EPA advertised $CO_2$ values for each vehicle, respectively, over the five pre-defined test routes for *Vehicles A* through *C*. Additionally, Table 4.6 summarizes the average values and standard deviations (1σ) computed over two consecutive repetitions of a given test route. In general, and as expected, highway driving showed lowest $CO_2$, whereas urban/suburban driving conditions lead to highest $CO_2$ emissions factors.

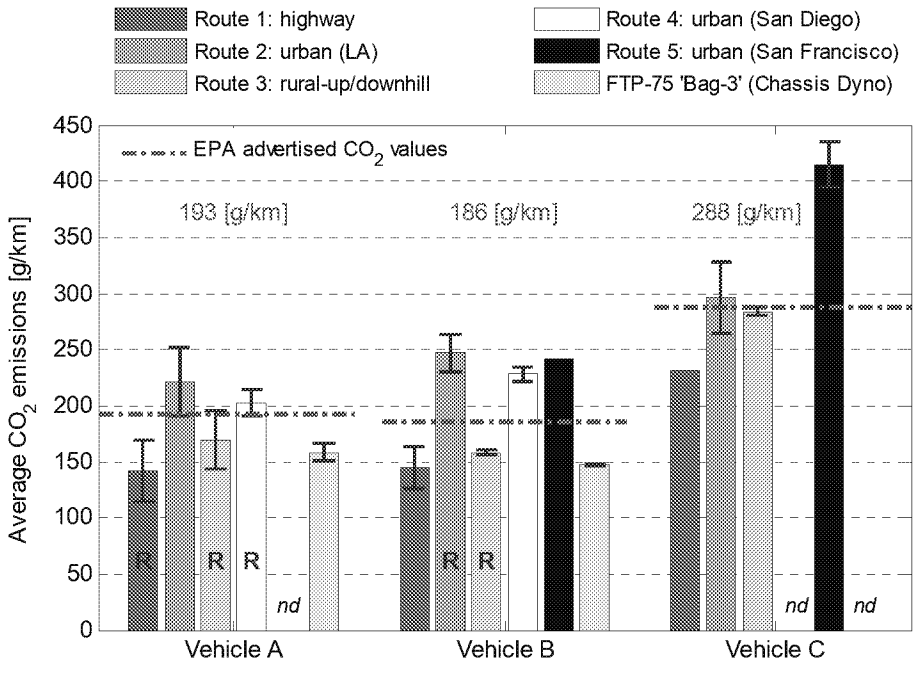


**Figure 4.9: Average $CO_2$ emissions of test vehicles over the five test routes compared to EPA advertised $CO_2$ values for each vehicle; repeat test variation intervals are presented as ±1σ; Route 1 for Vehicle A includes rush-hour/non rush-hour driving, '*R*' designates routes including a test with DPF regeneration event, '*nd*' - no data available**

Since both *Vehicle A* and *B* were equipped with the same engine their $CO_2$ consumption pattern appear similar in Figure 4.9. Routes 1 and 2 are characterized by higher average vehicle

speeds and reduced amount of stop/go conditions (especially for highway Route 1) which translates into lower vehicle acceleration events and thus, lower $CO_2$ emissions ultimately leading to improved fuel economy over these routes as shown in Figure 4.15.

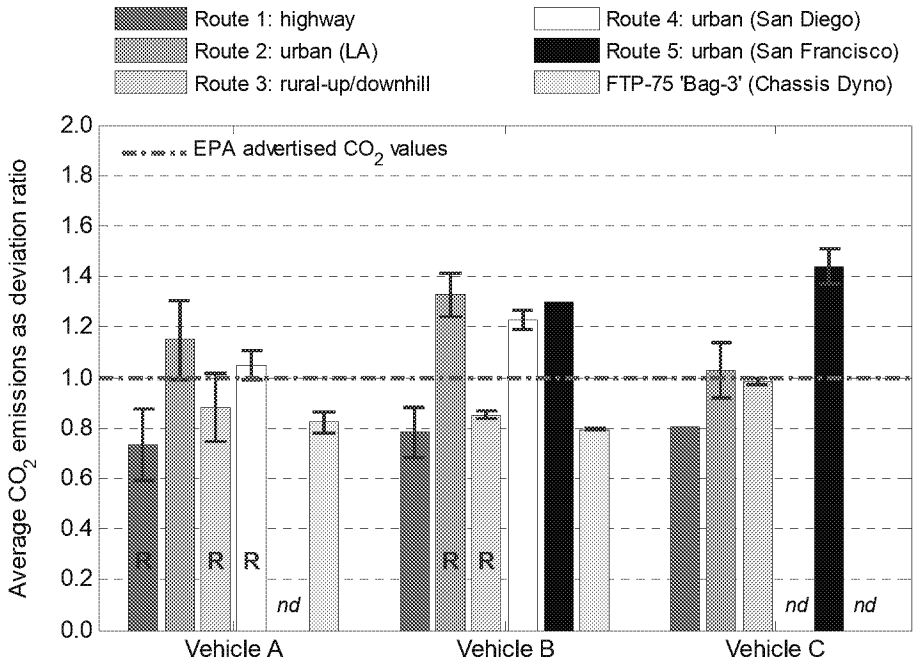


**Figure 4.10: Average $CO_2$ emissions of test vehicles over the five test routes expressed as deviation ratio from the EPA advertised $CO_2$ values; repeat test variation intervals presented as ±1σ, '*R*' designates routes including a test with DPF regeneration event, '*nd*' - no data available**

**Table 4.6: Average $CO_2$ emissions in [g/km] of test vehicles over the five test routes; σ is standard deviation over two consecutive test runs, Route 1 for Vehicle A includes rush-hour/non rush-hour**

| Route | | Vehicle A | Vehicle B | Vehicle C |
|---|---|---|---|---|
| Route 1: highway | μ | **141.9** | **145.6** | **231.8** |
| | σ | *27.0* | *18.8* | - |
| Route 2: urban (LA) | μ | **221.7** | **246.9** | **296.3** |
| | σ | *30.1* | *16.2* | *32.1* |
| Route 3: rural-up/downhill | μ | **169.8** | **158.6** | **283.6** |
| | σ | *25.6* | *2.5* | *3.6* |
| Route 4: urban (San Diego) | μ | **202.3** | **228.2** | - |
| | σ | *11.5* | *6.8* | - |
| Route 5: urban (San Francisco) | μ | - | **241.8** | **414.4** |
| | σ | - | - | *20.2* |

On the other hand, urban driving conditions lead to increased fuel consumption, hence, more $CO_2$ emissions as seen for urban routes 2, 4, and 5. Differences between $CO_2$ emissions factors

for *Vehicle A* and *B* could be attributed to varying traffic patterns over a given route, influences of ambient conditions as both vehicles were tested on a different day (however, within the span of two weeks during March), and most importantly variations in driving style as the experiments have been conducted with three different drivers.

Highway driving (i.e. Route 1) for *Vehicle A* includes non-rush-hour as well as evening rush-hour conditions causing the variability in $CO_2$ emissions factor seen in Figure 4.9. During rush-hour conditions, $CO_2$ emissions increased by ~31% from 123g/km to 161g/km. Furthermore, based on data for *Vehicles A* and *B*, it is observed that $CO_2$ emissions are generally increased during test runs with DPF regeneration events which could be explained by the oxidation of carbon from the DPF substrate as well additional fuel injected to augment exhaust gas and after-treatment temperatures in order to initiate and sustain DPF regeneration.

Overall, $CO_2$ emissions from *Vehicles A* and *B* compare well with $CO_2$ emissions observed during chassis dynamometer testing over the NEDC which consists of a dedicated urban/suburban (i.e. '*Bag 1*') and highway (i.e. '*Bag 2*') driving portion. The urban/suburban driving portion of the NEDC exhibited 212.3g/km ±11.2g/km (±1σ, 3 tests of which are 2 with *Vehicle A* and 1 with *Vehicle B*), whereas the highway driving resulted in 148.0g/km ±12.9g/km (±1σ, same sample set) of $CO_2$ on the chassis dynamometer.

Finally, increased variability was observed over the two urban routes in Los Angeles and San Francisco (i.e. Routes 2 and 5) for *Vehicle C*, which can be attributed to differences in driving style between the two drivers, as well as changing traffic patterns between repeated test runs. Furthermore, the topographical differences between Routes 2 and 5 (flat vs. hilly) seem to influence the $CO_2$ emissions factor to a higher degree for *Vehicle C* as compared to *Vehicle B*. This could be caused by the heavier overall weight of *Vehicle C*, which was ~54% heavier than *Vehicle B*, as well as the larger engine (~52% larger displacement for *Vehicle C*), leading to more aggressive accelerations, especially under the hilly and often larger road grade conditions as experienced over Route 5 (i.e. San Francisco).

Figure 4.11 along with Figure 4.12 show average particulate mass (PM) emissions factors and their respective deviation ratio from the US-EPA Tier2-Bin5 standard, respectively, over the five pre-defined test routes for *Vehicles A* and *B*. Additionally, Table 4.7 summarizes the average values and standard deviations (1σ) computed over two consecutive repetitions of a given test

route. It has to be noted that particulate masses reported in Figure 4.11 and Figure 4.12 are not directly measured masses via traditional filter samples, but rather inferred from a charge based real-time particle sensor as described in more detail in Section 3.3.2.2.

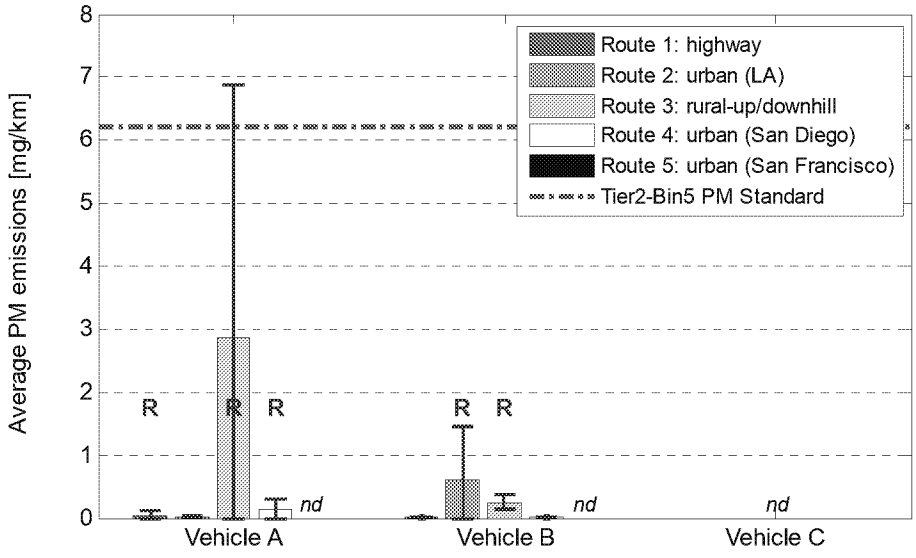


**Figure 4.11: Average PM emissions of test vehicles over the five test routes compared to US-EPA Tier2-Bin5 emissions standard; repeat test variation intervals are presented as ±1σ; Route 1 for Vehicle A includes rush-hour/non rush-hour driving, no PM data collected for Vehicle C, '*R*' designates routes including a test with DPF regeneration event, '*nd*' - no data available**

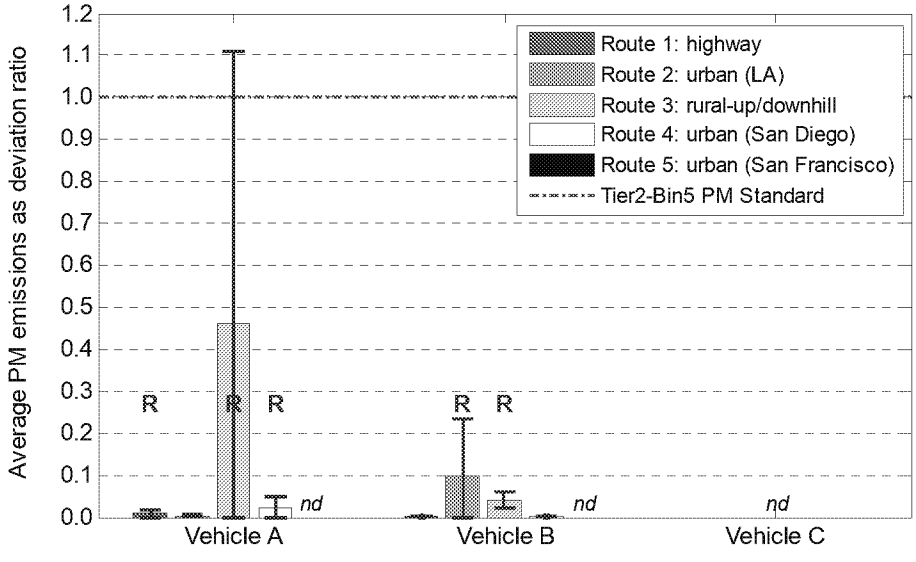


**Figure 4.12: Average PM emissions of test vehicles over the five test routes expressed as deviation ratio; uncertainty repeat test variation are presented as ±1σ; Route 1 for Vehicle A includes rush-hour/non rush-hour driving, no PM data collected for Vehicle C, '*R*' designates routes including a test with DPF regeneration event, '*nd*' - no data available**

In general, particulate mass emissions were observed to be well below the applicable US-EPA Tier2-Bin5 standard over all test routes for *Vehicles A* and *B* with the exception of Route 3 for *Vehicle A* which exhibited a DPF regeneration event during one of the test runs. Average PM emissions increased by two orders of magnitude from 0.01mg/km to 5.7mg/km between the test run with and without DPF regeneration for Route 3.

**Table 4.7: Average PM emissions in [mg/km] of test vehicles over the five test routes; σ is standard deviation over two consecutive test runs, Route 1 for Vehicle A includes rush-hour/non rush-hour**

| Route | | Vehicle A | Vehicle B | Vehicle C |
|---|---|---|---|---|
| Route 1: highway | μ | **0.051** | **0.007** | - |
| | σ | *0.058* | *0.001* | - |
| Route 2: urban (LA) | μ | **0.015** | **0.613** | - |
| | σ | *0.012* | *0.839* | - |
| Route 3: rural-up/downhill | μ | **2.858** | **0.250** | - |
| | σ | *4.023* | *0.117* | - |
| Route 4: urban (San Diego) | μ | **0.137** | **0.005** | - |
| | σ | *0.160* | *0.001* | - |
| Route 5: urban (San Francisco) | μ | - | - | - |
| | σ | - | - | - |

Figure 4.13 along with Figure 4.14 show average particulate number (PN) emissions factors and their respective deviation ratio from the European Euro 5b/b+ standard (i.e. $6x10^{11}$ #/km, same as Euro 6b effective Sept. 2014 for LDVs (Class M)), respectively, over the five pre-defined test routes for *Vehicles A* and *B*. Additionally, Table 4.8 summarizes the average along with minimum and maximum values computed over two consecutive repetitions of a given test route. Similarly to PM emissions, particulate numbers presented herein are inferred from a charge based real-time particle sensor as described in more detail in Chapter 3.3.2.2.

The European Euro 5b/b+ standard (same level as Euro 6b, effective Sept. 2014 for LDVs) has been chosen for comparison as it is currently the only particulate number standard in legislation, and applicable to new vehicles sold within the confines of the European Union [4].

Increased variation in average particulate number emissions was observed for test routes that included DPF regeneration events during one of the route repetitions. DPF regeneration events lead to a one or two order of magnitude increase in PN emissions factors when compared to test runs without DPF regeneration as seen for Routes 1, 3, and 4 as well as Routes 2, and 3 for

*Vehicle A* and *B*, respectively. Route 3 for *Vehicle B* exhibited DPF regeneration events during both repeats (see Figure 4.50) thus, leading to the observed low variability between tests.

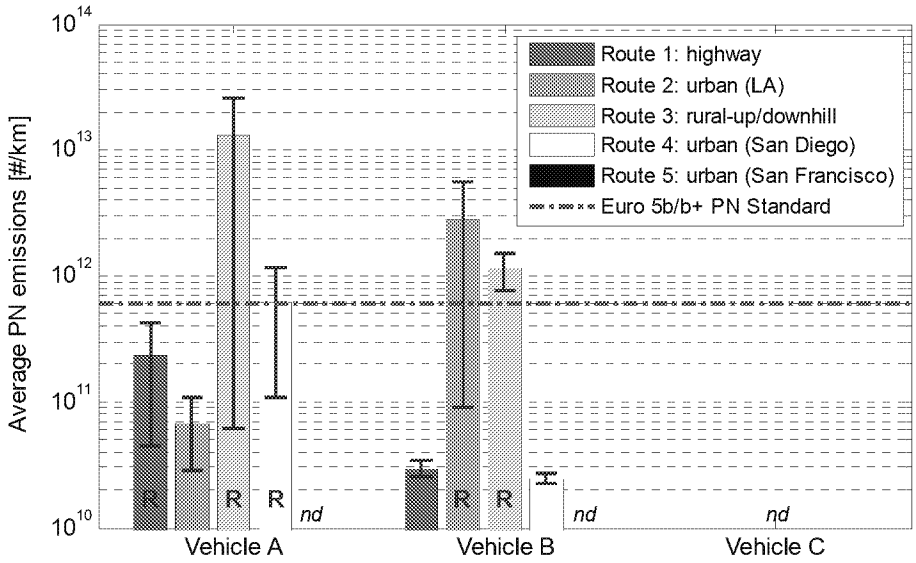


**Figure 4.13: Average PN emissions of test vehicles over the five test routes compared to Euro 5b/b+ emissions standard; repeat test variation intervals are presented as minimum/maximum test value; Route 1, Vehicle A includes rush-hour/non rush-hour driving, no PM data collected for Vehicle C, '*R*' designates routes including a test with DPF regeneration event, '*nd*' - no data available**

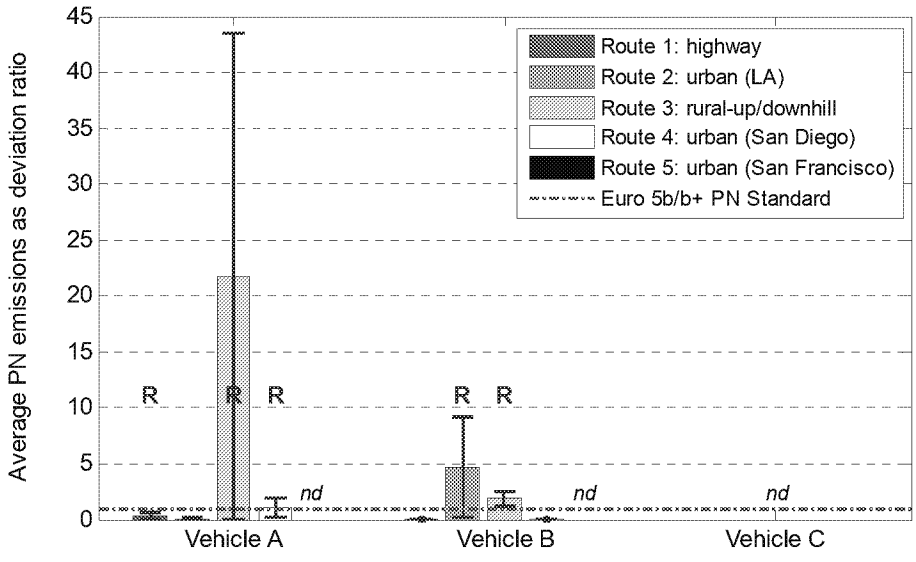


**Figure 4.14: Average PN emissions of test vehicles over the five test routes expressed as deviation ratio; repeat test variation intervals are presented as minimum/maximum test value, no PM data collected for Vehicle C, '*R*' designates routes with DPF regeneration event, '*nd*' - no data available**

In general, average PN emissions factors remain an order of magnitude below the applicable Euro 5b/b+ standard for all routes/tests that did not include DPF regeneration events. However,

for routes/tests with DPF regeneration particle number emissions increase rapidly and exceed the Euro 5b/b+ standard in most cases (i.e. Route 3, 4 for *Vehicle A*; Route 2, 3 for *Vehicle B*).

**Table 4.8: Average, minimum, and maximum PN emissions in [#/km] of test vehicles over the five test routes; Route 1 for Vehicle A includes rush-hour/non rush-hour**

| Route | | Vehicle A | Vehicle B | Vehicle C |
|---|---|---|---|---|
| Route 1: highway | **μ** | **2.32E+11** | **2.98E+10** | - |
| | *Min* | *4.43E+10* | *2.54E+10* | - |
| | *Max* | *4.20E+11* | *3.41E+10* | - |
| Route 2: urban (LA) | **μ** | **6.85E+10** | **2.80E+12** | - |
| | *Min* | *2.88E+10* | *9.05E+10* | - |
| | *Max* | *1.08E+11* | *5.51E+12* | - |
| Route 3: rural-up/downhill | **μ** | **1.31E+13** | **1.14E+12** | - |
| | *Min* | *6.24E+10* | *7.65E+11* | - |
| | *Max* | *2.61E+13* | *1.52E+12* | - |
| Route 4: urban (San Diego) | **μ** | **6.28E+11** | **2.48E+10** | - |
| | *Min* | *1.09E+11* | *2.25E+10* | - |
| | *Max* | *1.15E+12* | *2.70E+10* | - |
| Route 5: urban (San Francisco) | **μ** | - | - | - |
| | *Min* | - | - | - |
| | *Max* | - | - | - |

Figure 4.15 a) and b) present average fuel economy values in units [km/L] and [mpg], respectively, over the five pre-defined test routes for vehicles A through C. Additionally, Table 4.9 summarizes the average values and standard deviations (1σ) computed over two consecutive repetitions of a given test route.

As fuel economy values are derived via carbon balance with $CO_2$ emissions being the dominant fraction, they essential become a mirror of $CO_2$ emissions fractions. Therefore, any observations discussed earlier for $CO_2$ emissions are valid as well for fuel economy results, hence, in general, and as expected, highway driving showed increased fuel economy over urban/suburban driving conditions.

Average fuel economy for highway driving with *Vehicles A* and *B* was 45.3 mpg ±8.6mpg (±σ1) and 43.7mpg ±5.7mpg (±σ1), respectively, and 27.3 mpg (no repetition) for *Vehicle C* which is ~39% lower compared to *Vehicles A* and *B*. On the other hand, urban/suburban driving results in average fuel economies of 30.0mpg ±2.9mpg (±σ1) and 26.6 mpg ±1.4mpg (±σ1) for

*Vehicles A* and *B*, respectively, and 18.5mpg ±4.0mpg (±σ1) for *Vehicle C* which is 35% lower compared to *Vehicles A* and *B*. Overall, urban/suburban driving leads to a 32-39% reduction in fuel economy over highway driving.

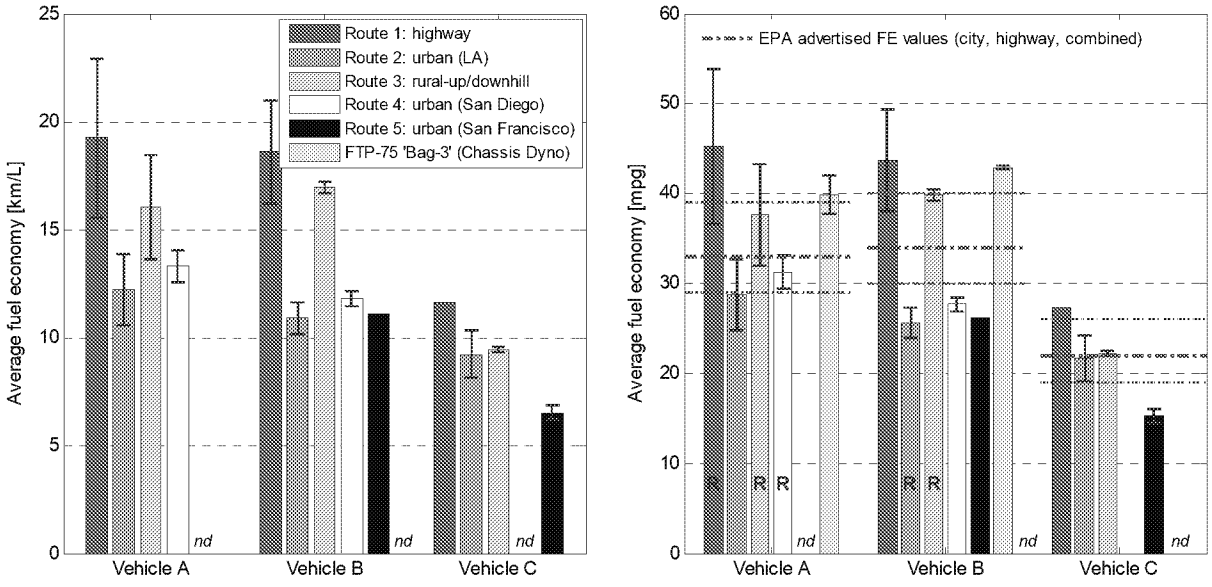


**Figure 4.15: Average fuel economy of test vehicles over the five test routes in km/L and mpg; repeat test variation intervals are presented as ±1σ; Route 1 for Vehicle A includes rush-hour/non rush-hour driving**

**Table 4.9: Average fuel economy in [mpg] of test vehicles over the five test routes; σ is standard deviation over two consecutive test runs, Route 1 for Vehicle A includes rush-hour/non rush-hour**

| Route | | Vehicle A | Vehicle B | Vehicle C |
|---|---|---|---|---|
| Route 1: highway | μ | **45.3** | **43.7** | **27.3** |
| | σ | *8.6* | *5.7* | - |
| Route 2: urban (LA) | μ | **28.7** | **25.6** | **21.7** |
| | σ | *3.9* | *1.7* | *2.6* |
| Route 3: rural-up/downhill | μ | **37.6** | **39.9** | **22.3** |
| | σ | *5.7* | *0.6* | *0.3* |
| Route 4: urban (San Diego) | μ | **31.3** | **27.7** | - |
| | σ | *1.8* | *0.8* | - |
| Route 5: urban (San Francisco) | μ | - | **26.2** | **15.3** |
| | σ | - | - | *0.8* |

Figure 4.16 depicts average engine work values and standard deviations (1σ) in units [kWh] over the five pre-defined test routes for vehicles A through C. The average engine work presented herein is inferred from estimated real-time engine power calculated according to

Equation 12, and based on an assumed calorific value for the test fuel and combustion efficiency as well as the real-time fuel consumption derived from a carbon balance using the measured exhaust constituents as input parameter. The calorific value for the diesel fuel was selected as 43,500kJ/kg and the combustion efficiency as 0.35. It can be noticed form Figure 4.16 that the engine of *Vehicle C* produces more work as compared to *Vehicles A* and *B* which can be explained by the overall heavier vehicle and larger engine for *Vehicle C*.

$$\dot{P}(t) = Calori_{fuel} \cdot \dot{Fuel}_{CB}(t) \cdot \eta_{comb} \cdot \frac{1}{1000} \qquad \textbf{Eq. 12}$$

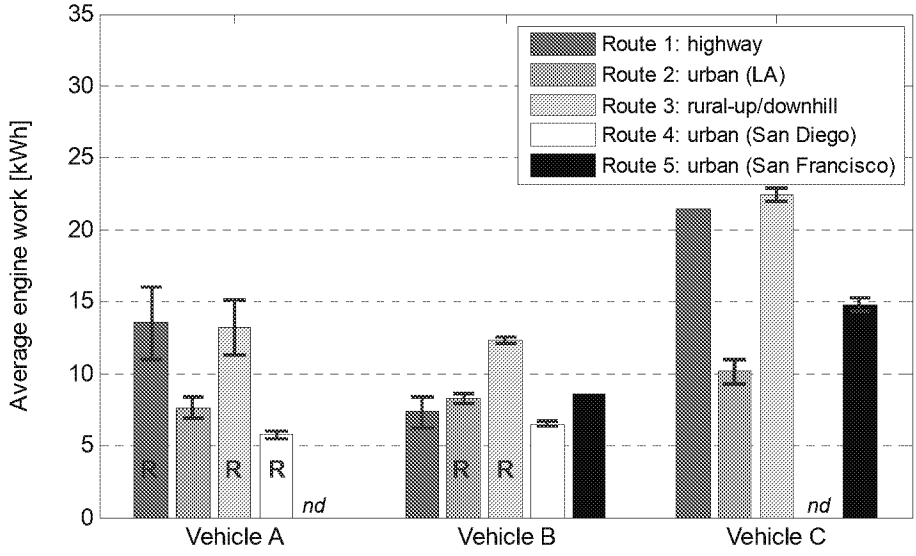


**Figure 4.16: Average engine work of test vehicles over the five test routes, calculated from carbon balance and combustion efficiency; repeat test variation intervals are presented as ±1σ; Route 1 for Vehicle A includes rush-hour/non rush-hour driving**

### 4.1.2 Emissions over Cross-Multi-State Driving Route

This section will report averaged emissions factors for gaseous and particulate matter emissions from *Vehicle B* over the cross-multi state driving route. Each figure in this section will present averaged emissions factors for route portions between Los Angeles and Seattle that comprise predominantly highway driving with the addition of two routes representative of urban/suburban driving in Seattle, WA and Sacramento, CA. Additionally, average values and standard deviations (1σ) computed separately for highway and urban/suburban portions of the

route as well as the grand average over the entire cross-multi state driving route are included to the right of each individual graph.

Figure 4.17 along with Figure 4.18 show average $NO_x$ emissions factors and their respective deviation ratio from the US-EPA Tier2-Bin5 standard, respectively. Over the entire route, $NO_x$ emissions factors were on average 0.26g/km ±0.21g/km (±1σ) or approx. 6 times exceeding the US-EPA Tier2-Bin5 standard. $NO_x$ emissions factors for urban/suburban driving portions were observed at twice the level of highway-only route portions with 0.52g/km ±0.27g/km versus 0.24g/km ±0.19g/km $NO_x$, respectively. For highway driving average, $NO_x$ emissions factors were close to $NO_x$ emissions observed during Route 1 (i.e. highway) driving (i.e. 0.344g/km ±0.096g/km), considering the large variation in $NO_x$ emissions over the highway portions of the cross-multi state route. Urban driving in Seattle (i.e. Route 6) exhibits $NO_x$ emissions factors at a similar level as seen for the pre-defined urban Routes 2, 4 and 5 shown in Figure 4.3. On the other hand, urban/highway driving in Sacramento (i.e. Route 7) shows greatly reduced $NO_x$ emissions compared to other urban routes, which is primarily due to the large share of highway driving contained in this route segment (> 60% by distance), thus, causing the large variability seen for total urban/suburban average $NO_x$ emissions factor.

However, more interesting is the large variation in $NO_x$ emissions factors over highway driving and in particular portions of the route where $NO_x$ emissions were observed below the US-EPA Tier2-Bin5 standard. In order to provide a possible explanation, Figure 4.17 needs to be interpreted in light of the vehicle speed and altitude graphs for the cross-multi state driving route shown in Figure 3.18 a) and b), respectively. Increased $NO_x$ emissions during route portions 1 and 2 as well as 8 through 11 (see Figure 4.17) coincide with up/downhill driving conditions while crossing mountain ranges near Los Angeles and in Northern California/Southern Oregon, respectively, with elevation changes of up to 1200 meters. On the other hand, $NO_x$ emissions at or below the US-EPA Tier2-Bin5 standard (see route portions 3 through 6 in Figure 4.17) were observed while traveling northbound on Interstate 5 through the San Joaquin Valley characterized by low or negligible changes in altitude (i.e. near zero road grade), and with the vehicle operated in cruise-control mode at approximately 120km/h.

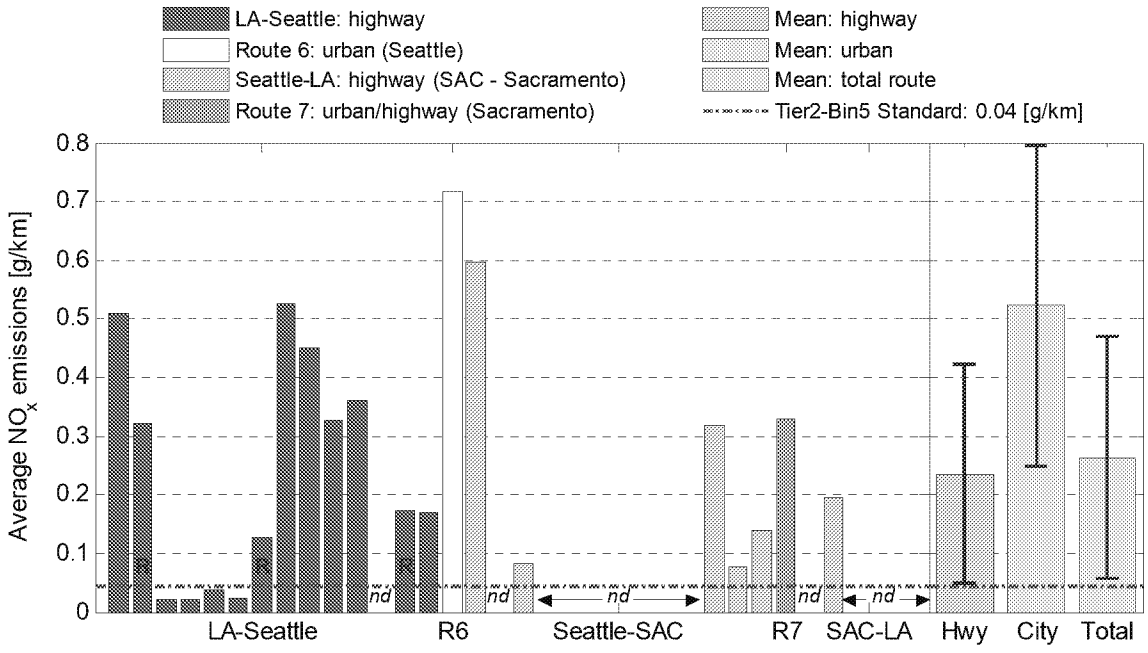


**Figure 4.17: Average $NO_x$ emissions of test vehicle over cross-multi-state driving route portions compared to US-EPA Tier2-Bin5 emissions standard; repeat test variations are presented as ±1σ, '*R*' designates segments including a DPF regeneration event, '*nd*' - no data available**

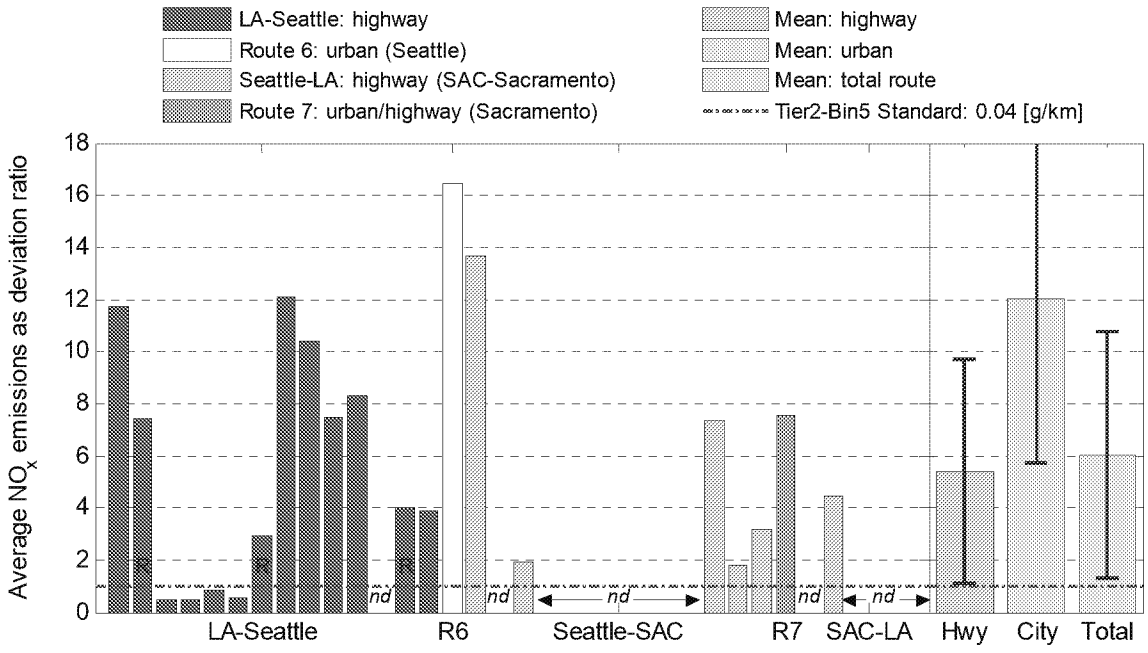


**Figure 4.18: Average $NO_x$ emissions of test vehicle over cross-multi-state driving route portions expressed as deviation ratio; repeat test variations are presented as ±1σ, '*R*' designates segments including a DPF regeneration event, '*nd*' - no data available**

Figure 4.19 along with Figure 4.20 show average CO emissions factors and their respective deviation ratio from the US-EPA Tier2-Bin5 standard, respectively. In general, and as expected,

CO emissions were observed at two orders of magnitude below the applicable standard and no specific pattern could be identified from the results.

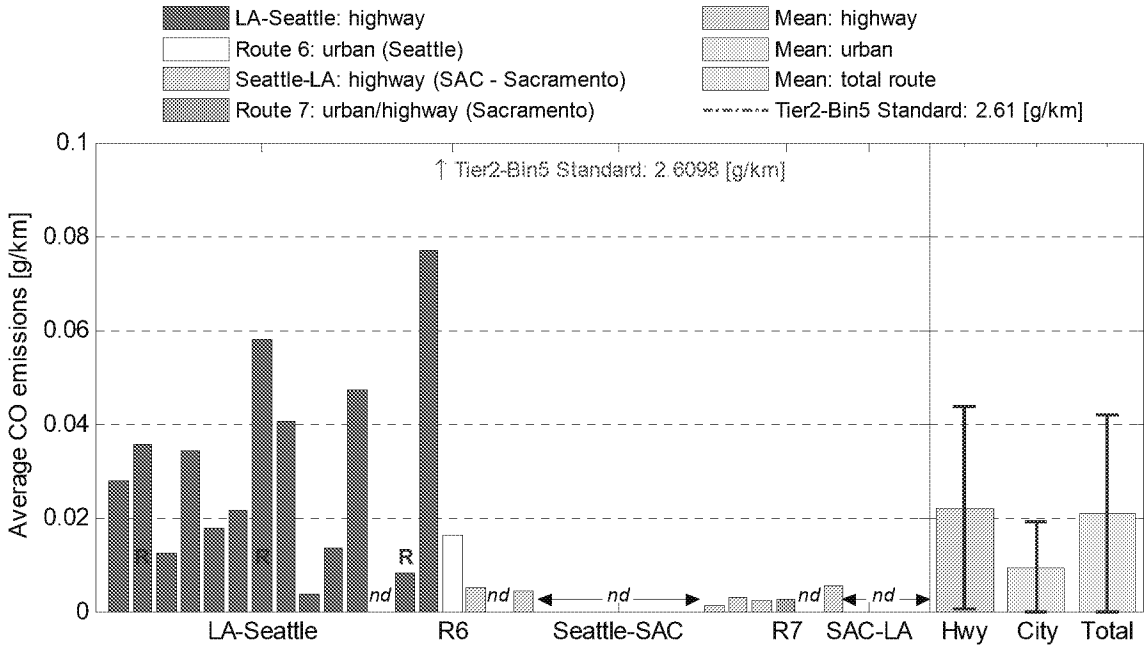


**Figure 4.19: Average CO emissions of test vehicle over cross-multi-state driving route portions compared to US-EPA Tier2-Bin5 emissions standard; repeat test variations are presented as ±1σ, '*R*' designates segments including a DPF regeneration event, '*nd*' - no data available**

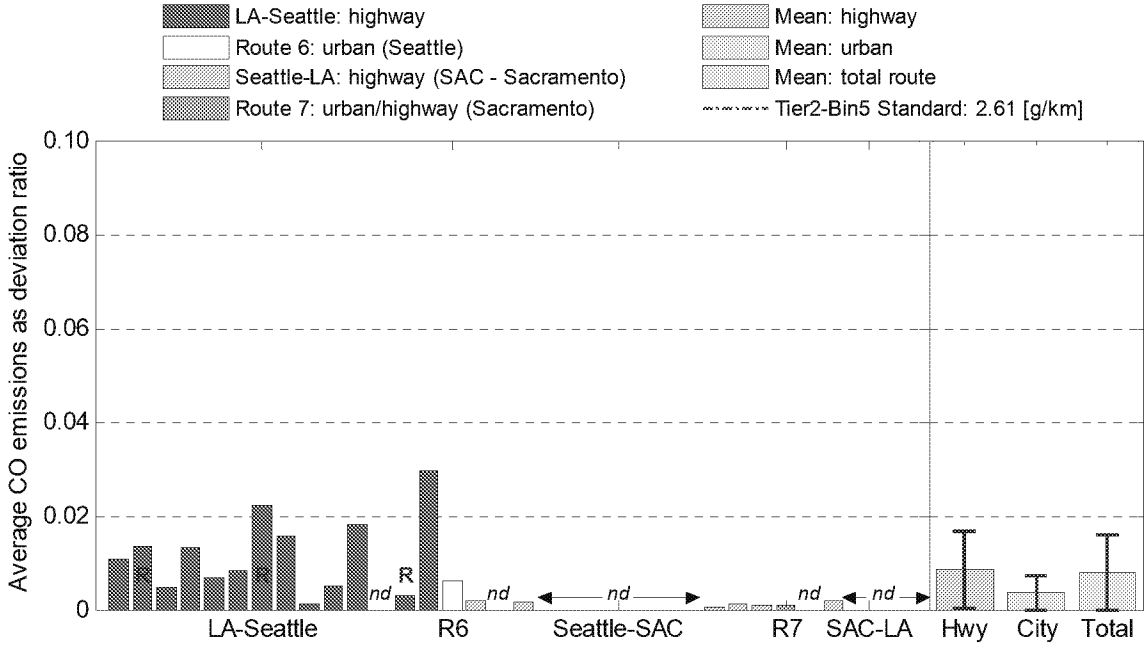


**Figure 4.20: Average CO emissions of test vehicle over cross-multi-state driving route portions expressed as deviation ratio; repeat test variations are presented as ±1σ, '*R*' designates segments including a DPF regeneration event, '*nd*' - no data available**

Similarly, Figure 4.21 along with Figure 4.22 show average THC emissions factors and their respective deviation ratio from the US-EPA Tier2-Bin5 standard, respectively, which were well below the applicable emissions standard.

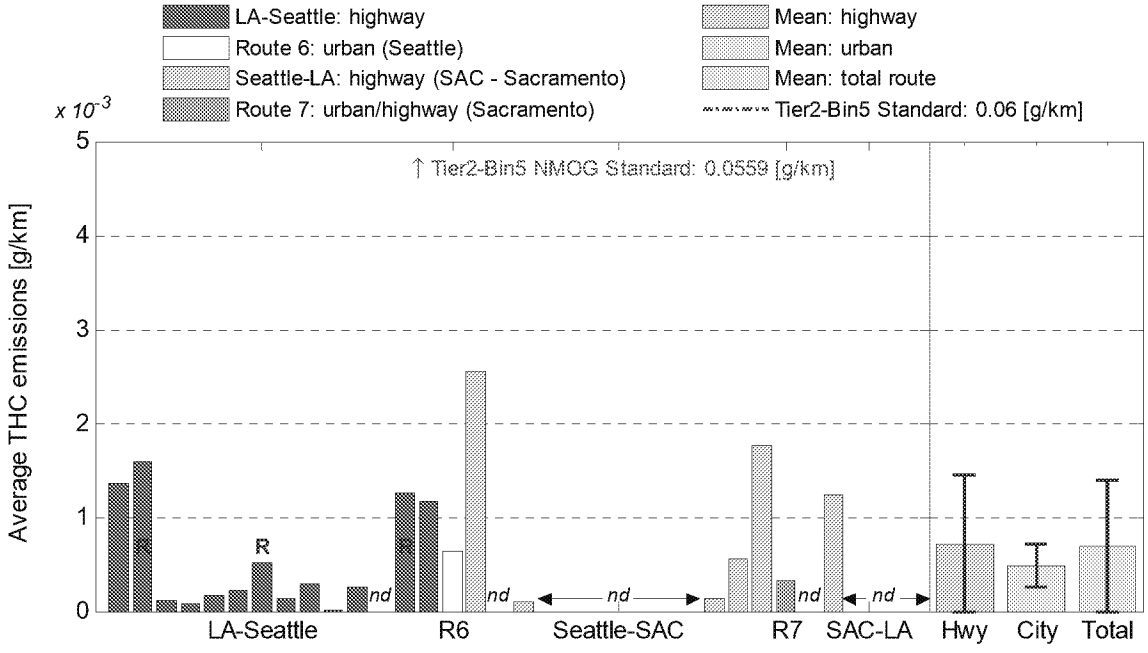


**Figure 4.21: Average THC emissions of test vehicle over cross-multi-state driving route portions compared to US-EPA Tier2-Bin5 emissions standard; repeat test variations are presented as ±1σ, '*R*' designates segments including a DPF regeneration event, '*nd*' - no data available**

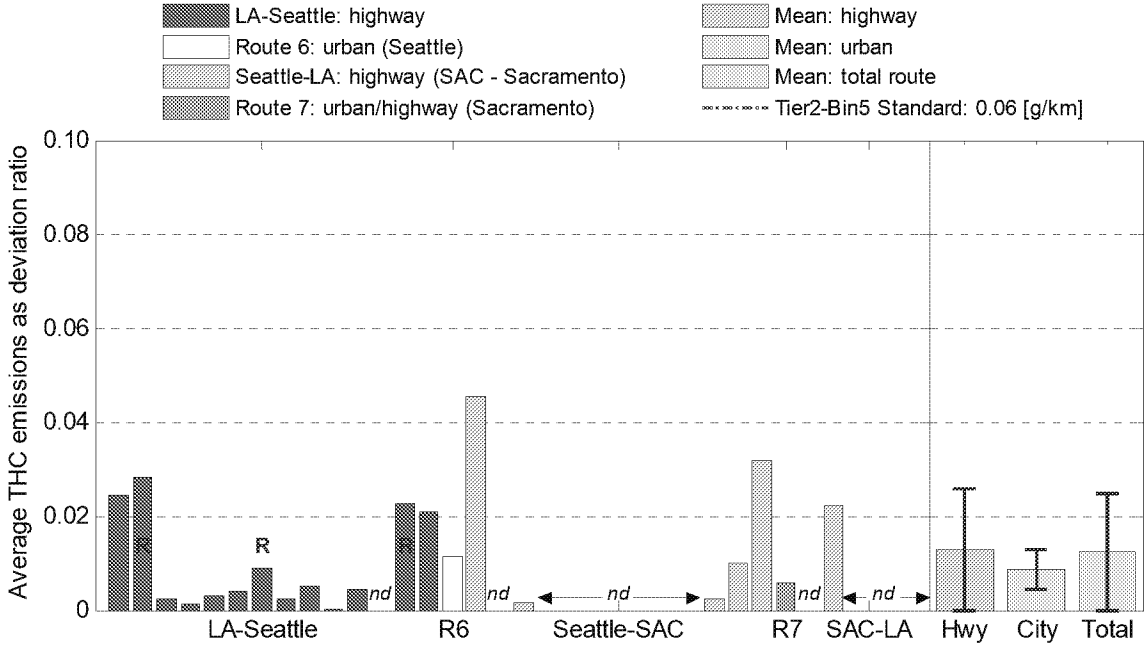


**Figure 4.22: Average THC emissions of test vehicle over cross-multi-state driving route portions expressed as deviation ratio; repeat test variations are presented as ±1σ**

Figure 4.23 along with Figure 4.24 show average $CO_2$ emissions factors and their respective deviation ratio from the EPA advertised $CO_2$ value for *Vehicle B* (i.e. 186g/km), respectively, over the individual sub-portions of the cross-multi state driving route.

As already has been observed for the pre-defined test routes (see Figure 4.9) $CO_2$ emissions are in general lowest for highway driving, whereas urban/suburban driving conditions lead to increased $CO_2$ emissions factors (155g/km ±14.4g/km vs. 178g/km ±19.9g/km). It has to be noted again that the second urban route presented in Figure 4.23 (i.e. Route 7) includes a proportionally large amount of highway driving and, thus, skews the $CO_2$ emissions factor for this route towards a lower value as was typically experienced for *Vehicle B* over urban driving conditions (e.g. see Route 2, 4, 5, and 6). On average, $CO_2$ emissions are ~16.7% below the EPA advertised $CO_2$ value for *Vehicle B* during highway operation. Increased $CO_2$ emissions as observed for route portions 7 and 8 coincide with larger elevation changes and therefore steeper road grades as can be seen from Figure 3.18 thus, resulting in increased engine load demand and thereby emitting more $CO_2$ on a distance-specific basis.

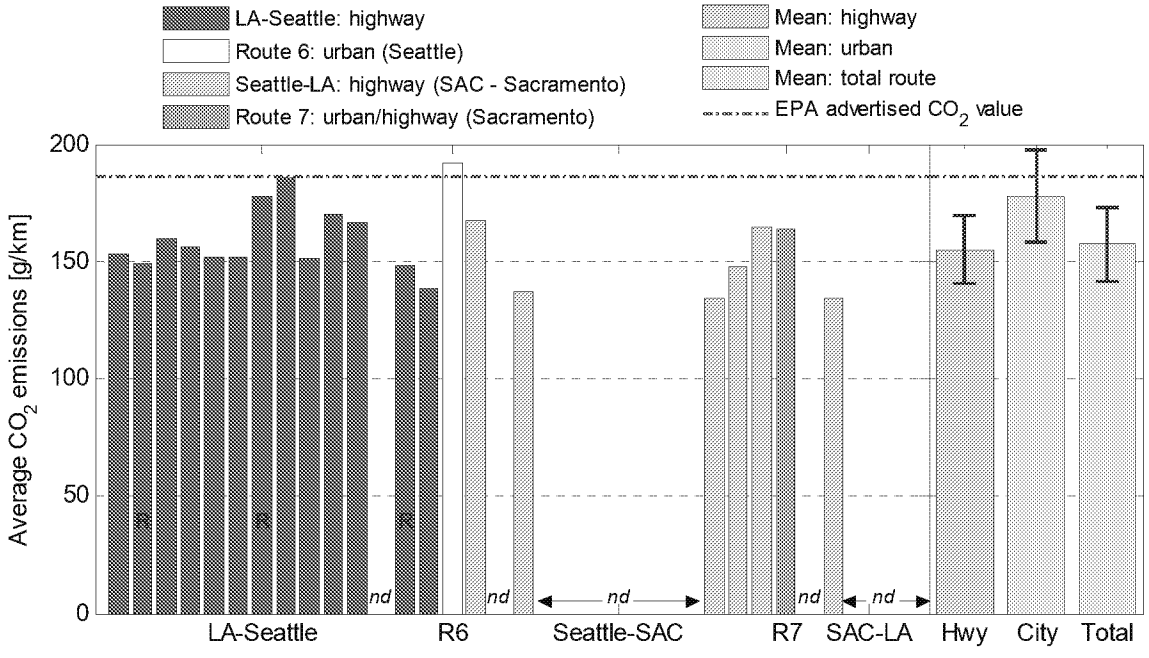


**Figure 4.23: Average $CO_2$ emissions of test vehicle over cross-multi-state driving route portions compared to EPA advertised $CO_2$ value for Vehicle B; repeat test variations are presented as ±1σ, '*R*' designates segments including a DPF regeneration event, '*nd*' - no data available**

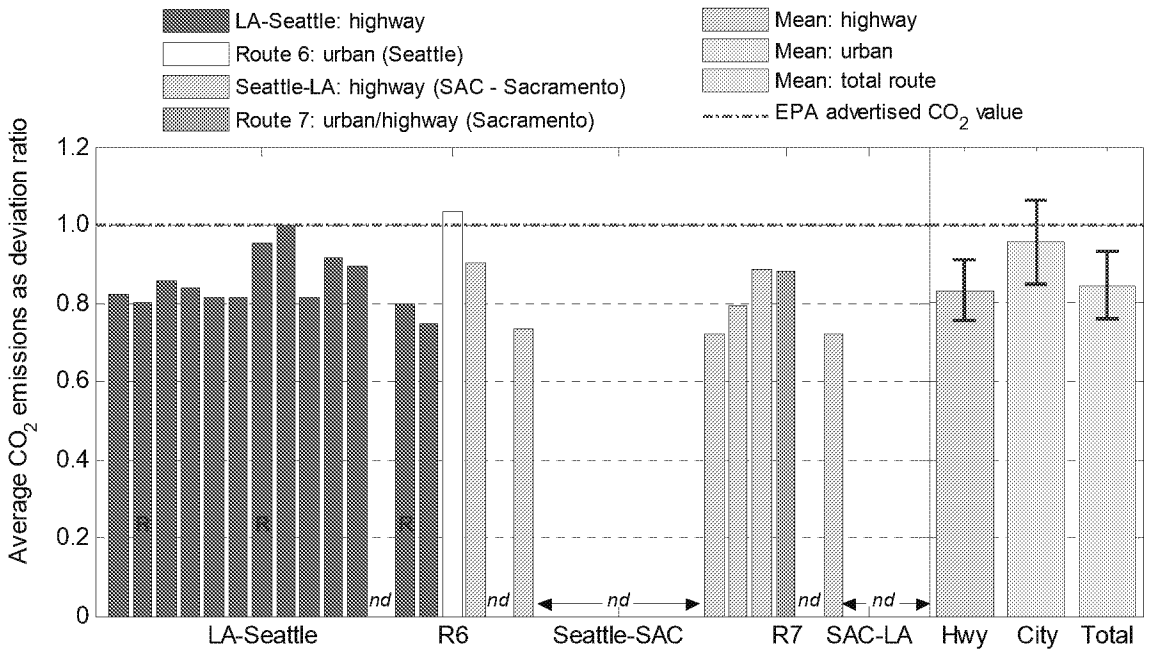


**Figure 4.24: Average $CO_2$ emissions of test vehicle over cross-multi-state driving route portions expressed as deviation ratio; repeat test variations are presented as ±1σ, '*R*' designates segments including a DPF regeneration event, '*nd*' - no data available**

Figure 4.25 shows average particulate matter mass emissions factors whereas Figure 4.26 presents average particulate matter number emissions factors along with the respective regulatory standards, specifically, US-EPA Tier2-Bin5 for PM and Euro 5b/b+ for PN. It has to be noted again that both PM and PN emissions are inferred from real-time particle charge measurements using the Pegasor particle sensor.

In general, PM emissions are on the order of 0.01mg/km ±0.005mg/km (±1σ), thereby nearly 100% (99.89%) below the US-EPA Tier2-Bin5 standard. From Figure 4.25 three portions of the cross-multi state driving route, namely, portions 2, 7, and 13 stand out showing distinctly different PM emissions levels as compared to all other route portions. This is due to DPF regeneration events occurring during these three route portions leading to a nearly 700 fold increase in PM emissions to 4.55mg/km ±0.003mg/km (±1σ). However, even during DPF regeneration events PM emissions levels remain ~27% below the regulatory standard of 6.2mg/km (i.e. US-EPA Tier2-Bin5), owing to the diesel particulate filters ability to retain particulate matter mass emissions with high efficiency from the exhaust gas stream.

Figure 4.26 shows a similar picture for particulate number emissions factors with PN levels typically on the order of $3.01 \times 10^{10}$#/km (min: $2.03 \times 10^{9}$#/km /max: $9.12 \times 10^{10}$#/km) during both

highway and urban/suburban driving conditions. However, during DPF regeneration events as observed during route portions 2, 7, and 13 PN emissions factors increase by 2 to 3 orders of magnitude to $2.08 \times 10^{13}$#/km $\pm 1.36 \times 10^{10}$#/km ($\pm 1\sigma$, including only PN for portions 7 and 13), thereby, exceeding the Euro 5b/b+ PN standard by more than an order of magnitude (factor 35).

Previous studies [32 and 33] have shown that particle number concentrations downstream the PM trap can momentarily increase during, and within a limited time period after, experiencing a regeneration event. During regeneration of a wall-flow type DPF the '*cake-layer,*' as referred to the soot layer deposited on top of the filter substrate and responsible for the high particle retention efficiency of wall-flow type DPF's (>99%), is partially oxidized, thus, momentarily reducing the filtration efficiency of the DPF [32]. Within a usually short, but ultimately depending on engine load, period after the regeneration event the '*cake-layer*' will be built up again and the DPF will resume its maximum filtration efficiency.

A more detailed discussion of DPF regeneration events and the frequency of their occurrence as observed for *Vehicle B* is presented in Section 4.3.2.

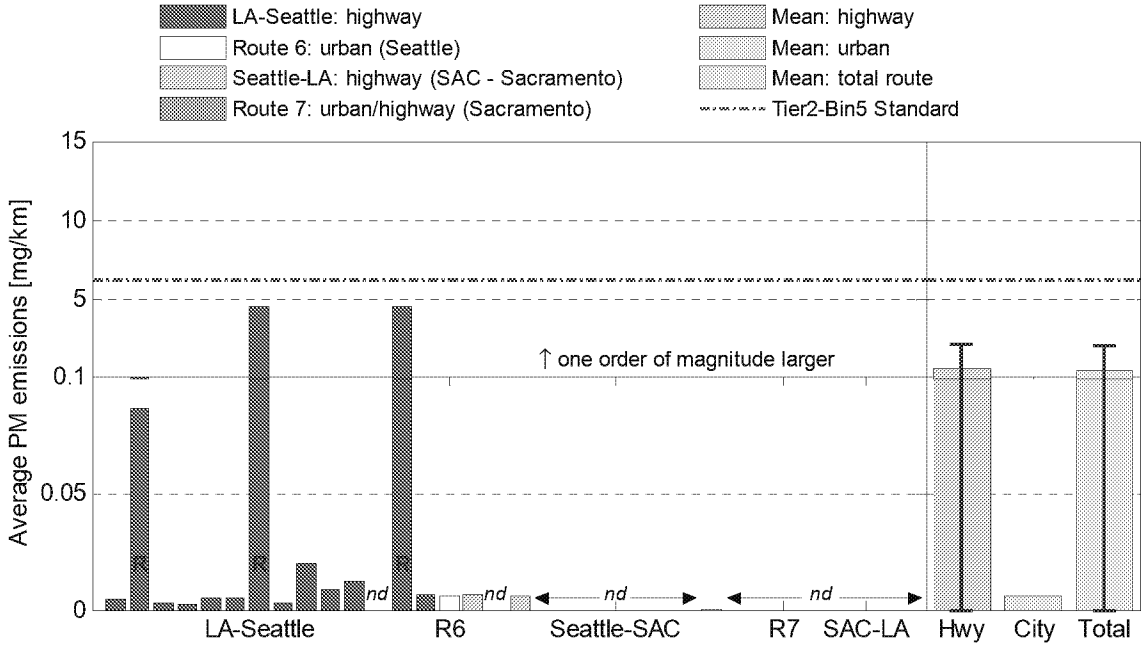


**Figure 4.25: Average PM emissions of test vehicle over cross-multi-state driving route portions compared to US-EPA Tier2-Bin5 emissions standard; repeat test variations are presented as ±1σ, '*R*' designates segments including a DPF regeneration event, '*nd*' - no data available**

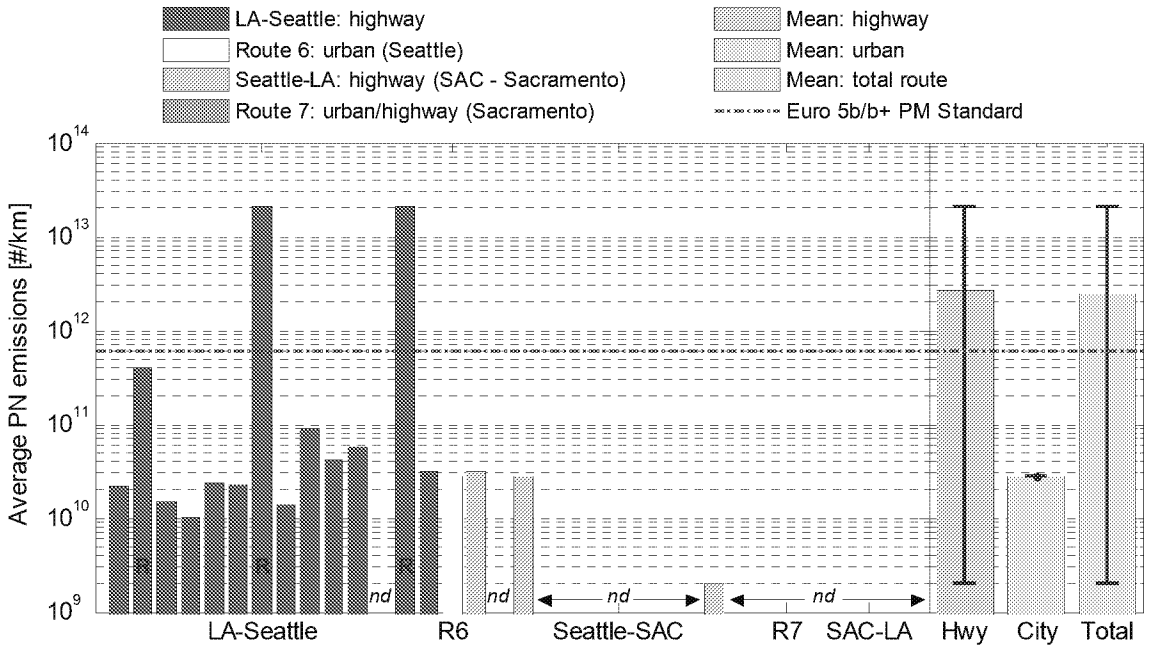


**Figure 4.26: Average PN emissions of test vehicle over cross-multi-state driving route portions compared to Euro 5b/b+ emissions standard; repeat test variations are presented as minimum/maximum test value, total city emissions are only based on Route 6 (R6), '*R*' designates segments including a DPF regeneration event, '*nd*' - no data available**

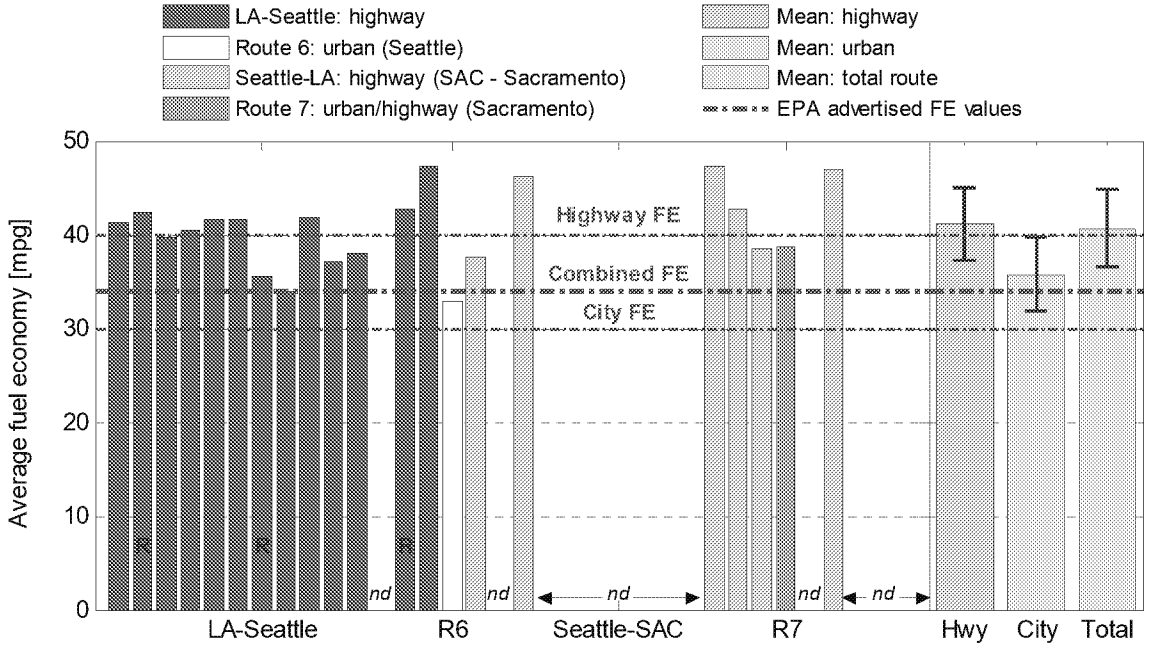


**Figure 4.27: Average fuel economy of test vehicle over cross-multi-state driving route portions expressed as mpg; repeat test variations are presented as ±1σ), '*R*' designates segments including a DPF regeneration event, '*nd*' - no data available**

Finally, Figure 4.27 shows average fuel economy values in units of [mpg] for the entire cross-multi state driving route. On average, fuel economy was 41.2mpg ±3.9mpg (±1σ) during highway driving conditions, spanning from 33.98mpg to 47.2mpg during route portions 8 and 26, respectively. Lowest fuel economy coincides with uphill driving, whereas highest fuel economy values were observed during downhill slopes while crossing the mountain ranges in Northern California/Southern Oregon (see Figure 3.18 for altitude reference). Furthermore, urban/suburban driving (i.e. Route 6) has been shown to result in ~20% reduced fuel economy over highway driving.

## 4.2 On-Road $NO_x$ Emissions

This chapter will present $NO_x$ emissions calculated based on the averaging window method over pre-defined test routes for all three vehicles (see Section 4.2.1) and over the cross-multi state driving route for *Vehicle B* (see Section 4.2.2).

The averaging windows were calculated following recommendations outlined in the European regulation [3] with the total mass of $CO_2$ in [g], emitted over a given vehicle certification chassis dynamometer cycle chosen as the reference criterion to determine window size. Two reference cycles were chosen, namely, FTP-75 and NEDC as actual $CO_2$ emissions data was available for both these cycles from *Vehicle A* and *B*, collected during chassis dynamometer testing at CARB's El Monte facility. Table 4.10 lists the respective $CO_2$ mass emissions emitted over the reference cycles. No actual $CO_2$ emissions data were available for *Vehicle C*, therefore, $CO_2$ values were instead taken from EPA certification documents for the FTP-75 cycle. Additionally, averaging window based $NO_x$ emissions will be presented as deviation ratios from the US-EPA Tier2-Bin5 standard for $NO_x$ (i.e. 0.043g/km) as described by Equation 11.

**Table 4.10: Window size criterion for AWM; total $CO_2$ mass over FTP-75 and NEDC (evaluated at CARB El Monte chassis dynamometer laboratory for Vehicle A and B; taken from EPA certification document for Vehicle C)**

| Vehicle | $CO_2$ over FTP-75 [g] | $CO_2$ over NEDC [g] |
|---|---|---|
| Vehicle A | 2921.9 | 1938.6 |
| Vehicle B | 2944.8 | 1841.8 |
| Vehicle C | 5042.5 [1)] | 5042.5 [2)] |

[1)] *$CO_2$ mass value for FTP-75 according to EPA certification documents (see http://www.epa.gov/otaq/crttst.htm)*
[2)] *$CO_2$ mass value for FTP-75 chosen since no NEDC specific values available from EPA certification documents*

### 4.2.1 $NO_x$ Emissions over Pre-Defined Test Routes

Cumulative frequency plots for averaging window $NO_x$ emissions in [g/km] and deviation ratios from the regulatory standard are presented for *Vehicle A* in Figure 4.28 along with Figure 4.29, for *Vehicle B* in Figure 4.30 along with Figure 4.31, and finally for *Vehicle C* in Figure 4.32 along with Figure 4.33, respectively. Total $CO_2$ emitted over the NEDC was chosen as reference value for calculating AWM-$NO_x$ emissions results presented in the above mentioned figures. Overall, the LNT equipped *Vehicle A* shows the highest, while the urea-SCR after-treatment based *Vehicle C* the lowest $NO_x$ emissions.

In general, highway driving (i.e. Route 1) shows lowest $NO_x$ emissions whereas rural-up/downhill driving conditions (i.e. Route 3) contribute to the largest amounts of $NO_x$ observed. For *Vehicles A* and *B*, about 30-40% of the $NO_x$ emissions emitted during Route 3 are below levels observed for urban driving and close to what was seen for highway conditions. Contrarily, *Vehicle C* emitted significantly more $NO_x$ during the rural-up/downhill route as compared to any of the other urban or highway routes (see Figure 4.32), with about 50% of the emissions released exceeding ~10 times the UA-EPA Tier2-Bin5 standard. This agrees well with route average $NO_x$ emissions presented earlier in Figure 4.3 and Figure 4.4. However, when comparing results for Route 3 between *Vehicles C* and *B* (see Figure 4.32 vs. Figure 4.30), close similarities in shape and magnitude can be noticed for the cumulative frequencies. The large increase in $NO_x$ emissions observed during the rural-up/downhill driving over other test routes could be attributed to the fact that the emissions presented herein are normalized for distance traveled rather total work produced by the engine. This impacts results from heavier vehicles (*Vehicle C* was ~54% heavier than *Vehicles A* and *B*) with larger and more powerful engines while operating over routes comprising increased altitude changes since proportionally more work needs to be done by the engine to move the vehicle uphill over a finite increment of distance.

The impact of DPF regenerations onto $NO_x$ emissions is especially pronounced for *Vehicle A*, visible as significant differences in cumulative frequency graphs between repetitions of routes with and without regeneration event (i.e. Route 1, 3, and 4). It has to be noted that this observation might be confounded for Route 1 as the test exhibiting the DPF regeneration event was also experiencing heavy evening rush-hour traffic conditions, thereby additionally affecting $NO_x$ emissions. However, owing the increased difference between both test runs for Route 1, as compared to the differences seen between test runs for Route 3 and 4, it could be justified as a

combined effect of DPF regeneration and increased stop-go conditions due to rush-hour traffic. Figure 4.36 shows a direct comparison of continuous averaging window $NO_x$ emission over Route 3 between two repeats, one with (i.e. Test 1) an the other without (i.e. Test 2) DPF regeneration event. The location of the regeneration event can be identified from the PN concentration and exhaust gas temperature (measured at the exhaust tailpipe outlet) graphs in the lower part of Figure 4.36, with the duration of the event observed to be on the order of 14min and thereby in agreement with [31]. During regeneration events averaging window $NO_x$ emissions are found to nearly double from ~3g/km to ~5.5g/km for Route 3 for example (see Figure 4.36). Similar behavior was observed for Routes 1 and 4 for *Vehicle A* between tests with and without DPF regeneration. A possible explanation for the observed increase in $NO_x$ emissions during DPF regeneration events for the LNT equipped *Vehicle A* was given earlier in Section 4.1.1. This distinct impact of DPF regenerations onto $NO_x$ emissions was not observed for the other test vehicles.

In general for *Vehicle A*, 50% of $NO_x$ emissions over all test routes were exceeding the US-EPA Tier2-Bin5 standard by a factor of 20 to 40 as seen from Figure 4.29, with none of the routes exhibiting $NO_x$ emissions at levels below the regulatory standard. On the other hand, for *Vehicle B* 50% of the $NO_x$ emissions were observed to exceed the US-EPA Tier2-Bin5 standard by 5 to 20 times for the majority of the test routes. One repeat of Route 1 exhibited lower $NO_x$ emissions with 5% of total accumulated averaging window $NO_x$ observed to fall below the standard.

Finally, as seen from Figure 4.32 and Figure 4.33 *Vehicle C* presents a vastly different averaging window $NO_x$ emissions pattern compared to *Vehicles A* and *B*, with the majority of the highway and urban/suburban driving routes exhibiting 80 to 90% of $NO_x$ emissions below the US-EPA Tier2-Bin5 standard. Figure 4.34 and Figure 4.35 provide a zoomed in view of the x-axis for Figure 4.32 and Figure 4.33, respectively. A significant variability in magnitude of $NO_x$ emissions between repetitions of the urban routes (i.e. Routes 2 and 5) can be noticed from Figure 4.34. Possible explanations for the observed test-to-test variability include changing traffic patterns and driving style as test drivers were changed between repeats of a given test route. Indeed, one of the tests for Route 5 was ~16min shorter and encountered more aggressive vehicle accelerations, possibly partially causing the observed increase in $NO_x$ emissions.

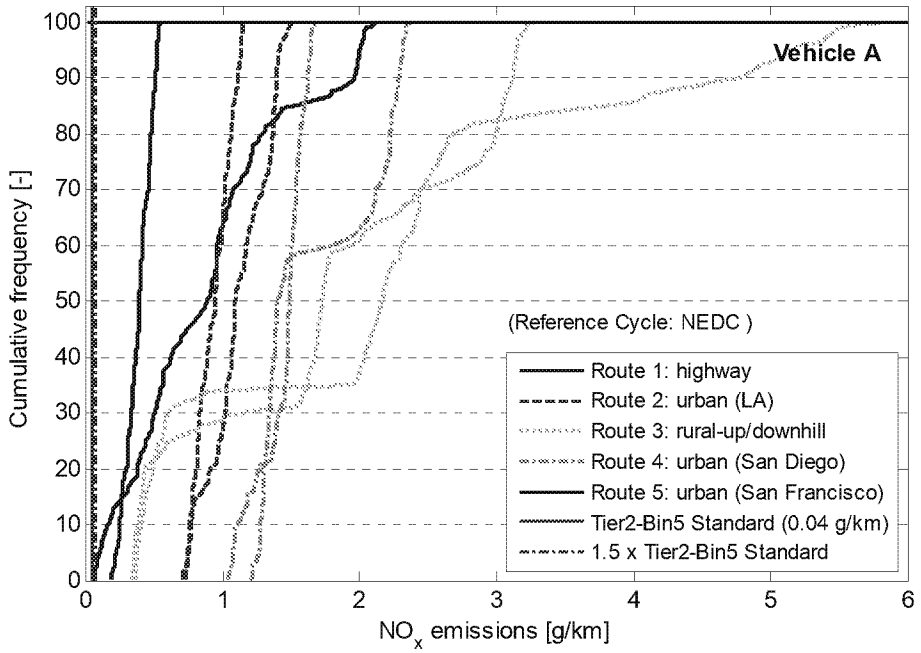


**Figure 4.28: Averaging window $NO_x$ emissions for Vehicle A over the five test routes compared to US-EPA Tier2-Bin5 emissions standard; AWM reference metric is $CO_2$ emissions over NEDC; Route 1 includes rush-hour/non rush-hour driving**

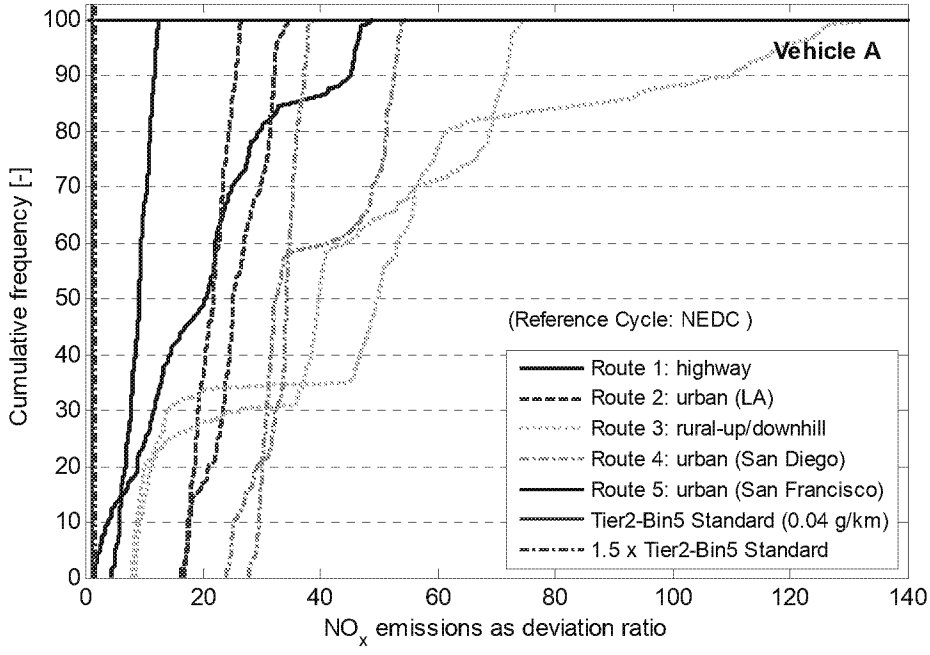


**Figure 4.29: Averaging window $NO_x$ emissions for Vehicle A over the five test routes expressed as deviation ratio; AWM reference metric is $CO_2$ emissions over NEDC; Route 1 includes rush-hour/non rush-hour driving**

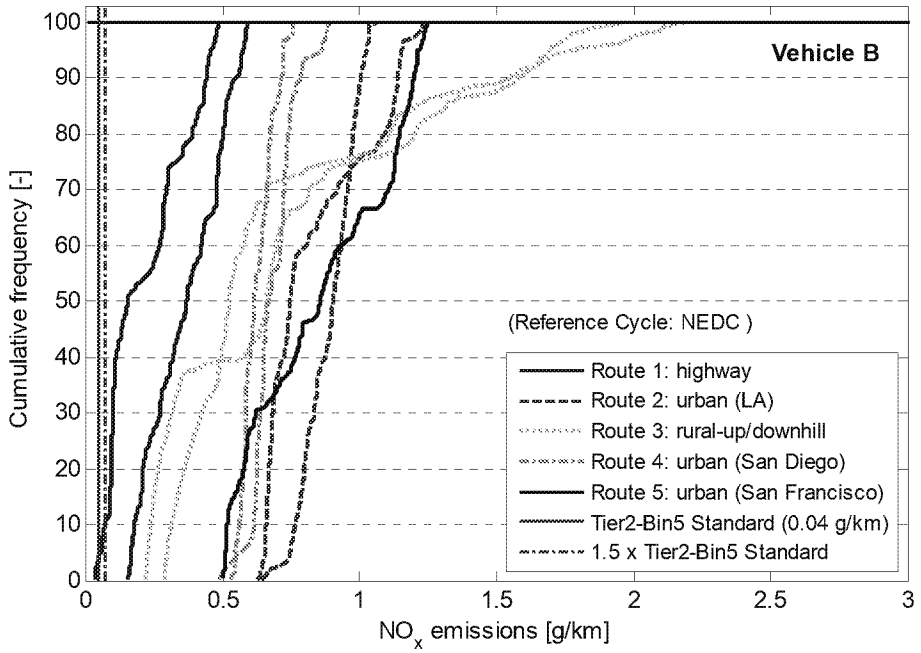


**Figure 4.30: Averaging window $NO_x$ emissions for Vehicle B over the five test routes compared to US-EPA Tier2-Bin5 emissions standard; AWM reference metric is $CO_2$ emissions over NEDC**

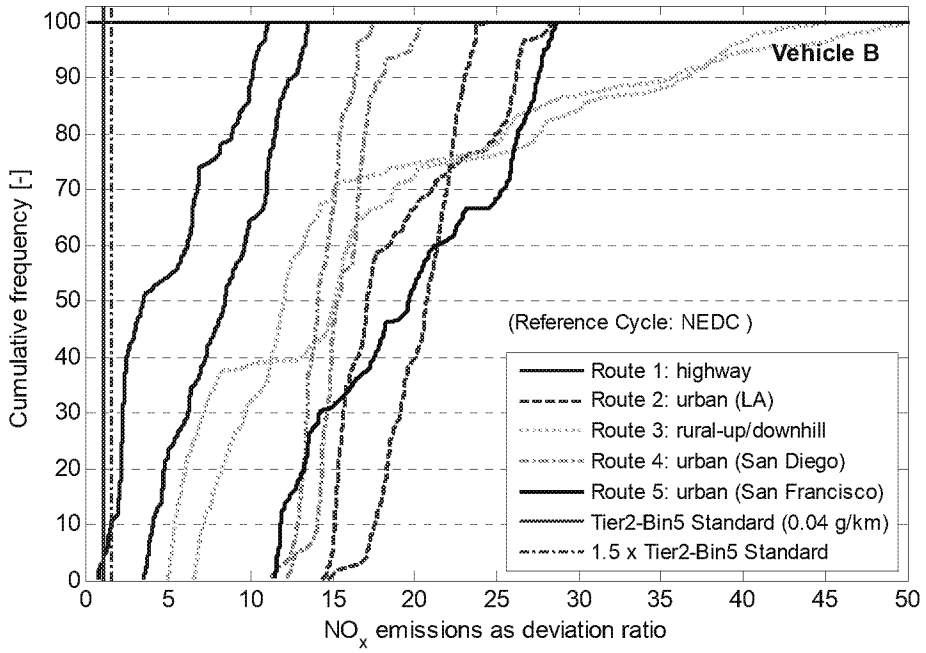


**Figure 4.31: Averaging window $NO_x$ emissions for Vehicle B over the five test routes expressed as deviation ratio; AWM reference metric is $CO_2$ emissions over NEDC**

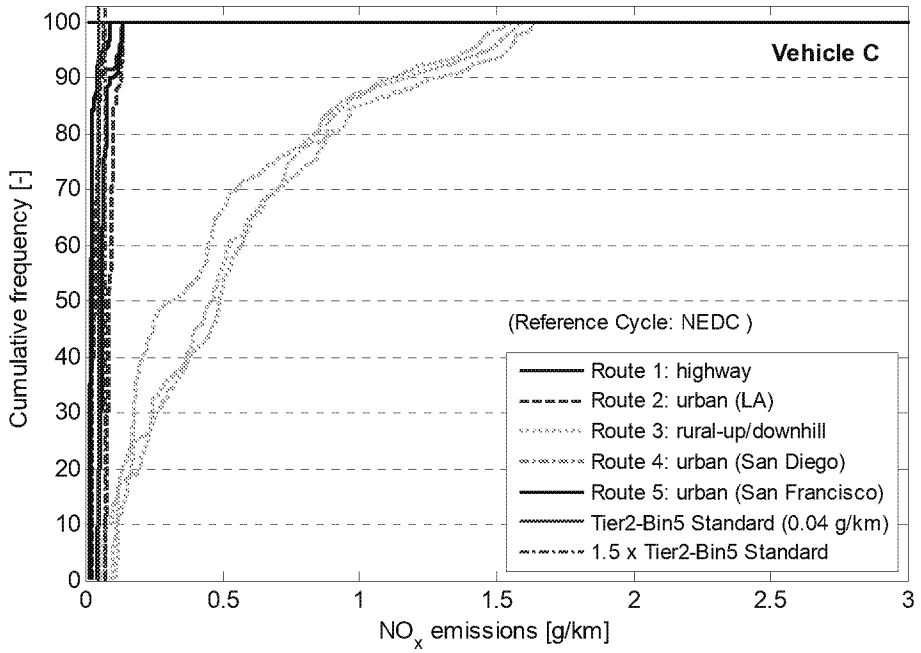


**Figure 4.32: Averaging window $NO_x$ emissions for Vehicle C over the five test routes compared to US-EPA Tier2-Bin5 emissions standard; AWM reference metric is $CO_2$ emissions over NEDC**

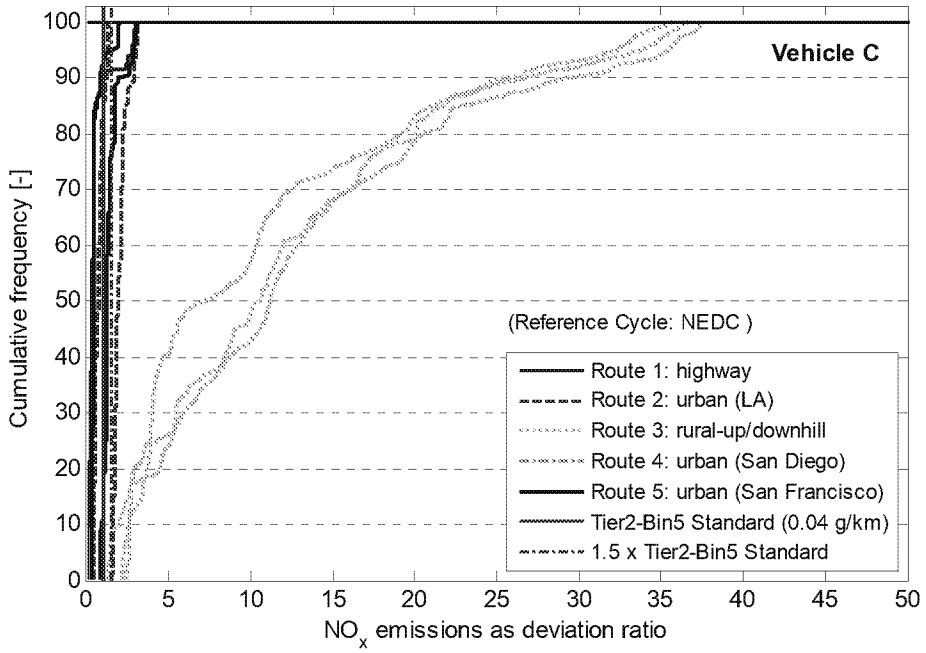


**Figure 4.33: Averaging window $NO_x$ emissions for Vehicle C over the five test routes expressed as deviation ratio; AWM reference metric is $CO_2$ emissions over NEDC**

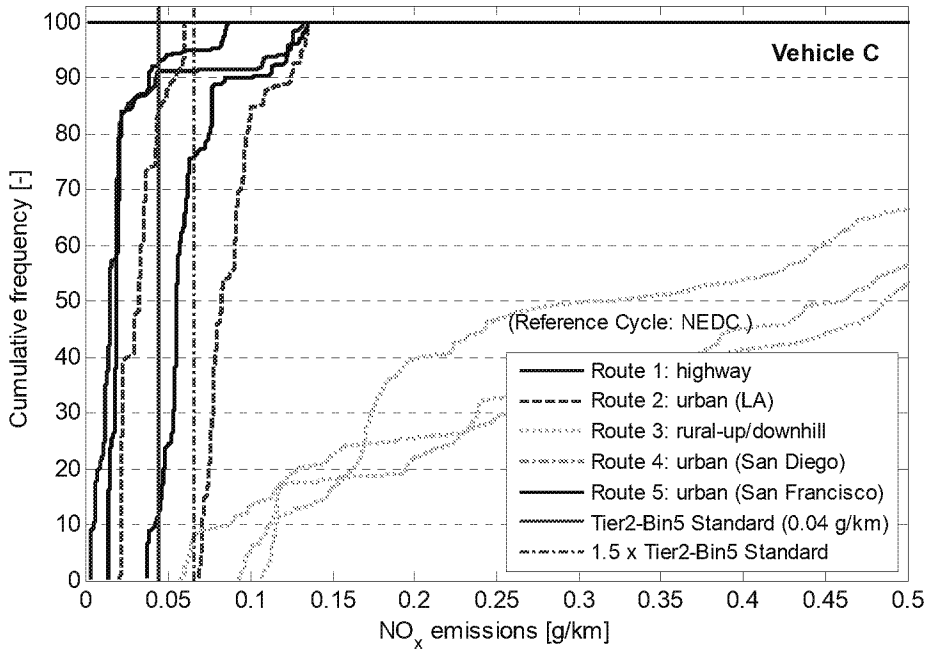


**Figure 4.34: Zoomed x-axis of Figure 4.32 showing averaging window $NO_x$ emissions for Vehicle C over the five test routes compared to US-EPA Tier2-Bin5 emissions standard**

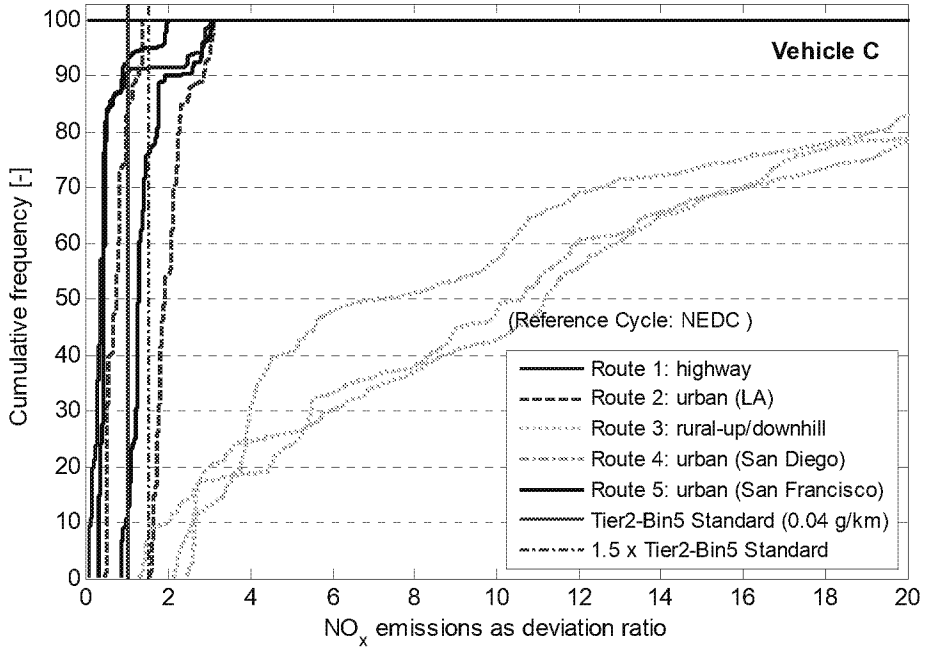


**Figure 4.35: Zoomed x-axis of Figure 4.33 showing averaging window $NO_x$ emissions for Vehicle C over the five test routes expressed as deviation ratio**

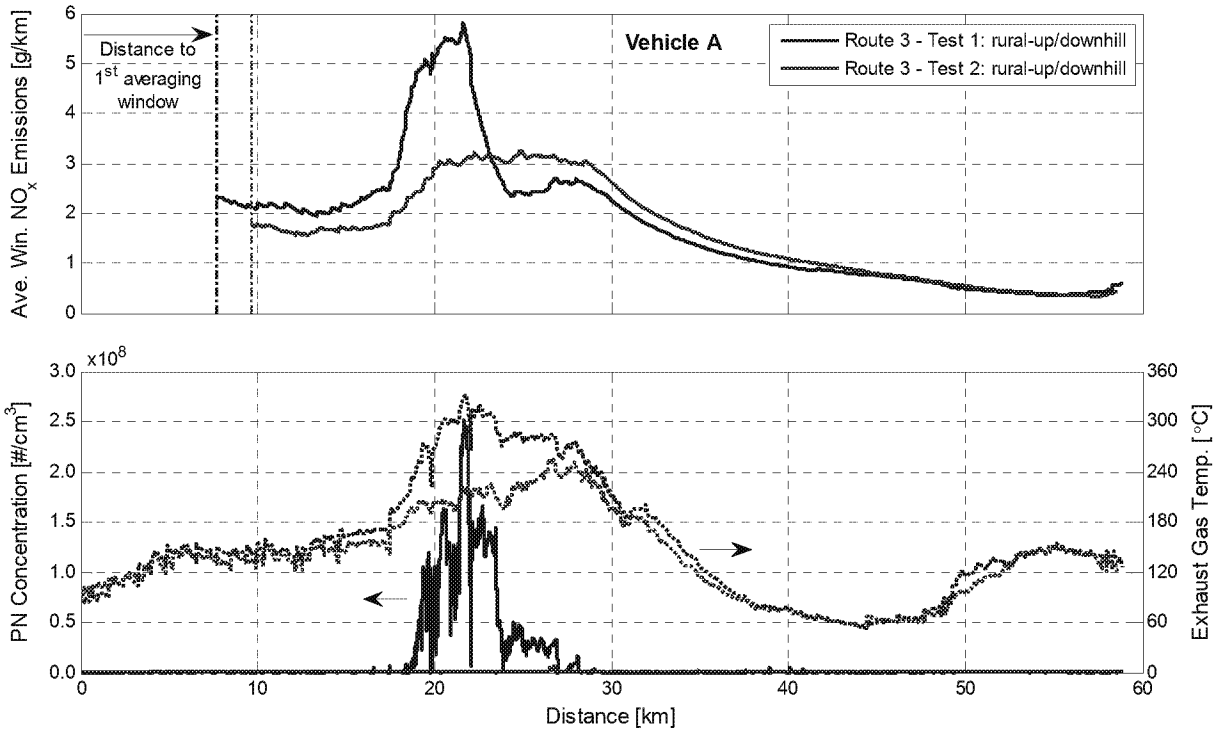


**Figure 4.36: *a*) Continuous averaging window $NO_x$ emissions, and *b*) particle number concentrations and exhaust gas temperatures (at exhaust tip) vs. distance for Route 3; test 1 with and test 2without DPF regeneration**

Figure 4.37 through Figure 4.40 depict cumulative frequencies for averaging window $NO_x$ emissions along with their deviation ratios from the US-EPA Tier2-Bin5 $NO_x$ standard over the five pre-defined test routes, similarly to Figure 4.28 through Figure 4.35, however, with mass of $CO_2$ emitted over the FTP-75 cycle selected as window size threshold value (see Table 4.10).

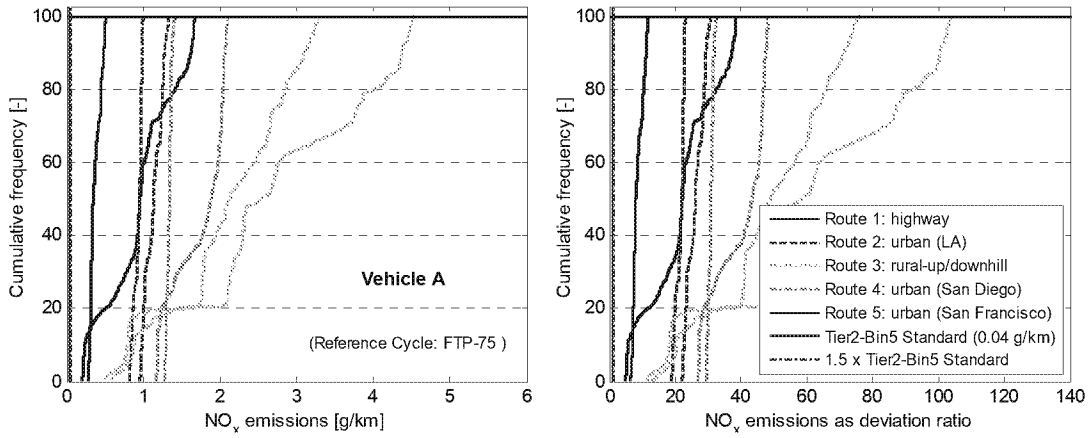


**Figure 4.37: Averaging window $NO_x$ emissions for Vehicle A over the five test routes compared to US-EPA Tier2-Bin5 emissions standard (*left*) and expressed as deviation ratio (*right*); AWM reference metric is $CO_2$ emissions over FTP-75; Route 1 includes rush-hour/non rush-hour driving**

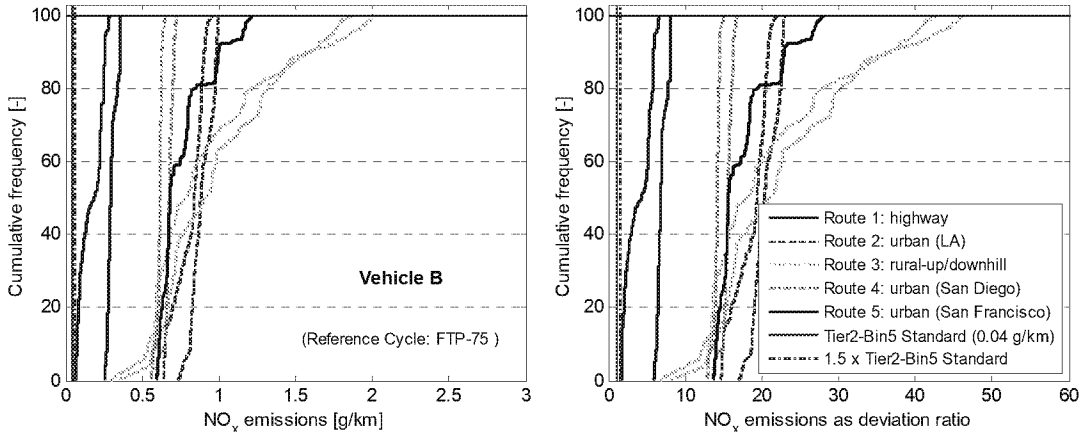


**Figure 4.38: Averaging window $NO_x$ emissions for Vehicle B over the five test routes compared to US-EPA Tier2-Bin5 emissions standard (*left*) and expressed as deviation ratio (*right*); AWM reference metric is $CO_2$ emissions over FTP-75**

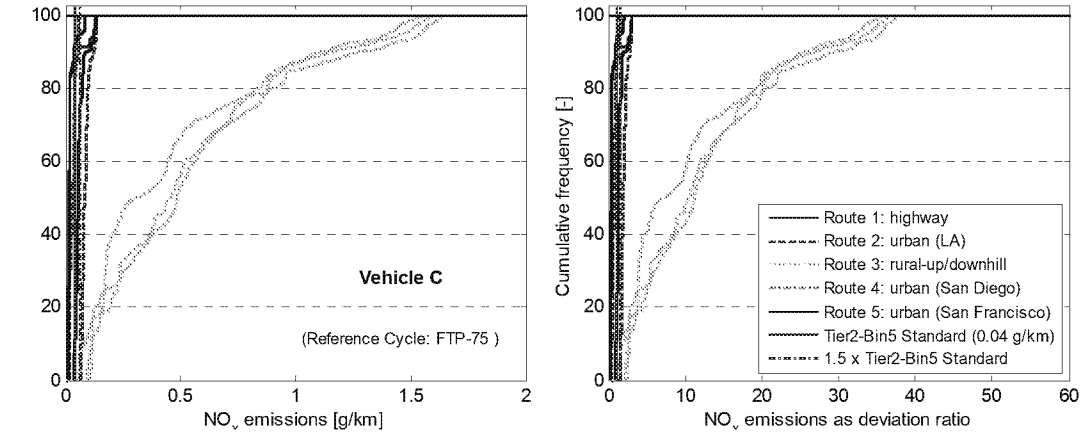


**Figure 4.39: Averaging window $NO_x$ emissions for Vehicle C over the five test routes compared to US-EPA Tier2-Bin5 emissions standard (*left*) and expressed as deviation ratio (*right*); AWM reference metric is $CO_2$ emissions over FTP-75**

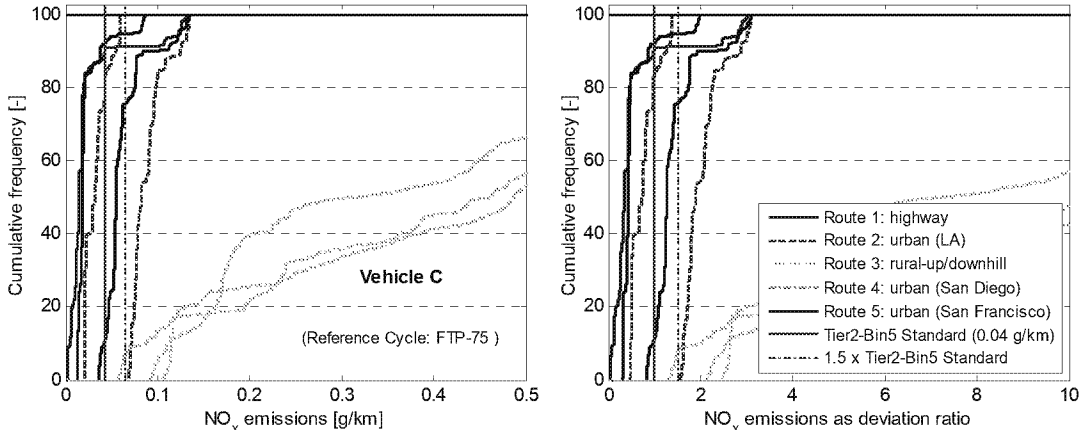


**Figure 4.40: Zoomed x-axis of Figure 4.39 showing averaging window $NO_x$ emissions for Vehicle C over the five test routes compared to US-EPA Tier2-Bin5 emissions standard (*left*) and expressed as deviation ratio (*right*)**

Figure 4.41 presents frequency distributions of exhaust gas temperatures for *Vehicles A* and *B* over two repeats of test Routes 1 through 4. These temperature distributions reflect exhaust gas temperatures measured by vehicle sensors (broadcasted via ECU CAN) downstream the DPF and upstream the $deNO_x$ after-treatment devices for *Vehicle A* and *B*, respectively.

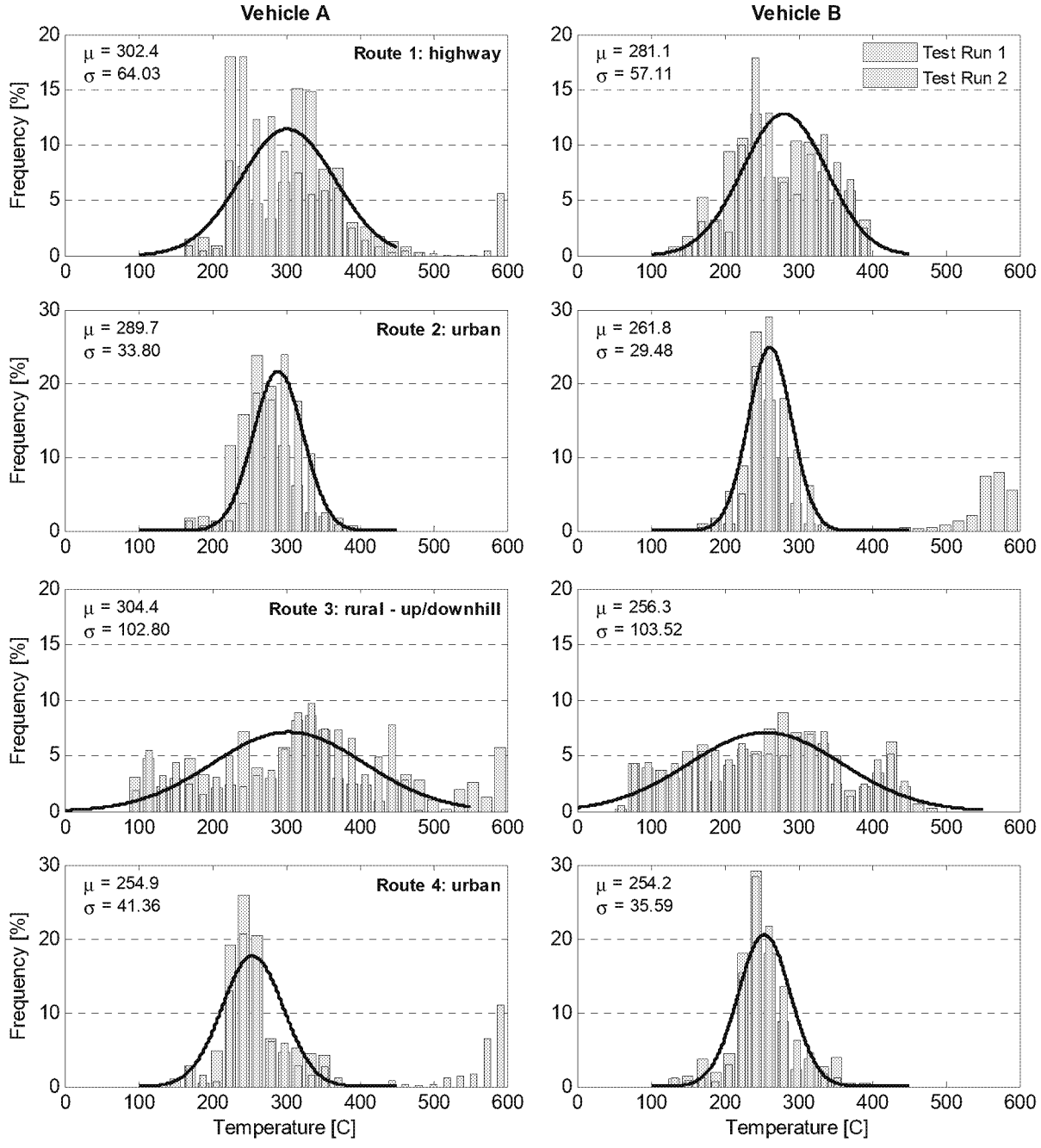


**Figure 4.41: Frequency distributions of exhaust gas temperatures at downstream DPF location for Vehicle A and B over Routes 1 through 4 with two repeats; data fitted by normal distribution (not including data for high temperature excursions during DPF regeneration events)**

Each temperature dataset is fitted by a normal distribution curve (bold dark line) which does not include any data points from the high temperature excursions observed for Vehicle A, Routes 1, 3, and 4 as well as for Vehicle B, Route 2 (see Figure 4.41). A distinct temperature distribution pattern can be noticed as a function of different driving conditions, namely, highway (i.e. Route 1), urban/suburban (i.e. Routes 2, 4), and rural-up/downhill (i.e. Route 3). Urban/suburban driving was found to exhibit narrow temperature distributions centered ($\mu$) around 255 to 280°C with a spread ($\sigma$) of 30 to 40°C, whereas highway driving conditions led to increased mean exhaust temperatures ($\mu$ = 280 to 300°C) owing to the elevated engine loads associated with high-speed driving, as well as a distinctively wider spread of the temperature distribution ($\sigma$ = 57 to 64°C). On the other hand, rural-up/downhill driving was observed to exhibit a relatively large range of varying exhaust gas temperatures with the majority of values falling between 100 and 500°C ($\mu$ = 255 to 300°C, $\sigma \approx$ 103°C). This is due to the particular characteristics of the test route (i.e. Route 3) that follows on the exact same street up and downhill to a turning point, leading to i) high exhaust temperature conditions during the uphill portion caused by increased engine load demand, and ii) low exhaust temperature conditions during the downhill portion where the vehicle predominantly coasts with fueling cut-off, thereby, effectively transforming the engine to an '*air-pump,*' pumping intake air at ambient temperatures through the engine and after-treatment system cooling its components (e.g. catalysts) down.

Route 1 - test 2, Route 3 - test 1, Route 4 - test 2 for *Vehicle A* as well as Route 2 - test 1 for *Vehicle B* show a distinct second mode in the upper temperature range centered around 600°C. The observed increase in exhaust gas temperature is due to DPF regeneration events occurring during some of the test runs, where elevated temperatures are required to initiate the periodic soot oxidation from the surface of the filter substrate.

### 4.2.2 $NO_x$ Emissions over Cross-Multi-State Driving Route

This section presents cumulative frequency plots for averaging window $NO_x$ emissions in Figure 4.42 (Zoom-in to x-axis shown in Figure 4.44) along with deviation ratios from the US-EPA Tier2-Bin5 standard for $NO_x$ (at full useful life) in Figure 4.43 for *Vehicle B* over individual portions of the cross-multi state driving route with total $CO_2$ emitted over the NEDC (see Table 4.10) chosen as reference value for calculating averaging window size.

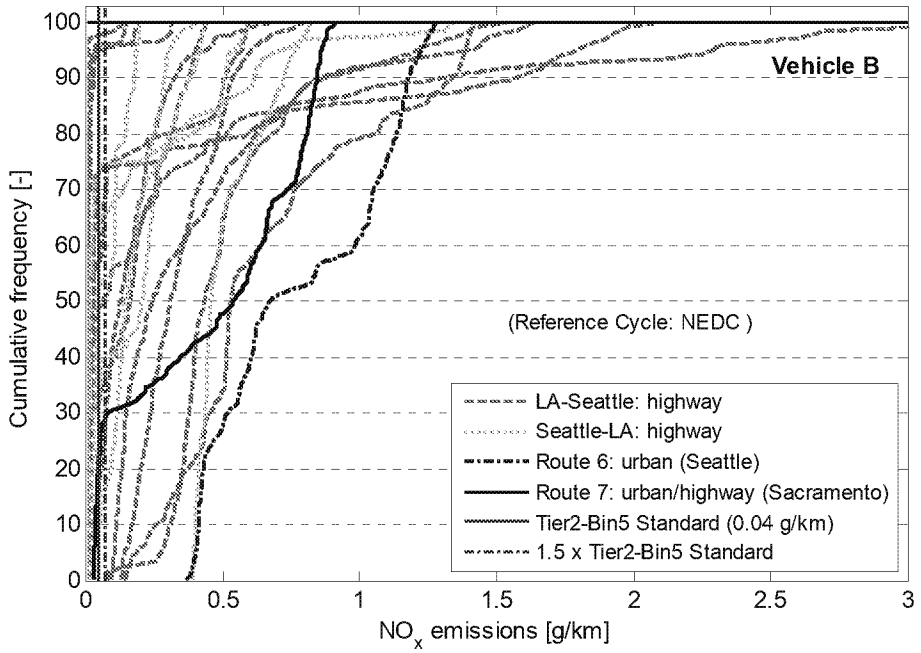


**Figure 4.42: Averaging window $NO_x$ emissions for Vehicle B over cross-multi-state driving route portions compared to US-EPA Tier2-Bin5 emissions standard; AWM reference metric is $CO_2$ emissions over NEDC**

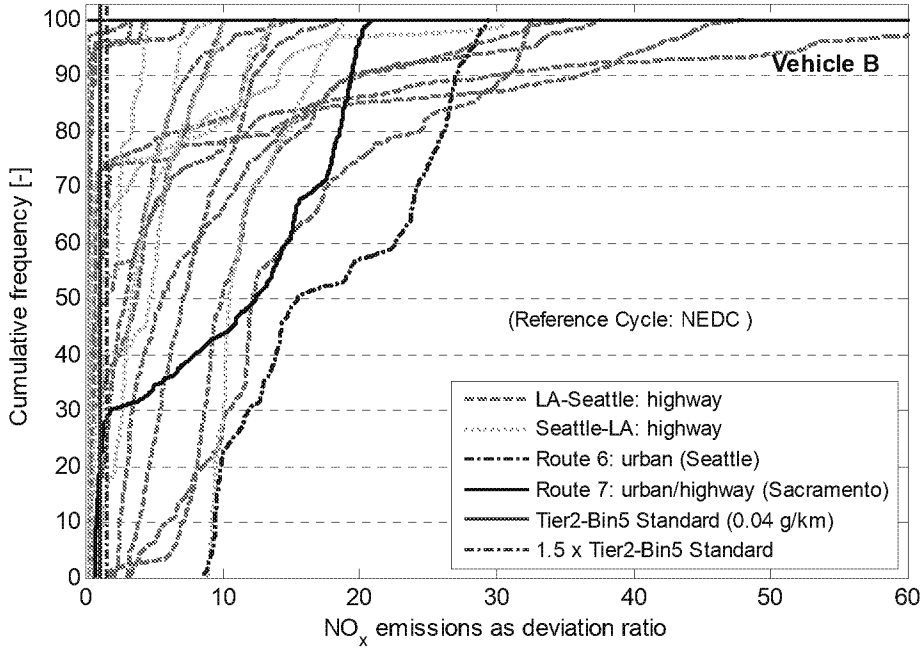


**Figure 4.43: Averaging window $NO_x$ emissions for Vehicle B over cross-multi-state driving route portions expressed as deviation ratio; AWM reference metric is $CO_2$ emissions over NEDC**

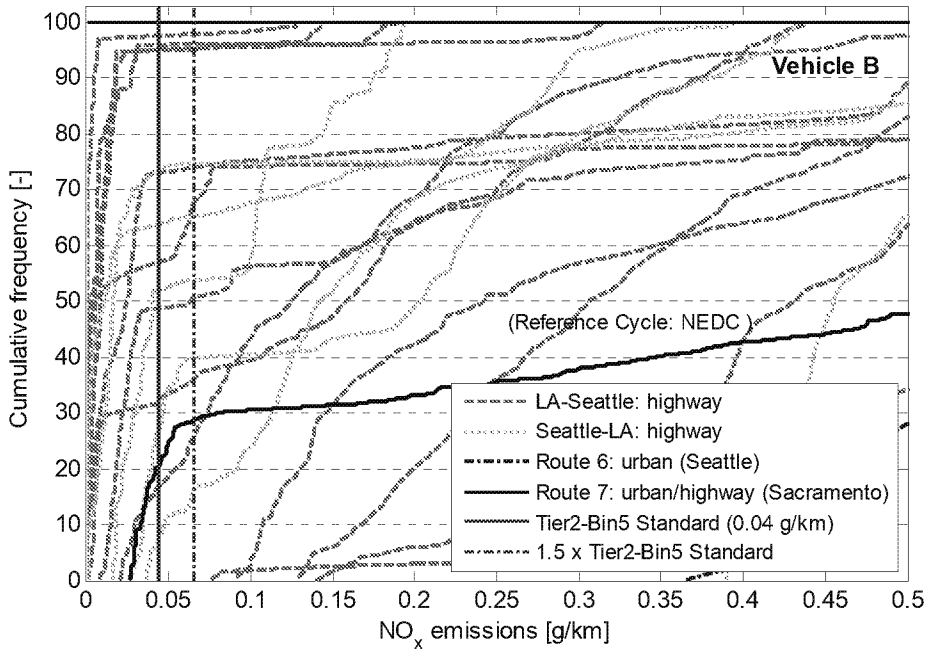


**Figure 4.44: Zoomed x-axis of Figure 4.42 showing averaging window $NO_x$ emissions for Vehicle B over cross-multi-state driving route portions compared to US-EPA Tier2-Bin5 emissions standard**

Overall, cumulative frequencies of averaging window $NO_x$ emissions over the majority of individual portions of the cross-multi state driving route agree with results seen from the pre-defined test routes (see Figure 4.30) for *Vehicle B*. It can be noticed that 50% of windowed $NO_x$ emissions during urban/suburban driving conditions (i.e. Routes 6 and 7) exceed the applicable standard by more than a factor of 10, similar to what was observed over urban Routes 2, 4, and 5. Route 7 exhibits a distinct change in $NO_x$ emissions as can be seen from Figure 4.44 (dark filled line). This is due to a significant portion of highway driving (> 60% by distance) contained in this route which accounts for ~20% of $NO_x$ emissions to be below the US-EPA Tier2-Bin5 standard whereas the smaller portion of the route (< 40% by distance) accounts for significantly increased $NO_x$ levels with 50% of the emissions deviating by 10 to 20 times from the standard.

On the other hand, Figure 4.44 also shows that under particular conditions, *Vehicle B* was observed to have $NO_x$ emissions well below the US-EPA Tier2-Bin5 level, specifically with route portions 3, 4, 5, and 6 exhibiting ~95% of windowed $NO_x$ emissions below the regulatory standard. It is worthy to mention that DPF regeneration events did not seem to noticeably affect $NO_x$ emissions from the urea-SCR based *Vehicle B* in the same manner as they were observed to influence $NO_x$ emissions rates from the LNT equipped *Vehicle A*.

## 4.3 On-Road Particle Number and Mass Emissions

This section will present and discuss particulate number and mass emissions concentrations over the pre-defined test routes for *Vehicles A* and *B* in Section 4.3.1 as well as over the cross-multi state driving route for *Vehicle B* in Section 4.3.2. It has to be noted that all PN and PM emissions concentrations presented herein are inferred from real-time particle measurements using a charge-type particle sensor (i.e. Pegasor particle sensor).

### 4.3.1 PN Emissions over Pre-Defined Test Routes

Figure 4.45 through Figure 4.52 present comparisons of raw particle number concentrations in units [#/cm$^3$] between two consecutive test runs for Routes 1 through 4 and *Vehicles A* and *B* plotted against driving distance. It has to be noted that for the purpose of this comparison PN concentrations reflect raw particle concentrations in the exhaust stream per unit volume (i.e. cm$^3$) and not total number of particles released from the engine which one could obtain by multiplying average PN concentration into total exhaust flow. Exhaust gas temperatures, as measured at the exhaust sample extraction point (i.e. at outlet of exhaust tip), are plotted along with PN concentrations to aid in identifying possible DPF regeneration events. To the right side of each continuous PN concentration and exhaust temperature graph is a bar chart providing PN emissions factors in [#/km] for each individual test (i.e. repetition of a given route) corresponding to PN results already presented in Figure 4.13 during Section 4.1.1.

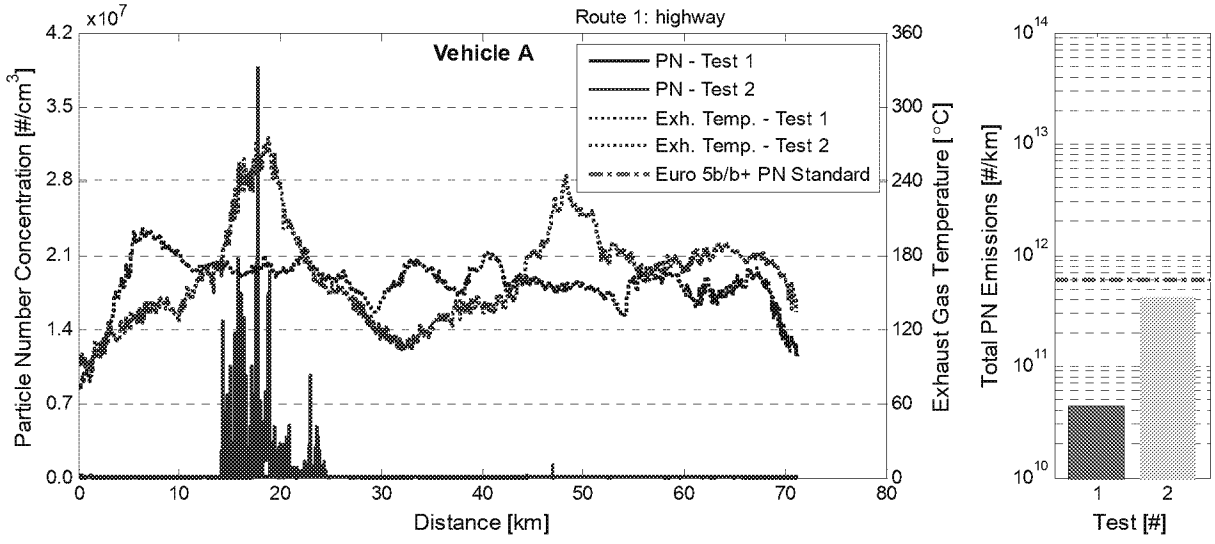


**Figure 4.45: Comparison of particle number concentrations between two tests of Route 1 for Vehicle A, DPF regeneration event during test 2**

Figure 4.45 and Figure 4.46 present PN emissions concentrations during highway driving (i.e. Route 1) for *Vehicles A* and *B*, respectively. *Vehicle A* can be noticed to have experienced a moderate DPF regeneration event between 15 and 25km into the test route leading to an order of magnitude increase in PN emissions factor for test 2 as compared to test 1. However, the observed regeneration event did not cause PN emission to exceed the Euro 5b/b+ PN standard. No DPF regeneration event is seen for *Vehicle B* during highway operation over Route 1.

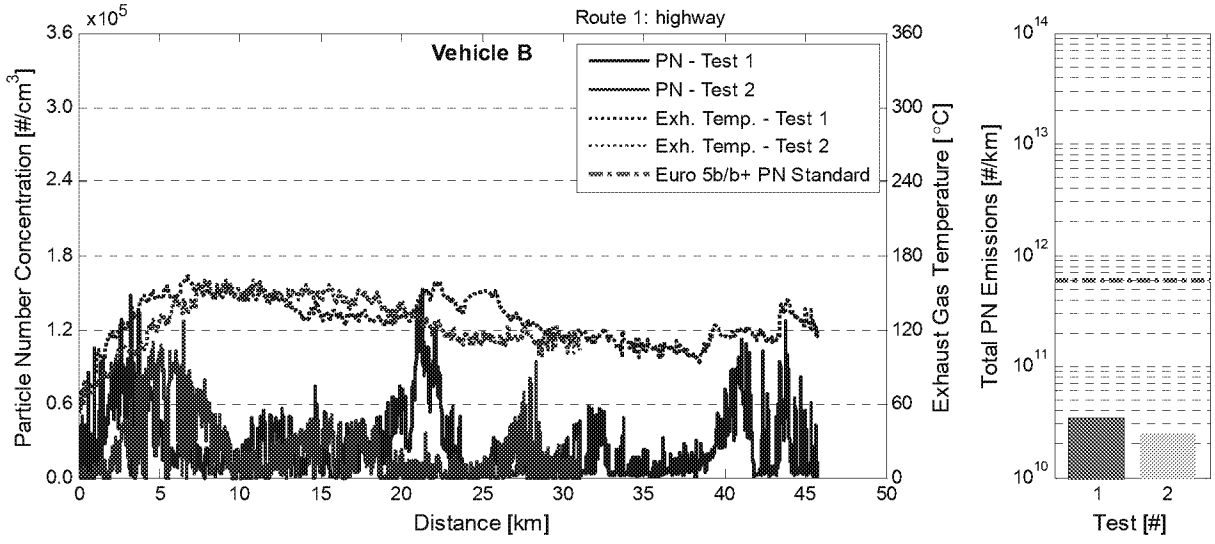


**Figure 4.46: Comparison of particle number concentrations between two tests of Route 1 for Vehicle B, No DPF regeneration event observed**

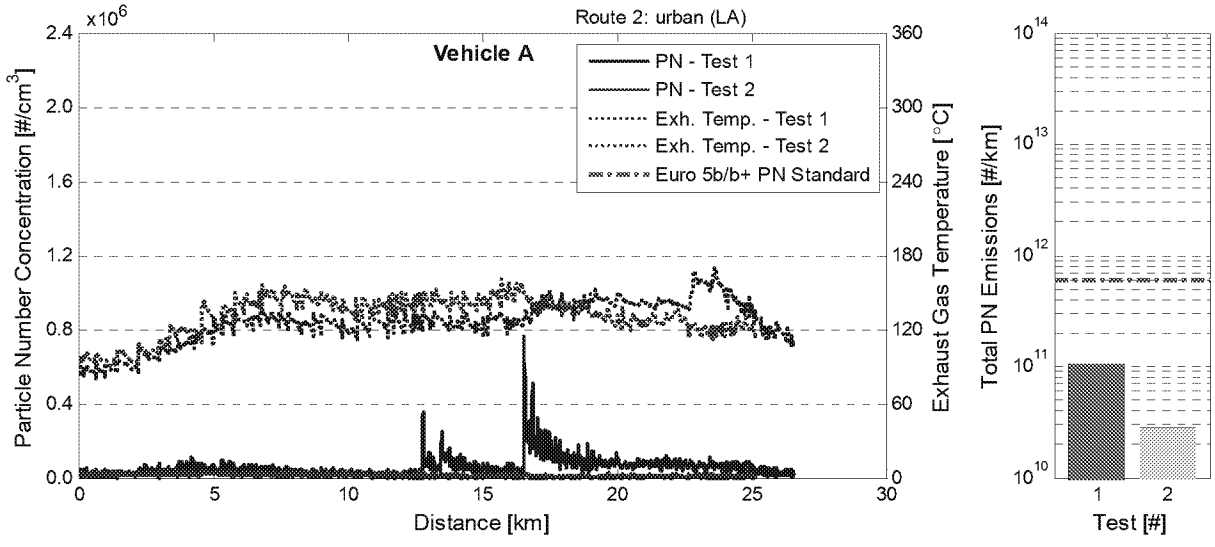


**Figure 4.47: Comparison of particle number concentrations between two tests of Route 2 for Vehicle A, No DPF regeneration event observed**

Figure 4.47 and Figure 4.48 show PN emissions concentrations during Route 2 for *Vehicles A* and *B*, respectively. Contrary to Route 1, during Route 2 driving *Vehicle B* exhibits a DPF regeneration event during the second half of the first test run as recognizable from either the significantly increased PN concentrations (> 2 orders of magnitude) or the increase in exhaust gas temperature by a factor of 2 when compared to test run 2 which lacks a regeneration event. Furthermore, the DPF regeneration event resulted in the PN emissions factor exceeding the applicable PN standard by an order of magnitude (i.e. $5.51 \times 10^{12}$#/km vs. $6.0 \times 10^{11}$#/km).

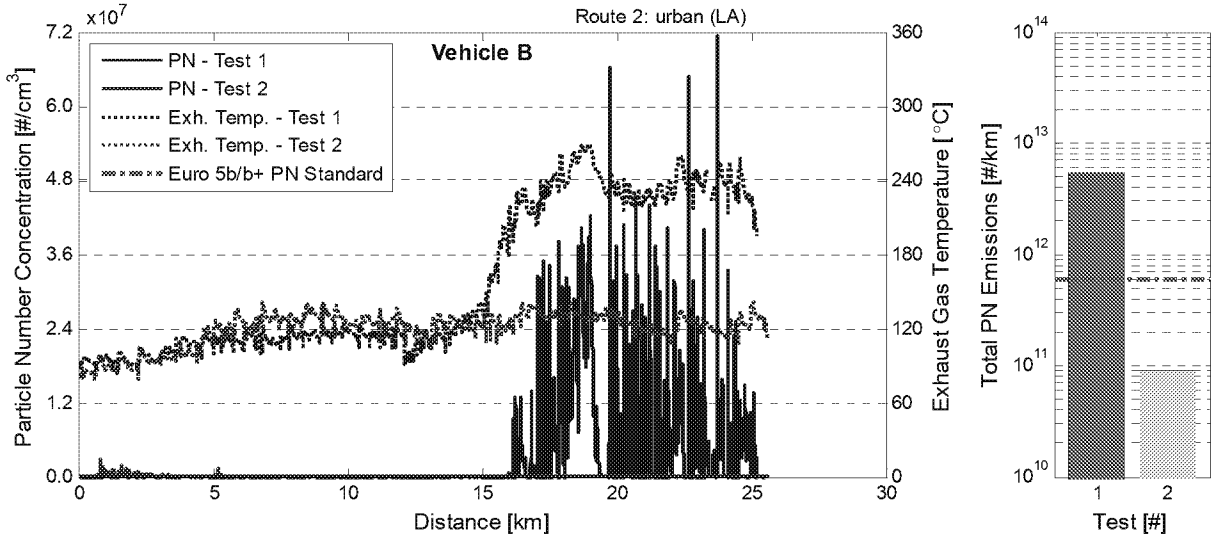


**Figure 4.48: Comparison of particle number concentrations between two tests of Route 2 for Vehicle B, DPF regeneration event during test 1**

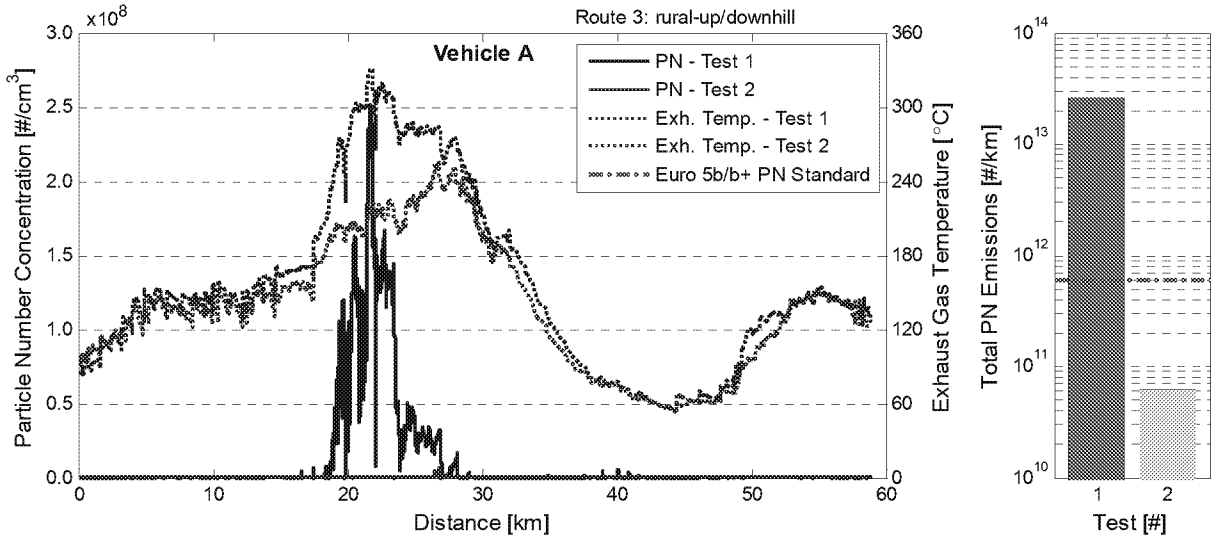


**Figure 4.49: Comparison of particle number concentrations between two tests of Route 3 for Vehicle A, DPF regeneration event during test 1**

Figure 4.49 and Figure 4.50 show PN emissions concentrations during Route 3 for *Vehicles A* and *B*, respectively, with DPF regenerations noticed for both vehicles. *Vehicle A* exhibited a regeneration event during the uphill portion of the first test run (at 18 to 27km) with the PN standard being exceeded by two orders of magnitude ($2.61 \times 10^{13}$#/km), whereas *Vehicle B* showed repeatable signs of moderate regeneration events at the same location for both test runs. Also, PN emissions factors for *Vehicle B* are exceeding the Euro 5b/b+ PN standard during both consecutive test runs of Route 3.

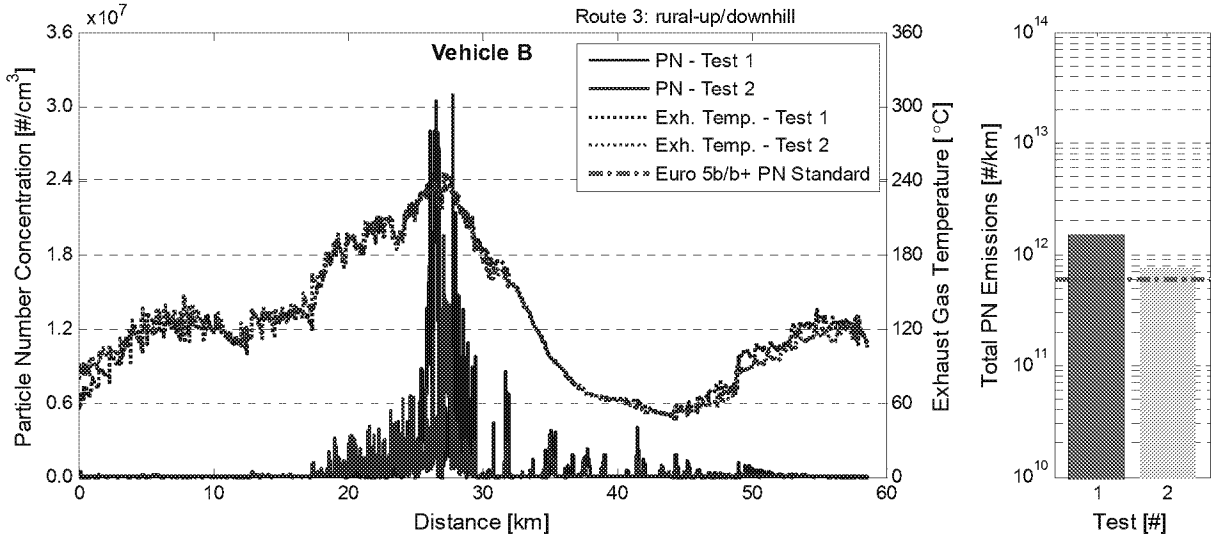


**Figure 4.50: Comparison of particle number concentrations between two tests of Route 3 for Vehicle B, DPF regeneration event during both tests**

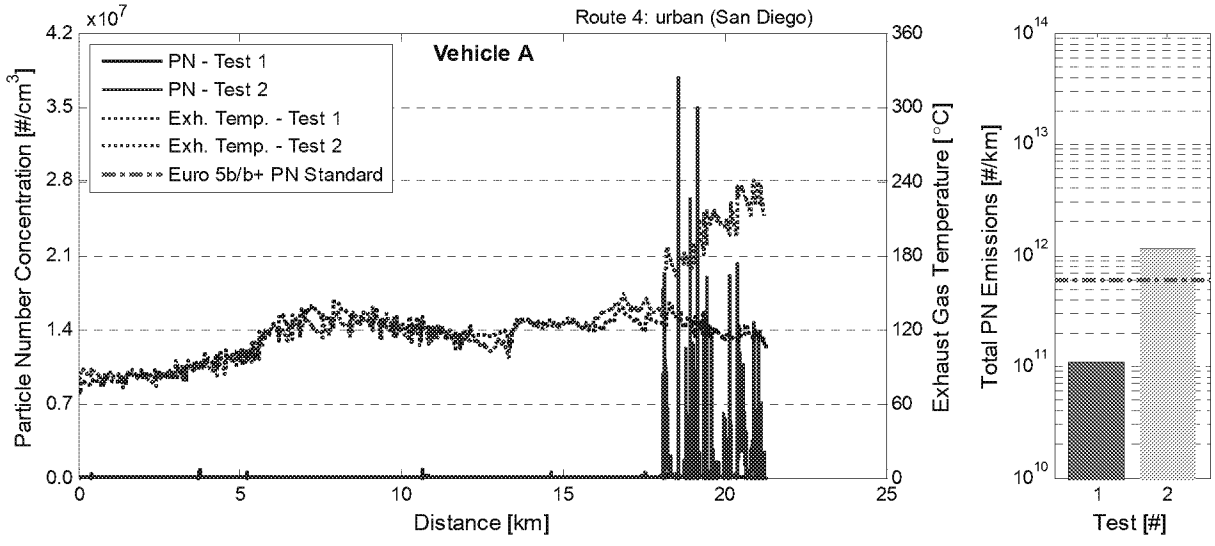


**Figure 4.51: Comparison of particle number concentrations between two tests of Route 4 for Vehicle A, DPF regeneration event during test 2**

Finally, Figure 4.51 and Figure 4.52 show PN emissions concentrations during Route 4 for *Vehicles A* and *B*, respectively. While *Vehicle B* does not experience any DPF regeneration event with PN emissions factors remaining well below the regulatory standard, *Vehicle A* exhibits the onset of a regeneration event towards the end of the second repetition leading to PN emissions one order of magnitude greater than observed for the test run without event.

Additionally, it is interesting to notice that while there was no DPF regeneration event occurring exhaust gas temperatures for both vehicles show a strong similarity. This can be explained by the fact that both *Vehicles A* and *B* are equipped with an identical engine that most likely is programmed with same or at least nearly same base calibration parameters. Also, the actual vehicle test weight only differed by 29kg between *Vehicle A* and *B* leading to similar load conditions for both engines during testing.

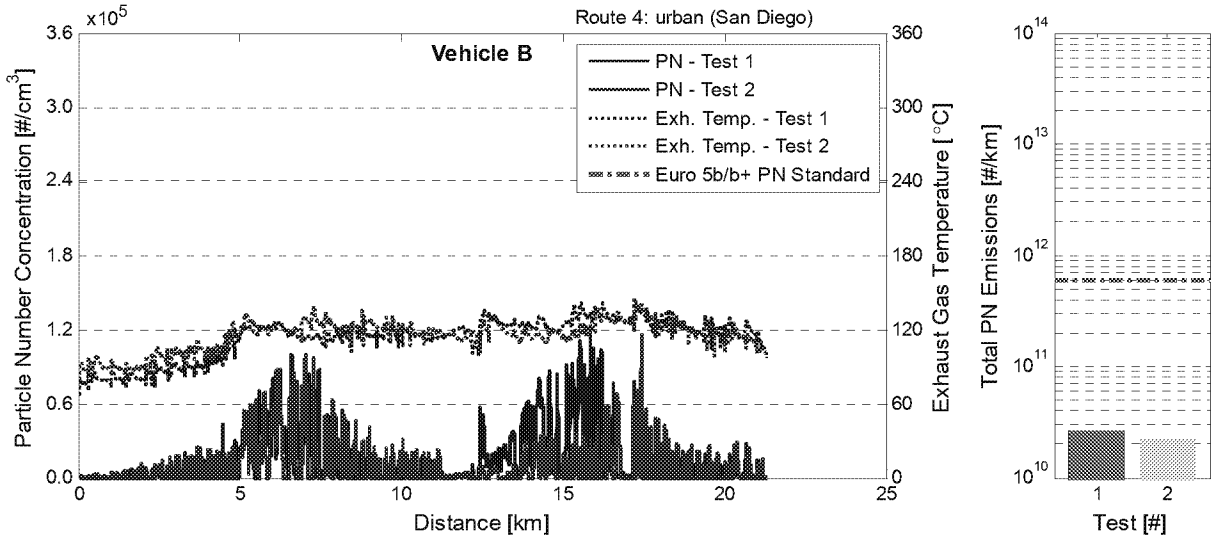


**Figure 4.52: Comparison of particle number concentrations between two tests of Route 4 for Vehicle B, No DPF regeneration event observed**

### 4.3.2 PM and PN Emissions over Cross-Multi-State Driving Route

This section presents raw particulate number and mass emissions concentrations in the exhaust stream in Figure 4.53 and Figure 4.54, respectively, for *Vehicle B* over the entire cross-multi state driving route. Four distinct DPF regeneration events can be noticed in Figure 4.53 from predominant particulate number concentration (blue line) spikes that increase by four orders of magnitude to $1.4 \times 10^8$ #/cm$^3$ over the typical concentration level of $2 \times 10^4$ #/cm$^3$. These events of drastic increase in particulate number concentrations are accompanied, as expected, by

excursions in exhaust gas temperatures as thermal conditions of after-treatment and exhaust stream are increased in order to initiate soot oxidation on the DPF substrate. Exhaust gas temperatures were observed to increase from typical levels throughout the route of ~320°C to ~560°C during the DPF regeneration events. It has to be noted that temperatures depicted in Figure 4.53 and Figure 4.54 were measured at post SCR location by an on-board temperature sensor, acquired via ECU CAN interrogation.

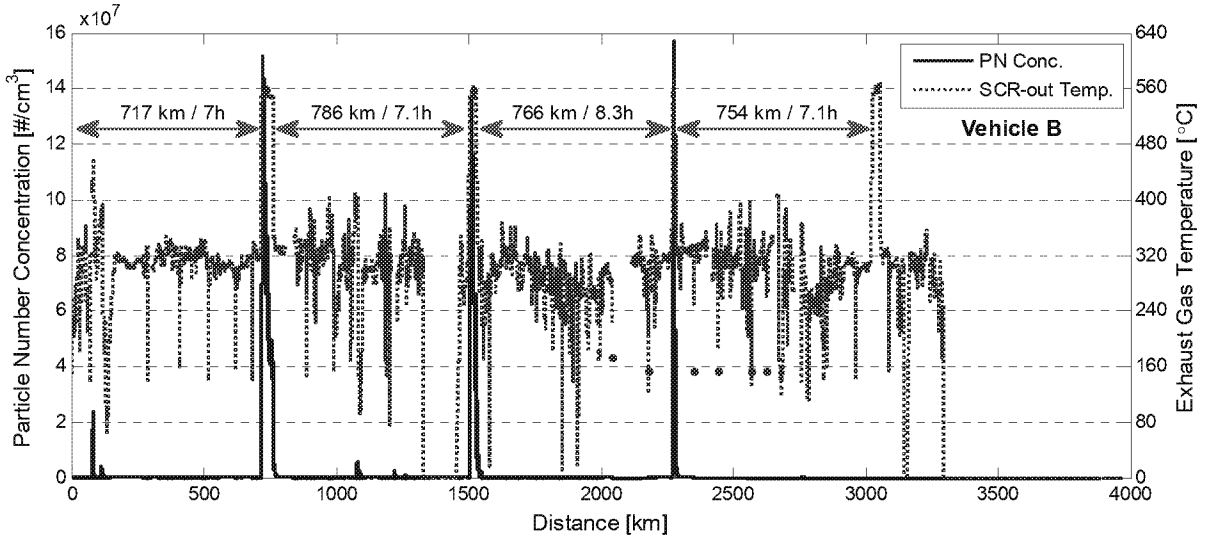


**Figure 4.53: Particle number concentration and exhaust gas temperature at SCR outlet location of test vehicle over cross-multi-state driving route; Note: PN concentration spikes indicate DPF regeneration events**

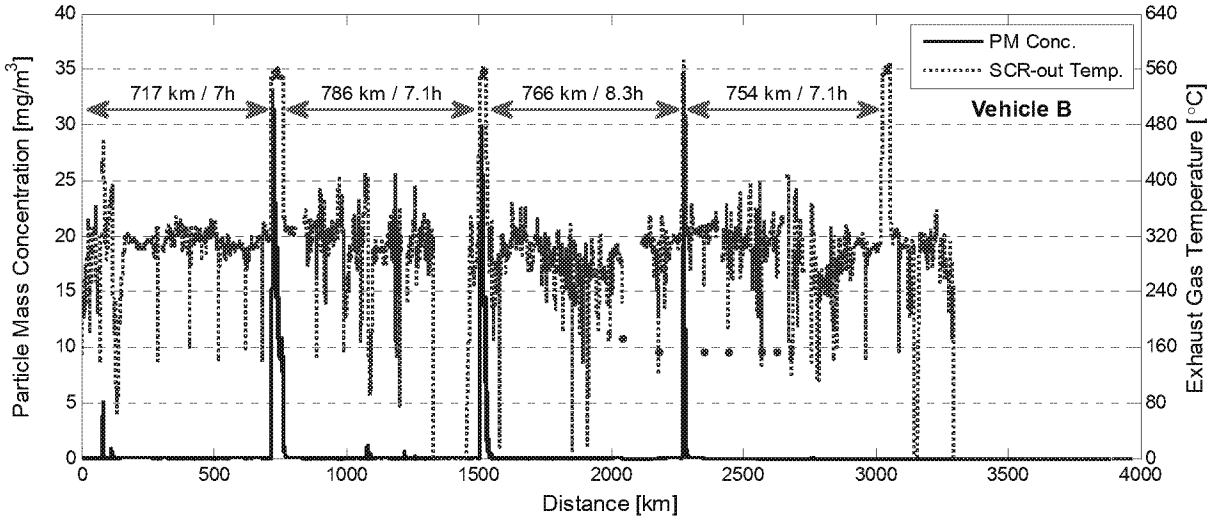


**Figure 4.54: Particle mass concentration and exhaust gas temperature at SCR outlet location of test vehicle over cross-multi-state driving route; Note: PN concentration spikes indicate DPF regeneration events**

Even though four distinct exhaust gas temperature excursions can be noticed from Figure 4.53, thus indicating four DPF regeneration events throughout the entire route, only three particulate number concentration spikes are observed. This is due to the fact that the real-time particle sensor was not operational after ~2600km as the electrical air compressor providing pressurized air to the sensor had failed. However, even though lacking actual particle measurements, but solely based on the preceding data it can be concluded with the necessary confidence that the temperature excursion around 3023km is indicative of a DPF regeneration event.

It is interesting to notice from Figure 4.53 that DPF regeneration events are nearly equally spaced both on a spatial (i.e. distance traveled) and temporal (i.e. duration between event) basis as can be seen from Table 4.11. On average the vehicle traveled approximately 756km ±29km (±1σ) between individual regeneration events which was observed to correspond to ~7.07hours ±0.06hours (±1σ, not including third event) on a temporal basis. Even though the distance traveled between events 2 and 3 is of similar length than for other events, the time required was observed to be ~17% longer (7.07hours vs. 8.3hours). A possible explanation for this difference is that the route between regeneration events 2 and 3 included low vehicle speed urban/suburban driving in and around Seattle, WA, leading to increased travel time to accumulate ~756km. Overall, these results ultimately lead to conclude that DPF regeneration intervals are predominantly distance based which agrees with descriptions given for after-treatment control strategies for Vehicle A in [31] (see from Figure 12 in [31]) which are most likely similar to *Vehicle B* as well as the same engine and DPF configurations are used in both vehicles. Furthermore, the observed average duration of a DPF regeneration event was 15min ±6min (±1σ) as seen from Table 4.11, thereby in agreement with system descriptions provided in [31].

**Table 4.11: Distance and time based DPF regeneration frequencies and duration for Vehicle B over cross-multi state driving route**

| Event [#] | Distance to event [km] | Distance based $f_{regen}$ [km] | Time to event [hr] | Time based $f_{regen}$ [hr] | Duration [min] |
|---|---|---|---|---|---|
| 1 | 717 | *717* | 7.0 | *7.0* | 22.4 |
| 2 | 1,503 | *786* | 14.1 | *7.1* | 15.2 |
| 3 | 2,269 | *766* | 22.3 | *8.3* | 7.5 |
| 4 | 3,023 | *754* | 29.5 | *7.1* | 15.8 |

# 5 CONCLUSIONS

Three light-duty diesel vehicles equipped with two different $NO_x$ abatement technologies, namely lean-$NO_x$ trap and urea-based selective catalytic reduction system, and certified to US-EPA Tier2-Bin5 and CARB LEV-II ULEV (CA) emissions standards were operated over a variety of pre-defined test routes exhibiting diverse driving conditions pertinent to major US population centers located in the state of California. Additionally, one vehicle, specifically *Vehicle B*, was driven over an extended distance of nearly 4000km predominantly composed of highway driving conditions between California and Washington State. Gaseous emissions of $NO_x$, CO, THC and $CO_2$ were measured using the OBS-2200 PEMS from Horiba Ltd., while particulate number and mass concentrations were inferred from real-time particle charge measurements employing a Pegasor particle sensor.

In summary, real-world $NO_x$ emissions were found to exceed the US-EPA Tier2-Bin5 standard (at full useful life) by a factor of 15 to 35 for the LNT equipped *Vehicle A*, by a factor of 5 to 20 for the urea-SCR fitted *Vehicle B* (same engine as *Vehicle A*) and at or below the standard for *Vehicle C* with exception of rural-up/downhill driving conditions, over five pre-defined test routes. Generally, distance-specific $NO_x$ emissions were observed to be highest for rural-up/downhill and lowest for high-speed highway driving conditions with relatively flat terrain. Interestingly, $NO_x$ emissions factors for *Vehicles A* and *B* were below the US-EPA Tier2-Bin5 standard for the weighted average over the FTP-75 cycle during chassis dynamometer testing at CARB's El Monte facility, with 0.022g/km ±0.006g/km (±1σ, 2 repeats) and 0.016g/km ±0.002g/km (±1σ, 3 repeats), respectively. Additionally, increased variability between consecutive test runs was observed for *Vehicle A* coinciding with DPF regeneration events, leading to an increase in $NO_x$ emissions by 97% (0.41 g/km to 0.81g/km), 19% (1.38g/km to 1.63g/km), and 38% (1.24g/km to 1.72g/km) for Routes 1, 3, and 4, respectively, between test runs with and without DPF regeneration events. This was speculated to be due to an extended duration of lean exhaust conditions and a lack of frequent enrichment of the exhaust gas ($\lambda < 1$) while DPF regeneration was ongoing, leading to an inhibition of necessary LNT regeneration ($D_eNOx$), and thus, causing the $NO_x$ storage catalyst to become saturated with $NO_x$ emissions that ultimately started to break through. The probability of this explanation is additionally supported by a detailed description of the after-treatment control strategy for *Vehicle A* presented elsewhere [31].

$NO_x$ emissions of *Vehicle B* over the cross-multi state driving route, comprising predominantly highway driving, were observed to be on average 0.26g/km ±0.21g/km (±1σ) or approximately 6 times exceeding the US-EPA Tier2-Bin5 standard. However, most interestingly $NO_x$ emissions were found to be below the regulatory standard for portions of the route characterized by low or negligible changes in altitude (i.e. near zero road grade), and with the vehicle operated in cruise-control mode at approximately 120km/h while traveling northbound on Interstate 5 through the San Joaquin Valley (see route portions 3 through 6 in Figure 4.17).

In general, CO and THC emissions were observed to be well below the regulatory level for all three test vehicles and driving conditions, with exception of Routes 1 and 2 for *Vehicle A* where THC emissions were seen to exceed the regulatory level by a small margin (< factor 1.25). Highest THC emissions for *Vehicle A* coincided with lowest $NO_x$ emissions however, no conclusive explanation can be presented herein for why this behavior was observed.

Highway driving showed lowest $CO_2$, whereas urban/suburban driving conditions lead to highest $CO_2$ emissions factors for all vehicles. Since both *Vehicles A* and *B* were equipped with the same engine and similar test weights (i.e. 1855kg vs. 1884kg), comparable $CO_2$ consumption patterns were observed in agreement with results obtained during chassis dynamometer testing over the NEDC for urban/suburban and highway driving portions. It has to be noted that the equivalent vehicle test weight during chassis dynamometer testing was 1701kg for both *Vehicles A* and *B*, or ~8% lower compared to vehicle weights during on-road PEMS testing. The equivalent test weight for *Vehicle C* for $CO_2$ emissions evaluation as per EPA procedure is 2495kg, or ~14% lower compared to the actual vehicle weight during on-road PEMS testing (i.e. 2903kg). Average fuel economy for highway driving with *Vehicles A* and *B* was 45.3 mpg ±8.6mpg (±σ1) and 43.7mpg ±5.7mpg (±σ1), respectively, and 27.3 mpg (no repetition) for *Vehicle C* which is ~39% lower compared to *Vehicles A* and *B*. On the other hand, urban/suburban driving results in average fuel economies of 30.0mpg ±2.9mpg (±σ1) and 26.6 mpg ±1.4mpg (±σ1) for *Vehicles A* and *B*, respectively, and 18.5mpg ±4.0mpg (±σ1) for *Vehicle C* which is 35% lower compared to *Vehicles A* and *B*. Overall, urban/suburban driving leads to a 32-39% reduction in fuel economy over highway driving.

Particulate matter mass emissions, inferred from PPS measurements, were observed below the US-EPA Tier2-Bin5 standard for *Vehicles A* and *B*. On the other hand, particulate number

emissions were found to exceed the Euro 5b/b+ PN standard during DPF regeneration events increasing by 2 to 3 orders of magnitude over emissions levels measured during none-regeneration events. It is noted that PN is not regulated in the United States. During the multi-state driving route, DPF regeneration frequency for *Vehicle B* was established to be predominantly based on distance traveled, occurring after every 756km ±29km (±1σ), corresponding to ~7.07hours ±0.06hours for highway driving conditions.

It is noted that only three vehicles were tested as part of this measurement campaign with each vehicle being a different after-treatment technology or vehicle manufacturer; conclusions drawn from the data presented herein are confined to these three vehicles. The limited data set does not necessarily permit drawing more generalized conclusions for a specific vehicle category or after-treatment technology.

# 6 REFERENCES


1 Weiss, M., Bonnel, P., Hummel, R., Manfredi, U., Colombo, R., Lanappe, G., Le Lijour, P., and Sculati, M., "Analyzing on-road emissions of light-duty vehicles with Portable Emission Measurement Systems (PEMS)," JRC Scientific and Technical Reports, EUR 24697 EN, (2011).

2 "US EPA, Fuel Economy Guide Web Site," Available at http://www.fueleconomy.gov, Last updated: March 17, (2014).

3 COMMISSION REGULATION (EU) No 582/2011, Official Journal of the European Union, May 25th, (2011).

4 COMMISSION REGULATION (EU) No 459/2012, Official Journal of the European Union, May 29th, (2012).

5 "US EPA, Emission Standards Reference Guide: Vehicle Weight Classifications," Available at http://www.epa.gov/otaq/standards/weights.htm, Last updated: November 14, (2012).

6 "Control of Air Pollution From New Motor Vehicles: Tier 2 Motor Vehicle Emissions Standards and Gasoline Sulfur Control Requirements; Final Rule," US Environmental Protection Agency, Federal Register Vol. 65, No. 28, pp. 6698 - 6870, February 10th, (2000).

7 Weiss, M., Bonnel, P., Hummel, R., and Steininger, N., "A complementary emissions test for light-duty vehicles: Assessing the technical feasibility of candidate procedures," JRC Scientific and Technical Reports, EUR 25572 EN, (2013).

8 Ericsson, E., "Variability in urban driving patterns," Transportation Research Part D, Vol. 5, pp. 337-354, (2000).

9 Delgado-Neira, O.F., "Driving Cycle Properties and their Influence on Fuel Consumption and Emissions," Ph.D. Dissertation, West Virginia University, (2012).

10 Delgado, O.F., Clark, N.N., and Thompson, G.J. "Method for translation of in-use fuel consumption and $NO_x$ emissions between different heavy-duty vehicle routes," Proceedings of the ASME 2011 Internal Combustion Engine Division Fall Technical Conference, Paper No. ICEF2011-60108, Morgantown, WV, October 2nd - 5th, (2011).

11 "The Federal Test Procedure & Unified Cycle," California Air Resources Board's Emissions Inventory Series, Volume 1, Issue 9, (*not dated*).

12 Praveen, R. B., "Measurement of Road Grade for In-use Emissions Testing Assessment," Master's Thesis, West Virginia University, December, (2012).

13 "Control of Emissions from New and In-Use Highway Vehicles and Engines," US Environmental Protection Agency, Federal Register, Title 40, Vol. 86, Subpart B, §86.158-08(c), pp. 555, (2008).

14 California Air Resources Board, "Enhanced Supplemental Federal Test Procedures Rulemaking - SFTP II," Meeting Presentation, Sacramento, (2010).

15 Horiba Ltd., "On Board Emission Measurement System OBS-2200 - Instruction Manual," March, (2009).

16 Khalek, I., "PM-PEMS Measurement Allowance Determination," Final Report, SWRI, Project 03.14936.12, June, (2010).

17 Bonnel, P., Carriero, M., Forni, F., Alessandrini, S., Montigny, F., Demircioglu, H., and Giechaskiel, B., "EU-PEMS PM Evaluation Program - First Report," JRC Scientific and Technical Reports, EUR 24543 EN, (2010).

18 Mamakos, A., Carriero, M., Bonnel, P., Demircioglu, H., Douglas, K., Alessandrini, S., Forni, F., Montigny, F., and Lesueur, D., "EU-PEMS PM Evaluation Program - Second Report - Study of Post DPF PM/PN," JRC Scientific and Technical Reports, EUR 24793 EN, (2011).

19 Mamakos, A., Carriero, M., Bonnel, P., Demircioglu, H., Douglas, K., Alessandrini, S., Forni, F., Montigny, F., and Lesueur, D., "EU-PEMS PM Evaluation Program - Third Report - Further Study on Post DPF PM/PN Emissions," JRC Scientific and Technical Reports, EUR 24883 EN, (2011).

20 Giechaskiel, B., Carriero, M., Bonnel, P., Schindler, W., Scheder, D., Bassoli, C., and Niemela, V., "Feasibility of Particulate Mass and Number Measurement with Portable Emission Measurement Systems (PEMS) for In-Use Testing," SAE Technical Paper Number 2011-24-0199, (2011).

21 Wei, Q., Rooeny, R., "The On-Board PM Mass Calibration for the Real-Time PM Mass Measurement," SAE Technical Paper Number 2010-01-1283, (2010).

22 Pegasor Ltd., "PPS Brochure," www.pegasor.fi, Finland, Accessed June, (2011).

23 Tikkanen, J., and Ntziachristos, L., "Pegasor Particle Sensor (PPS) - Potential solution for On-Board Diagnosis of Particle Filter Operation - First Results and Development Potential," 4th Biennial Conference – Emissions Solutions in Transportation, Ann Arbor, MI, October 5-8, (2009).

24 Besch, M.C., Thiruvengadam, A., Kappanna, H.K., Cozzolini, A., Carder, D.K., and Gautam, M., "Assessment of Novel In-Line Particulate Matter Sensor with Respect to OBD and Emissions Control Applications," Proceedings of the ASME 2011 ICE Division Fall Technical Conference, ICEF2011-60142, Paper Accepted for Publication, (2011).

25 Ntziachristos, L., Amanatidis, S., Rostedt, A., Janka, K., and Tikkanen, J., "Optimization of the Pegasor Particle Sensor for Automotive Exhaust Measurements," 23rd CRC Real World Emissions Workshop, San Diego, CA, April 7th-10th, (2013).

26 Ntziachristos, L., Amanatidis, S., Rostedt, A., Keskinen, K., Janka, K., and Tikkanen, J., "Calibration and performance of a novel particle sensor for automotive application," EAC - 2012, European Aerosol Conference, Granada, Spain, September 2nd-7th, (2012).

27 United Nations, ECE/TRANS/WP.29/GRPE/2012, Regulation No.49, Annex 4, Appendix 8, "Particle Number Emissions Measurement Equipment," (2012).

28 Tikkanen, J., Janka, K., Rostedt, A., Röbel, M., Amanatidis, S., and Ntziachristos, L., "Dilution Artifacts. A Significant Source of Error from Absolute Concentration and Possibly Difficult to Reproduce. PMP vs. Raw Exhaust," 17th ETH Conference on Combustion Generated Nanoparticles, Zurich, Switzerland, June 23rd - 26th, (2013).

29 Code of Federal Regulations, Title 40, Part 1065, "Engine-Testing Procedures," Available at http://ecfr.gpoaccess.gov/cgi/t/text/text-idx?c=ecfr&sid=024e8bd580a1b0936f51ab7cfb1615f1&rgn=div5&view=text&node=40:32.0.1.1.10&idno=40, Last Accessed: September 30, (2013).

30 "Light-Duty Vehicle Greenhouse Gas Emission Standards and Corporate Average Fuel Economy Standards; Final Rule," US Environmental Protection Agency, Federal Register Vol. 75, No. 88, May 7th, (2010).

31 Hadler, J., Rudolph, F., Dorenkamp, R., Kosters, M., Mannigel, D., and Veldten, B., "Volkswagen's New 2.0l TDI Engine for the Most Stringent Emission Standards - Part 2," MTZ Worldwide, Vol. 69, June, (2008).

32 Suresh, A., Khan, A., and Johnson, J.H., "An Experimental and Modeling Study of Cordierite Traps - Pressure Drop and Permeability of Clean and Particulate Loaded Traps," SAE Technical Paper No. 2000-01-0476, (2000).

33 Besch, M.C., Thiruvengadam, A., Kappanna, H.K., Cozzolini, A., Carder, D.K., Gautam, M., and Tikkanen, J., "Assessment of Novel In-Line Particulate Matter Sensor with Respect to OBD and Emissions Control Applications," Proc. of the ASME 2011 ICE Division Fall Technical Conference, Paper No. ICEF2011-60142, Morgantown, WV, Oct. 2nd-5th, (2011).

34 Andersson, J., Clarke, D., and Giechaskiel, B., "UN-GRPE Phase 3 Inter-Laboratory Correlation Exercise: Updated Framework and Laboratory Guide for Heavy-Duty Engine Testing." Working Paper No.GRPE-PMP-22-4, 22nd PMP working meeting, December (2007).

35 Giechaskiel, B., Ilara, P., and Andersson, J. "Particle Measurement Programme (PMP) light-duty inter-laboratory exercise: Repeatability and reproducibility of the particle number method," Aero. Sci. Technol., Vol. 42, Issue 7, pp. 528-543, (2008).

36 Andersson, J., Mamakos, A., Giechaskiel, B., Carriero, M., and Martini, G., "Particle Measurement Programme (PMP) Heavy-duty Inter-laboratory Correlation Exercise (ILCE_HD)," Final Report, Joint Research Center, Institute for Energy, EUR 24561 EN, (2010).

37 Johnson, K., Durbin, T.D., Jung, H., Chaudhary, A., Cocker III, D.R., Herner, J.D., Robertson, W.H., Huai, T., Ayala, A., and Kittelson, D., "Evaluation of the European PMP Methodologies during On-Road and Chassis Dynamometer Testing for DPF Equipped Heavy-Duty Diesel Vehicles," Aerosol Science and Technology, Vol. 43, pp. 962–969, (2009).

38 Zheng, Z., Johnson, K.C., Liu, Z., Durbin, T.D., Hu, S., Huai, T., Kittelson, D.B., and Jung, H.S., "Investigation of solid particle number measurement: Existence and nature of sub-23 nm particles under the PMP methodology," Journal of Aerosol Science, Vol. 42, pp. 883-897, (2011).

39 Jung, H., Zheng, Z., Durbin, T.D., and Johnson, K.C., "Issues associated with solid particle measurement," ARB Chairman's air pollution seminar series, January 24th, (2012).

40 Thiruvengadam, A., Besch, M.C., Carder, D.K., Oshinuga, A., and Gautam, M., "Influence of Real-World Engine Load Conditions on Nanoparticle Emissions from a DPF and SCR

Equipped Heavy-Duty Diesel Engine," Environmental Science and Technology, Vol. 46, pp. 1907-1913, (2011).

41 Vaaraslathi, K., Keskinen, J., Giechaskiel, B., Solla, A., Murtonen, T., and Vesala, H., "Effect of Lubricant on the formation of Heavy-Duty Diesel Exhaust Nanoparticles," Environmental Science and Technology, Vol. 39, pp. 8497-8504, (2005).

42 Kittelson, D.B., Watts, W.F., Johnson, J.P., Thorne, C., Higham, C., Payne, M., Goodier, S., Warrens, C., Preston, H., Zink, U., Pickles, D., Goersamnn, C., Twigg, M.V., Walker, A.P., and Boddy, R., "Effect of fuel and lube oil sulfur on the performance of a diesel exhaust gas regenerating trap," Environmental Science and Technology, Vol. 42, pp. 9276-9282, (2008).

# 7 APPENDIX

## 7.1 Exhaust Emissions Calculations with Horiba OBS-2200

### 7.1.1 Time alignment of real-time emissions concentrations

The individual emissions concentrations are shifted to account for transport delays from the sampling plane (reference point) to the analyzer cells through the heated transfer line, heated filter and internal plumbing of the OBS. This is done in order to time-align the concentration values with the respective exhaust flow rates for calculation of time-specific mass emissions rates. Exhaust concentration alignment is automatically performed by the OBS software, hence; the emissions concentrations reported in the data sets (csv-files) are already time-aligned. Transport delay times ($T_{50}$) are calculated from spike-recovery tests during the calibration and initial setup of the OBS instrument. The csv-files report the delay times in column '*E*' in the file header.

### 7.1.2 Drift correction of real-time emissions concentrations

Drift corrections of the emissions concentrations are performed in order to account for possible analyzer drift over the measurement period. Prior to data collection over a test route, '*pre-zero*' and '*pre-span*' adjustments are performed for each analyzer. Upon completion of a test route, '*post-zero*' and '*post-span*' values are automatically collected by the OBS software for each analyzer. If the duration of a test route exceeds one hour (i.e. 3600 seconds), the OBS will automatically interrupt data collection for a period of 30 seconds to perform a '*post-zero*' and '*post-span*' check as well as make zero/span adjustments for each analyzer before continuing with data collection. Zero-drift and span-drift values are reported in columns '*I*' and '*J*', respectively of the csv-file. Using these values, the OBS software automatically performs a drift correction of the real-time emissions concentration values upon completion of data collection (e.g. end of test route) using Equation (1).

### 7.1.3 Averaging Window Method (AWM)

In this method emission rates are integrated along with one of the listed criteria from time $t = 0.0\ sec$ until the chosen criteria has reached a target value. The target values are normally derived from standardized test cycles used in certifying engine families in test cell. The time interval between $t_{start} = 0.0\ sec$ to $t_{end} = x.x\ sec$ where the integrated value of the chosen criteria

is equal to its target is called a window, and for a moving window method the process is repeated with a new starting time being $t_{start} = 0.0 + 1.0\ sec$ until a new window is achieved. Emissions rates of regulated pollutants are integrated for the above criteria windows, and have to meet the set in-use emissions standards. The criteria windows are valid only if the average engine power for each window is greater than or equal to 20% of maximum engine power. Similarly for an in-use test to be valid there should be at least 50% of criteria windows should be valid. If there are no 50% valid criteria windows in an in-use test then the window validity condition is reduced as low as 15% of maximum engine power in increments of 1% of average power. However, it has to be noted that averaging window emissions factors presented in this report are based on total emissions emitted over a given test route and are not corrected for any exclusion conditions such as exhaust temperature limits, altitude, DPF regeneration events or similar. Also, all averaging windows were considered for calculation and none were invalidated based on the 20% minimum power condition as outlined in the European Regulations No. 582/2011 [3]

## 7.2 Particle Number Measurement with European PMP Method

Streamlined with the introduction of PN limits (i.e. Euro 5b/b+ [4]), the European Union adopted a new methodology aimed at standardizing the measurement of total particle number concentrations by only counting solid particles having a diameter between 23nm and 2.5μm and that are thermally treated in order to reduce the volatile fraction, thus reducing measurement artifacts and variability [27]. This method has been previously developed under the Particle Measurement Program (PMP) of the United Nation's Economic Commissions for Europe - Group of Experts on Pollution and Energy (UN-ECE-GRPE) [34, 35, and 36] leading to the following operational definition of particle numbers: '*measurement of solid particles having a diameter between 23nm and 2.5μm and are of sufficiently low volatility to survive a residence time of 0.2sec at 300°C*' [37].

The sampling system comprises a volatile particle remover (VPR) and an ultrafine particle counter optimized for a 50% counting efficiency for 23nm size particles. The VPR is designed to remove the volatile and semi-volatile fractions in the exhaust sample, thereby aiming at suppressing particle nucleation and the formation of artifacts in the sample stream. A first stage hot dilution (at 150 to 400°C and dilution ratio of 10) is used to reduce particle concentration in

the sample before being directed into the evaporation tube (operated at 300 to 400°C) where the volatile and semi-volatile components are being transferred to a gaseous state. It follows a second cold dilution stage (dilution ratio between 10 to 15) to i) rapidly lowering the partial pressures of the gaseous components aimed at preventing their re-condensation, and ii) lowering the sample temperature to below 35°C prior to entering the particle counting device. The Pegasor particle sensor for example has the advantage of not having a very limited range requirement for sample inlet temperatures (up to ~800°C), thus allowing for direct measurement of raw exhaust gases and thereby ultimately reducing the magnitude of size dependent particle losses as occurring in the VPR.

However, the PMP approach for particle number measurements has come under scrutiny as recent studies have on one hand observed significant semi-volatile particles downstream the VPR [38, 39], and on the other hand measured increased concentrations of particles below the size of 23nm being emitted from DPF equipped vehicles. These ultrafine particles are believed to comprise sulfuric acid and assumed to be emitted from catalytic oxidation of sulfur from lubrication oil [40, 41, and 42]. Johnson et al. [37] evaluated the European PMP methodology during on-road vehicle testing and observed a significant portion of particles in the size range below 20nm even though the sample stream was thermally treated according to PMP requirements, thus questioning the applicability of the 23nm lower cut-point for particle measurements, as mandated by the European PMP regulation.

## 7.3 PEMS Comparison with CVS System for Gaseous Emissions

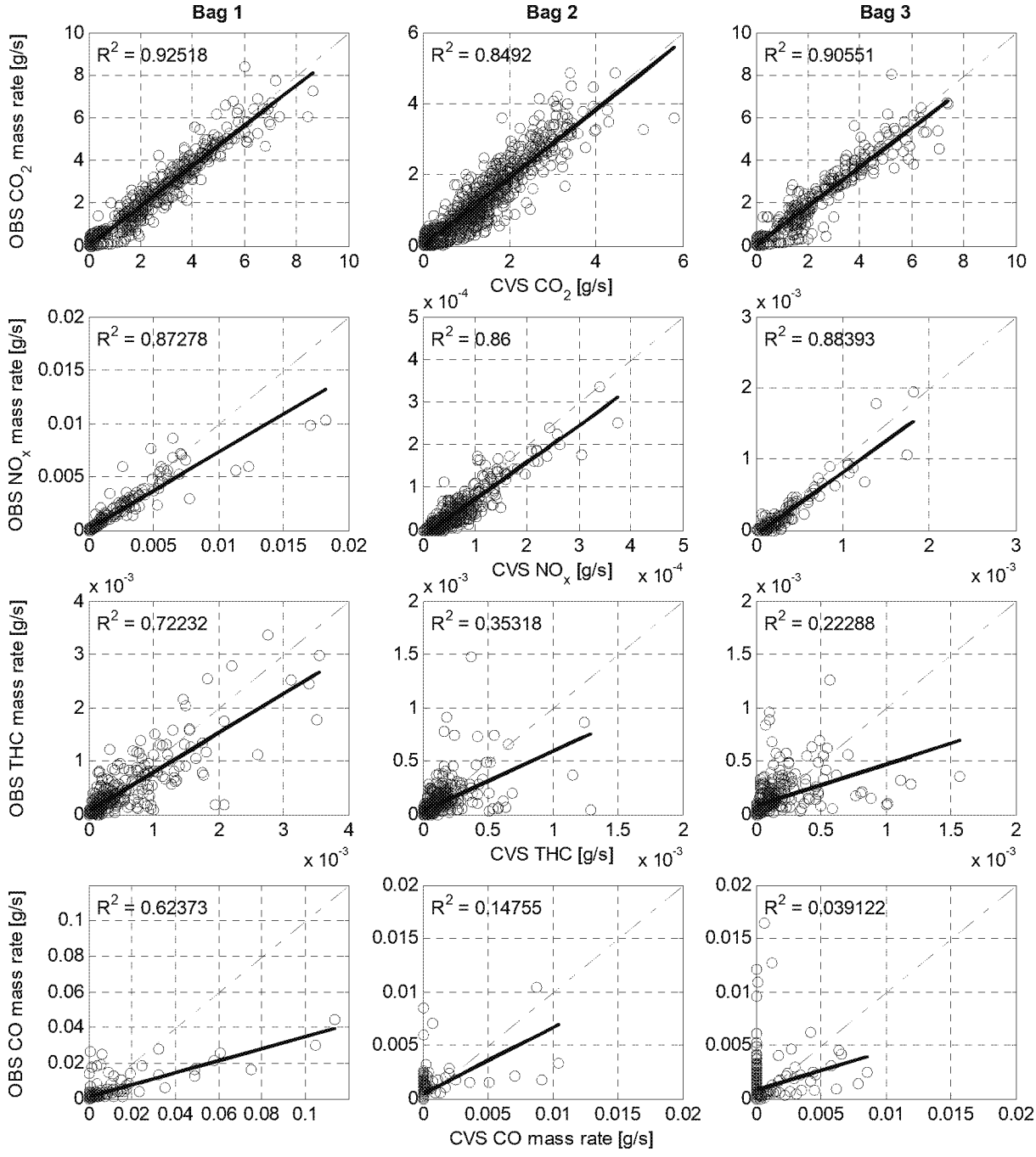


**Figure 7.1: Linear regression analysis between CVS laboratory (CARB, El Monte CA) and Horiba OBS-2200 PEMS measurements over the FTP-75 standard chassis dynamometer test cycle**

## 7.4 ULSD Fuel Analysis for Vehicles A and B

SGS HERGUTH LABORATORIES

# Certificate of Analysis
**Lab Number V7012631A**

Francisco Posada Sanchez
The International Council
on Clean Transportation
1225 "I" Street NW, Suite 900
Arlington VA 20005

03/12/13

Page 1

Client Code : THEICF Sample Date : 02/25/13 P.O. Number : POSTED CASH
Herguth ID : LABV7012631
Description : Commercial Grade Diesel Fuel
Oil Type : Diesel Fuel (GN_130)
Unit Type : Diesel Fuel (GN_DF001)

| Test Performed | Proc-Rev | Result | |
|---|---|---|---|
| Sulfur by Microcoulometry ASTM D3120 | 3120-3.1 | 5 | mg/kg |
| Density @ 15C ASTM D4052 | 4052-1.7 | 0.8355 | g/mL |
| Biodiesel Blend as FAME by FTIR HL-1141A | 1141A-1.1 | 0.32 | vol. % |
| Aromatic Content & PAH by SFC ASTM D5186 | 5186-1.0 | | |
| Mono-Aromatics ASTM D5186 | | 13.9 | % wt |
| Polynuclear Aromatic Hydrocarbons, PAH ASTM D5186 | | 1.7 | % wt |
| Total Aromatics ASTM D5186 | | 15.6 | % wt |
| Ultimate Analysis | 5291-1.0 | | |
| Carbon ASTM D5291 | | 86.16 | mass % |
| Hydrogen ASTM D5291 | | 13.67 | mass % |

REVISED REPORT supersedes lab # V7012631 and includes additional test results.
Data is reported per client specified testing request.
Fourier Transform Infrared Analysis (FTIR) of the fuel sample submitted shows the percent of Fatty Acid Methyl Ester (FAME) component in the ~1750 cm-1 wavenumber region. FAME is the major indicator for Biodiesel. The FTIR was calibrated based on standards prepared by blending Diesel with B100 Soy Biodiesel.
Aromatic Content & PAH by SFC and Ultimate Analysis was subbed out.

Respectfully Submitted,
SGS Herguth Laboratories, Inc.

cc: Francisco Posada Sanchez

Bobby R Licu, Evaluations Manager


*101 Corporate Place, Vallejo, CA 94590-6968 * Toll-Free Phone 1-800-645-5227 * Fax 1-707-554-0109 * www.herguth.com*